A Study to Evaluate Urban Heat Mitigation Design Strategies to Improve Pedestrian's Thermal Perception in Existing Canyons of Extreme Hot-Arid Cities.

The Case of Phoenix, Arizona

by

Abdullah Ali A Aldakheelallah

A Thesis Presented in Partial Fulfillment
of the Requirements for the Degree
Master of Science

Approved April 2020 by the
Graduate Supervisory Committee:

T Agami Reddy, Chair
Ariane Middel
Paul Coseo

ARIZONA STATE UNIVERSITY

May 2020

ABSTRACT

The rapid rate of urbanization coupled with continued population growth and anthropogenic activities have resulted in a myriad of urban climate related impacts across different cities around the world. Hot-arid cities are more vulnerable to induced urban heat effects due to the intense solar radiation during most of the year, leading to increased ambient air temperature and outdoor/indoor discomfort in Phoenix, Arizona. With the fast growth of the capital city of Arizona, the automobile-dependent planning of the city contributed negatively to the outdoor thermal comfort and to the people's daily social lives. One of the biggest challenges for hot-arid cities is to mitigate against the induced urban heat increase and improve the outdoor thermal. The objective of this study is to propose a pragmatic and useful framework that would improve the outdoor thermal comfort, by being able to evaluate and select minimally invasive urban heat mitigation strategies that could be applied to the existing urban settings in the hot-arid area of Phoenix. The study started with an evaluation of existing microclimate conditions by means of multiple field observations cross a North-South oriented urban block of buildings within Arizona State University's Downtown campus in Phoenix. The collected data was evaluated and analyzed for a better understanding of the different local climates within the study area, then used to evaluate and partially validate a computational fluid dynamics model, ENVI-Met. Furthermore, three mitigation strategies were analyzed to the Urban Canopy Layer (UCL) level, an increase in the fraction of permeable materials in the ground surface, adding different configurations of high/low Leaf Area Density (LAD) trees, and replacing the trees configurations with fabric shading. All the strategies were compared and analyzed to determine the most impactful and effective mitigation

strategies. The evaluated strategies have shown a substantial cooling effect from the High LAD trees scenarios. Also, the fabric shading strategies have shown a higher cooling effect than the Low LAD trees. Integrating the trees scenarios with the fabric shading had close cooling effect results in the High LAD trees scenarios. Finally, how to integrate these successful strategies into practical situations was addressed.

ACKNOWLEDGMENTS

I would like to convey my deep acknowledgments and appreciations to Professor Agami Reddy for his mentorship and guidance, during the last year it took me to complete my thesis. I would also like to thank my committee members, Professors Ariane Middel and Paul Coseo for their valuable comments and input.

I would like to extend my thanks to the SHaDE Lab research group at Arizona Sated University lead by Professor. Ariane Middel, for their continued support with instruments and equipment which made this study possible. Also, SHaDE Lab team members Saud AlKhaled and Florian Arwed for their supervision and guidance through the field measurements and simulation process.

Finally, my gratitude goes to my mother, brothers, and sisters who supported unconditionally throughout this journey, Last but not least, my wife Shatha for her sacrifices and care throughout the last two years.

TABLE OF CONTENTS

Page

CHAPTER Page

CHAPTER Page

CHAPTER Page

LIST OF TABLES

LIST OF FIGURES

Figure Page

Figure Page

Figure Page

Figure Page

Figure Page

Figure Page

Figure Page

Figure Page

Figure Page

Figure Page

\

LIST OF EQUATIONS

Equation Page

LIST OF ACRONYMS

ASHRAE	American Society of Heating, Refrigerating and Air Conditioning Engineers.
SEC	Saudi Electricity Company
UHI	Urban Heat Island
SUHI	Surface Urban Heat Island
BLHI	Boundary Layer Heat Island
CLO	Clothing Insulation
CLHI	Canopy Layer Heat Island
UBL	Urban Boundary Layer
UCL	Urban Canopy Layer
UCM	Urban Canopy Model
CFD	Computational Fluid Dynamics
LAD	Leaf Area Density
LSTs	Land Surface Temperatures
MET	Metabolic Equivalent of Task
PET	Physical Equivalent Temperature
ITS	Index Thermal Stress
LST	Local Standard Time
H/W	Building Height to Street Width
SVF	Sky View Factor
N-S	North-South
E-W	East-West

T_a	Air Temperature
T_{Srf}	Ground Surface Temperature
T_{MRT}	Mean Radiant Temperature
T_w	Wall Temperature
°C	Celsius
°F	Fahrenheit
W/m^2	Watt per Square Meter
$Btu/hr.ft^2$	British Thermal Unit per Hour per Square Feet
CDD	Cooling Degree Day
HDD	Heating Degree Day

1. INTRODUCTION

1.1. Statement of the Problem

1.1.1. The rapid growth effects on cities

The rapid rate of urbanization coupled with continued population growth and human activities have resulted in a myriad of urban climate effects across different cities around the world. According to the UN report, the population on the urbanized areas in 2019 was 54% of the worldwide population of 7.7 billion, and they projected that it would increase to 60% by 2050 with a total population of 9.7 billion. (World Population Prospects 2019). The fast growth is reflected in the urbanized areas and driving it to develop radically. As a result, the rapid development and the density of the population in cities have increased human activities. Therefore, anthropogenic heat drastically increased in urbanized areas; this is one primary reason for experiencing high ambient temperature during evening and nighttime in cities (Rosheidat, 2014). Further, this has resulted in Urban Heat Island (UHI) intensity increase in hot-arid cities. Many scholars have studied and identified the phenomena of UHI by the increment of air temperatures compared to the rural areas around the city because of the effects of the anthropogenic activities, urban surface energy balance, materials thermal properties and storage, and the intensive use of energy; causing the generation of heat (Oke, T.R., 1987; Kikegawa et al., 2006; Shahmohamadi et al., 2010). (UHI) intensity is controlled by the size of the city and the climatic characteristics (Arnfield, A. John, 2003). Oke reported that in a city with more than one million population could have a range of 1.0 to 3.0°C hotter annual

average temperatures than its rural areas (Oke, T.R., 1987). Also, nighttime temperatures in large cities can also stay 12C hotter than their rural environment during calm and clear nights (Oke, T. R., 1997).

1.1.2. The industrial revolution and cities growth

Since the industrial revolution at the start of the 19th century, the planning of cities was influenced by the industries and economy (Schivelbusch, 2014). Thus, the rapid growth caused environmental and social issues on the city scale (Mumford, 1981). And since then, scholars were investigating ways to solve industrial growth issues (Fishman, 1982). For instance, one option was to separate cities to zones depending on their function (e.g., Le Corbusier's Ville Radieuse). After that, the 20th century has seen a drastic change in city planning due to the fast success of the automobile industry (Mumford, 1981). The layout of cities was directly affected by cars, which was to facilitate car transportation and movement in the cities (Gehl, 2006). The fragmentation of cities was a result of new city planning change in the 20th century (Holston, 1999), and participated in reducing the social interactions on the city scale (Madanipour, 1998). Due to the preeminent car-centered planning, in the 1960s, a school of thought of activists and scholars like J. Jacobs, J. Gehl, D. Appleyard, and others rethought and investigated the social deteriorations and its extents in cities and called for (Cities for People). As a result of that, after the 2000s, the dissection and arguments of the human-centered urban design approaches were more in-depth and beyond the common gathering and meeting in outdoor spaces. In 2016, the UNESCO adopted a re-humanization cities approach (UNESCO, 2016).

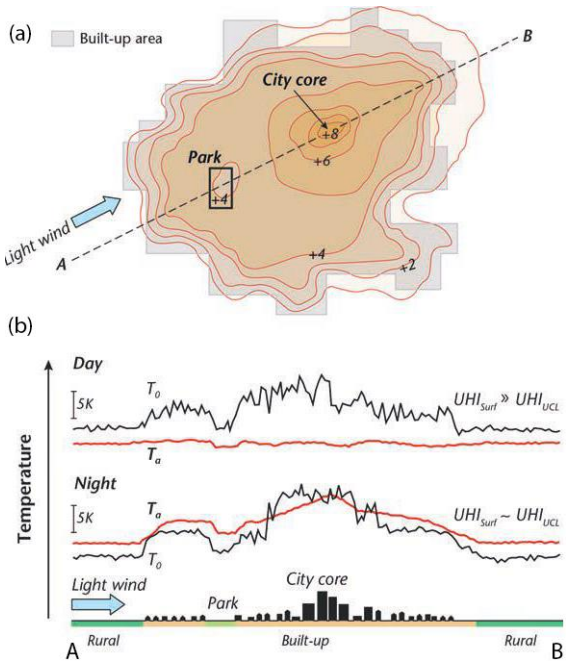

Figure. 1. 1. Schematic depiction of a typical UHI UCL at night in calm and clear conditions in a city on relatively level terrain. (a) Isotherm map illustrating typical features of the UHI and their correspondence with the degree of urban development. (b) 2D cross-section of both surface and screen-level air temperature in a traverse along the line A–B shown in (a) (Oke et al., 2017).

1.1.3. The spatial perception and extreme heat; the case of the City of Phoenix

Hot-arid cities are more vulnerable to induced urban heat magnitude due to the intense solar radiation during most of the year, which leads to the rise of the ambient air temperature and to outdoor/indoor discomfort. As a result, the energy demand for cooling will increase and will lead to significant energy consumption levels compared to a similar population in other cooler climates. Figure. 1. 1. shows a schematic depiction of a typical UHI Urban Canopy Layer (UCL) at night in calm and clear conditions in a city on relatively level terrain presented by Oke et al., (2017). Another instance is Riyadh in Saudi Arabia which has a similar hot-arid climate, with 80% of the electricity demand in households used for cooling (SEC, 2013). For that reason, one of the biggest challenges for hot-arid cities is to mitigate the induced urban heat and improve the outdoor thermal comfort, which could lead to a reduction in air-conditioning demands in indoor spaces. One way to achieve that is to rethink and study the urban microclimate in the existing

urban fabric on the UCL level, where it could have more substantial effect on the cities energy consumption more than focusing on the new developments. The outdoor cooling effects and energy consumption reduction that the new developments could make on the city scale will not have an enormous benefits to the city as whole. According to (World Population Prospects 2019), existing cities will only grow 25% by 2050 which is not a major factor in existing cities, so the new developments effects is unlikely to have a drastic reduction on the UHI intensity. Consequently, improving and rethinking the existing urban fabric is a necessity in order to mitigate the induced urban heat on the microclimate scale and reduce the ambient air temperature of the outdoor/indoor spaces on the city scale.

Therefore, Climate-sensitive approaches should be adopted to the urban and building designs in extreme heat and hot-arid climates to reduce the climatic significance on the pedestrians in the outdoor spaces. Accordingly, the air-conditioning loads in the indoor spaces will be reduced. The compact urban form is a successful application of the Climate-sensitive urban design approaches in ancient desert cities around the world. Bakarman described the Old Riyadh's neighborhood in Saudi Arabia, as an application of the Climate-sensitive approach:

> The old urban form reflects a high level of sensitivity to the local climate. It is highly dense to minimize the footprint of open spaces, which are vulnerable to extreme heat during the summer. Streets are narrow and aligned with a series of attached dwellings that are constructed on the property line with no setbacks. This kind of arrangement illustrates tightly bound relationships between streets and buildings and provides an efficient solution to cope with the severe hot and dry local climate. (Bakarman 2017, p.9).

However, due to the urbanization of the natural desert, concrete and asphalt as examples of the highest thermal storage materials were used extensively to build and

pave most of the cities surfaces. Golden (2004) have shown a thermal image Figure. 1. 2. of the City of Phoenix, where the roads, highways, parking structures, and the paved surfaces had the highest surface temperatures, which will result in higher absorption rates and retention of heat more than the natural desert surroundings (Golden, 2004). The urban fabric will release the stored heat as longwave radiation to the canopy layer at the nighttime. Moreover, anthropogenic heat and emissions from cars and HVAC units cause added heat to the canopy layer, which makes the urbanized areas hotter than the natural desert at night (Rosheidat 2014). Another reason for the induced heat in the urbanized area is the urban form and geometry itself, where it slows down the wind movement, which will reduce the advection effect and heat losses (Voogt & Oke, 1997).

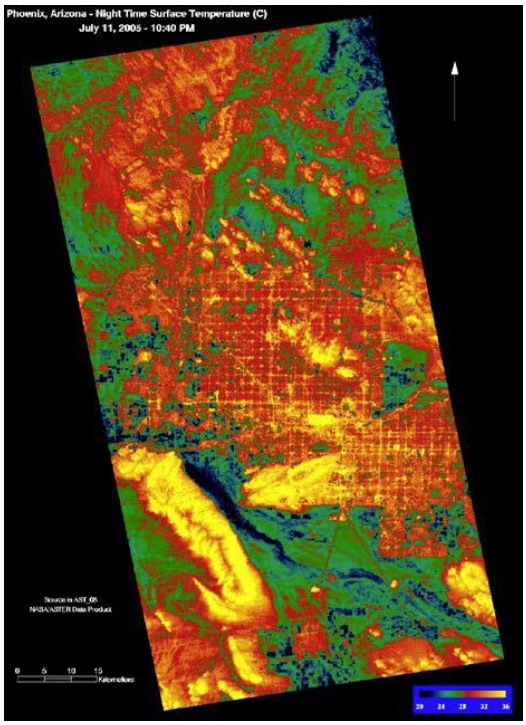

*Figure. 1. 2. Infrared image of Phoenix Metropolitan area at night on July 11, 2005, showing the hottest areas are where pavement is concentrated (streets/highways, airport, etc.). Source: ASU Center for Environmental Science Applications (CESA), retrieved on February 11,2014 at:*https://asterweb.jpl.nasa.gov/content/03_data/05_application_examples/urban/default.htm

In the City of Phoenix, the induced urban heat plays a critical role in the UHI intensity and negatively adverse the outdoor thermal comfort on the microclimate scale, provoking people to spend more time in air-conditioned indoor spaces. As a result, people's lives undesirably will be affected adversely in different aspects related to the socially, environmentally, economic, health and well-being, and result in increasing demands of energy consumption on the urban scale. With the fast growth of the capital city of Arizona, the automobile-dependent planning of the city contributed negatively to the outdoor thermal comfort and the daily people's social lives, which led to the extreme drop in the walkability, especially in the modern parts of the city. The drastic growth had its direct effect on social life and connection between residents on the city scale, also affected their health. Scholars like Abalkhail and al-Naim described the main reasons that led to the deterioration of daily social activity in a similar modern desert rapidly growing city; Riyadh, Saudi Arabia. First, the disregard of the pedestrians and sidewalks right-of-way in the new planning approaches. Second, the introduction of indoor shopping malls. Third, the influences of religious traditions on the spaces use. Fourth, microclimate discomfort while walking on the wide exposed streets with minimal and ineffective tree canopy shade, due to the car-dependent planning approach and the lack of apocopate urban canyons ratios, pedestrians were rare since the 1980s (Abalkhail and al-Naim, 2010). In the early 2000s, the reports have shown more than 98% of trips in Riyadh were by personal cars (ADA, 2003).

1.2. Aims, objectives, and research questions

Since the existing urban fabric is the dominant factor of the urban climate in cities, it is directly affecting the outdoor thermal comfort and the energy consumption in buildings. Also, due to the financial and time limitations for most of the cities around the world, it is unrealistic to have a drastic change in the existing urban form of the majority of the city. The primary goal of this study is to suggest suitable pragmatic configurations meant to enforce the spatial thermal perception experience with a stronger emphasis on design as the essential element of the manifestation of social patterns by improving the existing urban form. This is to be done by identifying suitable urban heat mitigation strategies that could be applied to the existing urban settings in the hot-arid Phoenix, without changing the building's footprint or any radical modification to the existing urban form. We shall start by evaluating existing conditions by thermal mapping and observation of various locations of an urban block to assist North-South oriented canyon in ASU Downtown campus in Phoenix, Arizona. After that, the data will be evaluated and analyzed for the local climates of the different locations. Then, we will investigate the effect of the local climate on outdoor thermal comfort and validated a computational fluid dynamics ENVI-Met model. After that, four mitigation strategies to the UCL level will be evaluated along with three incremental scenarios in each strategy (with the stipulation that the existing structures remain as they are), and then compared to find the most efficient performance. Afterwards, the successful and most efficient and resilient strategies will be integrated into two proposed scenarios and evaluated.

This research attempts to find answers to the following questions:

1- What is the most efficient/durable urban heat mitigation strategy that could be applied to the existing urban canyon, with respect to the pedestrian's thermal comfort?
2- To which level do the permeable surfaces on the ground level participate in outdoor thermal comfort for pedestrians?
3- Between the fabric shading devices and High/Low LAD trees, which one has the highest cooling effect in hot-arid Phoenix, Arizona?

1.3. Significance of the study

The rapid population growth caused an increase in energy demand internationally; thus, governments in many countries around the world are taking serious actions to reduce energy consumption on the city scale. For instance, funding renewable energy projects, promoting sustainable energy initiatives, and rethinking the smart cities. The State of Arizona is facing a puzzling challenge where the capital City of Phoenix experienced rapid growth since the early 1960s. Located in the middle of the desert of North America and to the northeast of the Sonoran Desert, Arizona, it lacks natural water sources. The City of Phoenix is projected to grow to more than 2 million by 2040 (The Maricopa Association of Governments, 2013). This study will contribute to the urban configuration/urban landscape fields in different ways. First, it will show the influence of the urban design/urban landscape on the local climate in downtown areas. Second, it will create a framework that could help to analyze, evaluate the existing urban situation and

then determine the suitable mitigation strategies that could improve the outdoor thermal comfort and walkability rates, which will reduce the energy consumption in buildings. Third, it will strengthen the understanding of the policymakers, and professionals in hot-arid regions of the range of opportunities that could be made to improve the outdoor thermal comfort, walkability, and improve the energy consumption on the neighborhood scale. Finally, the research will add to the limited literature on microclimate studies of the hot-arid climates as a whole, and more specifically to the southwest of the United States.

2. LITERATURE REVIEW

The effect of urbanization on human behavior and thermal comfort has been studied extensively throughout the last two decades. Also, the evaluation of urban energy consumption, especially for cooling and heating purposes, has been conducted through two different perspectives, namely: the impact of urbanization in terms of population growth and UHI. The effect of urban surface on air temperature (T_a) has been identified based on three main factors: material thermal properties (especially albedo), vegetation and shading effects, and the urban form. These factors also adopted as UHI mitigation strategies (Bakarman, 2017). For this study, only the role of material thermal properties, vegetation, and shading on UCL level, is discussed in detail regarding its impact on the outdoor thermal comfort levels. For a broad understanding of the problem, this study presents an overview of the urban design concepts, the practice of urban configuration, and Human-centered spaces. Moreover, it focusses on the UHI phenomenon in Phoenix and its contributions to the degradation of the microclimate as well as surface energy balance, urban & rural ground cover in Phoenix, and Urban Landscape & Shade. Finally, we present an overview of outdoor thermal comfort and review the human energy balance in urban spaces, the human thermal exchange on microclimate scale, and human thermal preference in urban spaces.

2.1. Urban Design

2.1.1. The practice of urban configuration

Urban design as a practice involving making urban configurations of spaces started in early history and applied to ancient cities (Carmona, 2014). The urban space's quality and arrangements were reflective of the traditions, religions, social norms, and economic and physical statue (Panofsky, 1951). The main goal of urban design is to connect people within the environment that they are living in (Kriege and Sauders, 2009). For that reason, many fields extensively studied that relationship between the human and its environments such as psychology, sociology, anthropology, urban topography, political science, and economic science (Carmona, 2014). Urban design is a multi-disciplinary field where architects, landscape architects, urban planners, town managers, etc. could be involved in it (Carmona, Tiesbell, Heath, and Oc, 2010). Many people have tried to define the urban design, and since it has different scopes it was hard to describe it, for example, a physical form of public policy; the bridge between planning and architecture sustainable and smart growth; mobility infrastructure; an artistic dimension of the city place-making; and visionary urbanism. (Carmona, et al., 2010; Krieger, 2009). Accordingly, this research will consider the urban design as one fundamental element of the spatial experiences for humans in the existing urban settings.

2.1.2. Human-centered spaces

The people’s lives in cities are affected by urban spatial, social, cultural, experiences (Madanipour, 2010). Many behavioral patterns happen in public urban

spaces (e.g., meet other people, enjoy their free time) (J. Jacobs, 1961). Thus, the quality of urban and human-centered space will be evaluated by its social sustainability, vitality, safety, and liveability, enjoyably, and walkability (Carmona et al., 2010; Cilliers and Timmermans, 2016; Gehl and Gemzoe, 2008; J. Jacobs, 1961; Lynch, 1984). The typical understanding of the spatial human behavior in the outdoor public spaces comes from the universal and standard human needs like comfort, enjoyment, and safety (Gehl and Gemzoe, 2008). For that reason, essential spatial aspects like human scale, walkability and seating rights, trees and microclimate comfort will improve the basic stream of accessibility, diversity, proximity, safety, and legibility rights (Bosselmann, 2012; Gehl, 2010; Moulay and Said, 2017; Burton and Mitchell, 2006). Thus, spatial behavior could be affected by; 1) Characteristics of users like; age, gender, socio-economic status, needs, and culture, etc. 2) Spatial experiences like; configuration, access, location, transparency, program, etc. (Gehl, 2010; Mehta, 2013). Those spatial aspects made a standard international set of practices and treatments of how the public spaces for human-centered urban design could be accomplished (NACTO and GDCI, 2016).

On the other hand, essential criticism to the universal practices in the urban design field and the re-humanizing cities, relate to the fact that the same strategies were considered with the same approaches around the world without looking at the local culture and climates (Lang, 2005; Madanipour, 2010; Fürst, 2009). The traveling, where urban design strategies could be taking as an international or standards, should be de-contextualized to be applicable in any given context (Maloutas, 2018). By being abstracted and simplified, the urban design traveling concepts could be a universal approach. However, the critical challenge of these urban design concepts is to integrate

them with local traditions and social norms (Knieling and Othengrafen, 2009; sayer, 1992, 2010). Thus, users typically tend to use the adopted traveling urban design concepts with the considerable influence of their local social norms and culture (Mehta, 2013; Raapoport, 1987). This behavior described as (parochialisation), where people use the urban spaces with an influence of their social norm roots and make the space exclusive to a specific social group (Reijndorp and Hajer, 2001). Hence, the social norms, cultures, religion, and traditions influencing the spatial behavior on the urban setting, the urban design key role is to create the suitable possible configurations to enforce the spatial experience with a stronger emphasis on design as the essential element of the manifestation of social patterns (Bosselmann, 2008; M. Camona, Tiesdell, Heath and Oc, 2010; Gehl and Gemzoe, 2008; Michelson, 1975, 1977). Therefore, we could define the human-centered urban space by being safe, accessible, walkable, delightful, livable, comfortable, sociable, and inclusive. Also, human-centered urban spaces inspire users to meet, bike, enjoy walking, and do daily life activities (Whyte, 1980; Gehl, 2010).

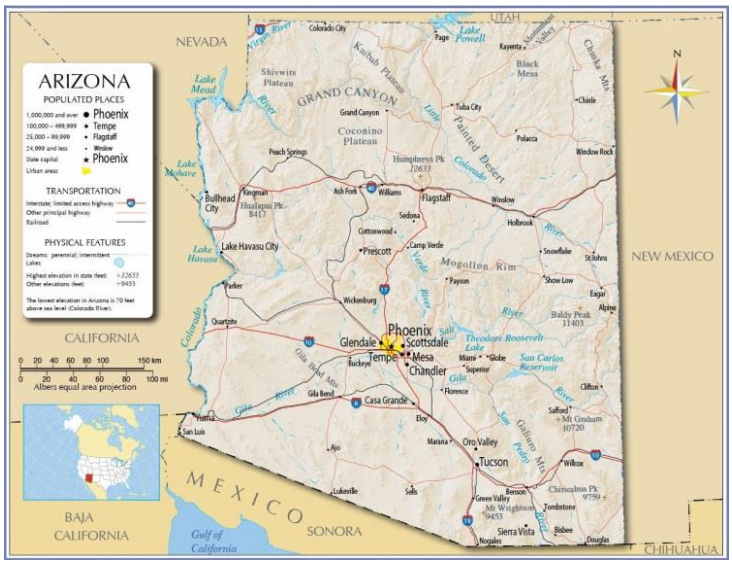

Figure. 2. 1. a map of the Phoenix, Arizona, http://www.orangesmile.com/common/img_city_maps/arizona-map-0.jpg

Figure. 2. 2. a map of the City of Phoenix, Arizona Www.google.com/maps

2.2. Phoenix Urban Climate

The City of Phoenix located in Maricopa County, AZ at 33° 29’ North, 112° 4’ West, and an elevation of 1,117 feet. The area experiences hot dry summers and mild winters. The average maximum temperature is 40 °C and the average minimum temperature is 15 °C. Precipitation is minimal, averaging 208 mm per year, and almost 1–2 mm in the summer (Western Regional Climate Center, 2019). The population of The City of Phoenix has grown from 105,000 to more than 1.6 million in 2018 in less than 70 years, to become the 6th major city in the US. (US Census Bureau, 2019). The City of Phoenix is projected to grow to more than 2 million by 2040 (The Maricopa Association of Governments, 2013).

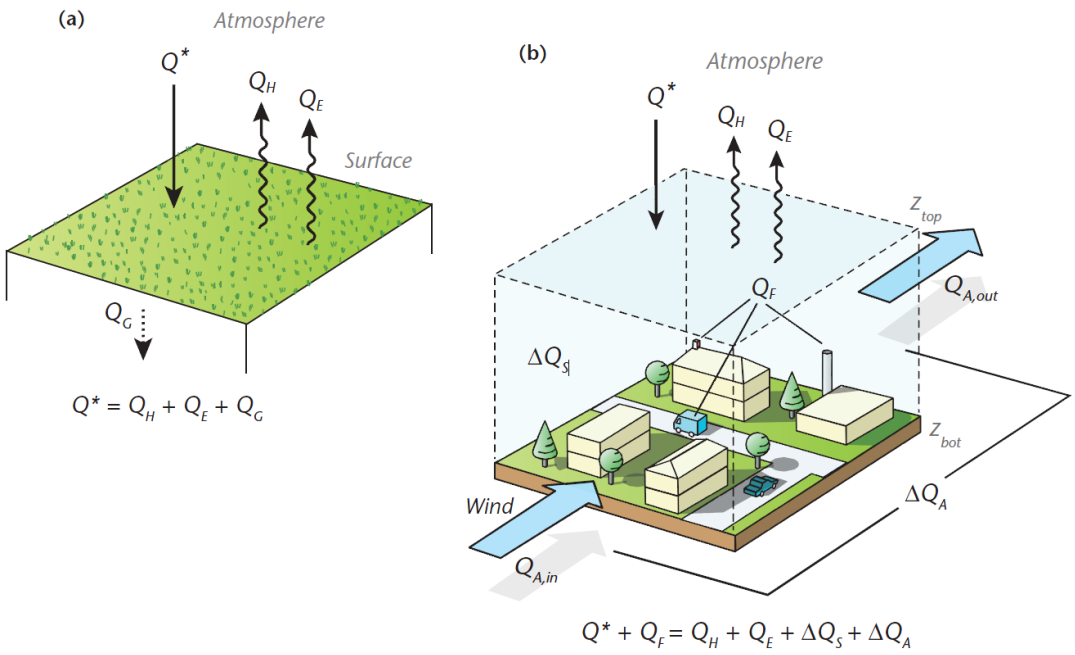

Figure. 2. 3. Schematic of the fluxes in the SEB of (a) a rural and (b) an urban building-soil-air volume. The volume that extends from the top of the RSL (ztop) down to a depth where there is no net conduction over the period of interest (zbot). Arrows are drawn in the direction the corresponding flux is considered positive. For ΔQS and ΔQA, they are positive if the internal energy of the volume increases (Modified after: Oke, 1987) (Oke et al., 2017).

Where; Q= Net all wave radiation, Q F = Anthropogenic heat flux, Q H = Delta of between the surface & atmosphere fluxes, Q E = Latent heat flux, ΔQ S = Heat storage flux, ΔQ A = Advection (Oke et al., 2017).*

2.2.1. Surface Energy Balance:

In the daytime, urban horizontal and vertical surfaces are exposed to solar radiation; the surface temperature will increase and interact with the air layer on top of them. The efficiency of the interchange of energy will be determined by the physical and thermal properties of the surfaces. Properties such as emissivity, thermal conductivity, density, specific heat capacity, thickness, moisture content, and albedo are important in analyzing the various heat flows. In Figure. 2. 3. a schematic diagram of Q* is presented showing net all wave radiation equations in the surface energy balance of (a) a rural and (b) an urban building-soil-air volume. The direct irradiation will increase the surface temperature, and the heat will be stored it in the urban fabric, which will be hotter than

the surrounding ambient temperature; the irradiated surfaces will reach a point where they start to increase the ambient temperature through sensible, latent, and radiative heat (Olgyay 1963, Asaeda 1996). The lowest 200m of the atmosphere absorbs the majority of the emitted infrared radiation from the horizontal surfaces, which will have a direct effect on the near-ground air temperature. When the difference between the urban surfaces and the air temperature above the surfaces is at its maximum, namely at noon, the amount of irradiated infrared will reach its highest levels and will be absorbed by the ambient temperature above the surfaces. Asaeda and Ca, (1996) recorded the highest rates of absorption was above asphalt surfaces, higher than concrete and soil surfaces by 60 W/m^2 at the lower layer of the atmosphere. In the early evening, the stored heat in the urban surfaces is released by direct and indirect radiation to the night sky as longwave radiations, which is correlated to the sky view factor as presented in Figure. 2. 4. (Nunez and Oke 1977, Oke 1981, Nakamura and Oke 1988, Erell et al. 2011). The efficiency of the heat discharge to the sky is associated with the sky view factor of the surfaces. Almost 90% of emitted longwave radiation is absorbed by the lower troposphere layer, mainly by clouds, water vapor, and carbon dioxide (Eriksson et al. 1982). The atmosphere will radiate the energy back to the urban surfaces, and this is why the re-radiated energy from the atmosphere is directly linked to the local climatic conditions like wind speed and direction, relative humidity, aerosols on the air, and cloud cover (Eriksson et al. 1982). In hot, dry climates and mostly free-clouds cover like Phoenix, the surface temperature will decrease drastically due to the nocturnal cooling due to the efficient discharge heat with the clear open sky (Eriksson et al. 1982).

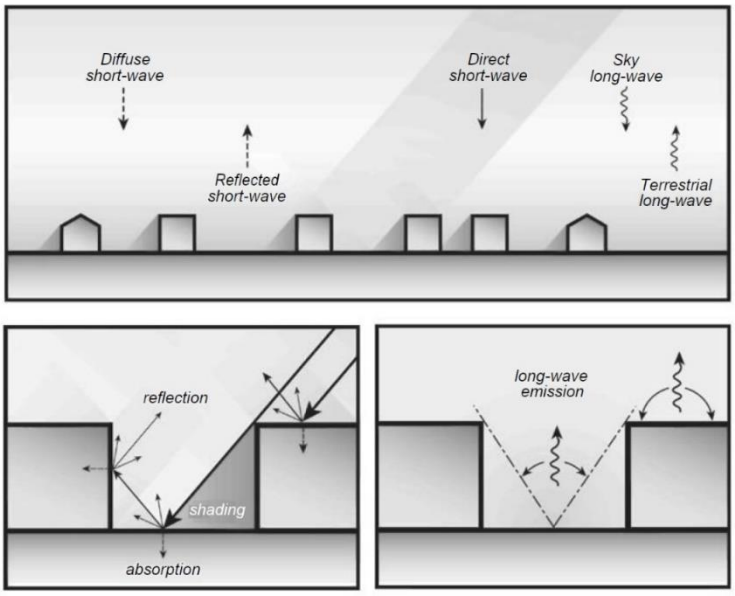

Figure. 2. 4. Generic effects of urban surface geometry on the penetration, absorption and reflection of solar radiation, and on the emission of long-wave radiation (Erell et al. 2011).

Vertical surfaces in urbanized areas tend to have higher surface temperatures by 0.5 – 1 °C than the horizontal ones with a highest sky view factor in the nighttime (Santamouris et al., 1999). The horizontal surfaces and paved materials on the ground level are a critical contributor for radiating heat to the surroundings in the summer nights (Asaeda et al., 1993). Asaeda et al., (1993) compared the emittance of asphalt and bare soil; the asphalt was emitting 200 W/m^2 of sensible heat and 150 W/m^2 longwave radiation more than the bare soil. The soil had a lower temperature because it contained higher moisture amount, which allowed the evaporation to reduce the surface temperature. On the other hand, the impermeable surfaces like asphalt do not allow moisture in the lower surfaces to get through, which reduces the chance of the evaporation effect and the reduction of the surface temperature (Asaeda and Ca 1993). Other studies have shown that high albedo and light cooler surfaces had higher reflectivity, which results in lower stored heat (Doll et al. 1985, Akbari et al. 1995, Taha

1997, Taha et al. 1997). However, Golden et al (2006) concluded that the high albedo did not have a noticeable effect on the surface temperature in Phoenix, AZ, compared to the capacity, thermal material storage, and thickness.

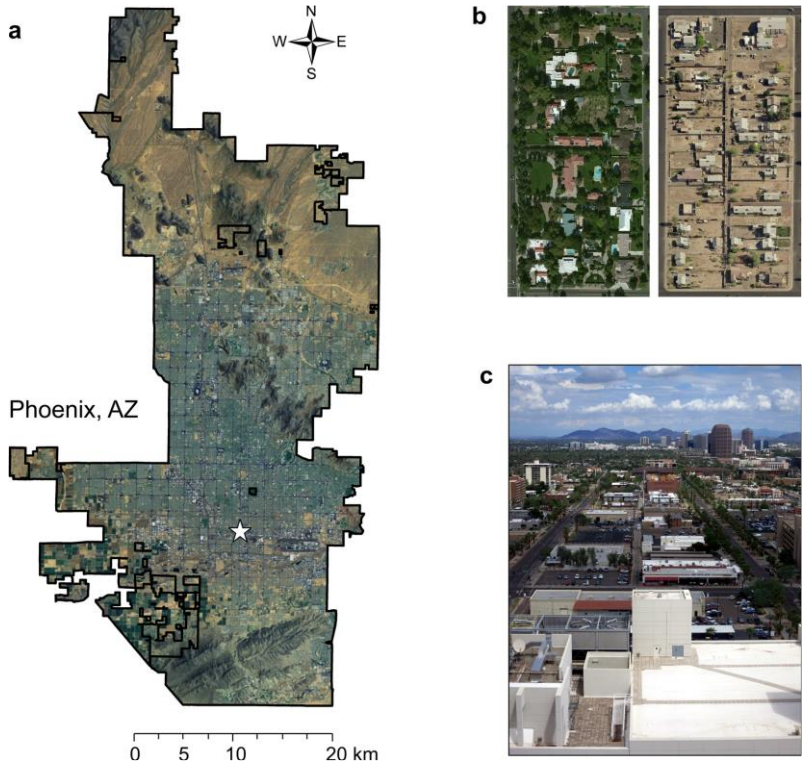

Figure. 2. 5. (a) Aerial view of the City of Phoenix, including downtown; (b) Phoenix neighborhood with high tree canopy cover and low tree canopy cover; and (c) cool roofs and street trees in Phoenix downtown (Middel et al. 2015).

2.2.2. Urban & Rural ground cover in Phoenix

Phoenix metropolitan area mostly surrounded by desert, and some of the agricultural fields which use a lot of irrigation and it became a source of moisture more than the natural desert Figure. 2. 5. Showing Aerial views of the City of Phoenix, including downtown area and how it is different than the rural areas. The rapid growth of the city replaced the agricultural fields with new developments, which reduces the

cooling effect from the agricultural fields due to the lack of the latent heat flux. The evapotranspiration or latent heat exchange process involving evaporation of water in the soil, and also described as microclimate modification strategy (McPherson and Simpson 1995). Most of the incoming radiation to the urban areas are stored as heat due to the high thermal mass materials used in cities. Moreover, although the natural desert has low reflectivity, as permeable surfaces, the natural desert allows the latent heat exchange, which will keep the surface temperature relatively cooler than the paved surfaces (Rosheidat, 2014). Furthermore, the surface temperature of the natural desert has shown an incremental rate than the urban paved surfaces, compared to the asphalt and concrete (Doll et al. 1985, Asaeda and Ca, 1993). Even though the lower layers under the natural desert have an almost similar amount of stored heat to the paved surface at night time, due to the low natural desert surface conductivity, it has a faster cooling rate than the urban paved surfaces. Also, the deep layers under the natural desert do not get much of the heat, due to its poor conductivity. The natural desert surfaces are permeable, and they allow evaporation exchange and latent heat flux losses, which creates a cooling effect. The cooling effect exceeds the surface layer and reaches the deeper natural desert layers due to the upward emittance (Rosheidat 2014). As a result, during night time, the air temperature above the natural desert becomes higher than the surface temperature of the natural desert suggesting that, the natural desert does not participate in heating air temperature in the night time. On the other hand, the paved surfaces like concrete and asphalt have higher surface temperature than the air above them, and they contribute to air temperature heating at night through radiation and sensible heat flux until the early mornings. Mainly because of the high thermal storage and the impermeable surfaces

materials thermal properties, which reduce the latent heat exchange with the surrounding atmosphere (Asaeda and Ca, 1996, Doll et al. 1985, Chalfoun 1991).

Figure. 2. 6. Examples of urban canyon cross sections, looking north along a north-south axis (Left) and west along an east-west axis (Right), illustrating climatic response in terms of basic geometry and secondary shading treatments (Erell et al. 2011).

Figure. 2. 7. Trees covering a pedestrian canyon. https://www.reddit.com/r/pics/comments/60ydks/vine_shaded_street_in_spain/

Figure. 2. 8. Shading fabrics covering a canyon. https://www.flickr.com/photos/44292341@N03/8118878644

2.2.3. Urban Landscape & Shade

The urban landscape is an essential aspect of the outdoor thermal comfort, only if it is designed with proper size and density. Landscape design could be an effective way to mitigate the induced urban heat in urbanized areas (McPherson et al. 1994, Akbari et al. 1995, Taha et al. 1997). McPherson et al, (1994) reported that the vegetation strategies could help mitigate the urban heat mainly by shade, evaporation, and changing the wind flow direction. The most useful role of the tree in dry, hot regions is its shading effect,

which is controlled by the shape of its crown and the density of its leaves. In Figure. 2. 6. an application of shading the urban canyon, showing the cross sections, looking north along a north-south axis (Left) and west along an east-west axis (Right), illustrating climatic response in terms of basic geometry and secondary shading treatments (Erell et al. 2011). Moreover, Figures. 2. 7. and 2. 8. illustrates two different shading strategies on the existing canyons. Shashua-Bar and Hoffman (2000) presented their study of an urban canyon in a hot-dry area, the local cooling effect was found to be due mainly to the shading effect of the trees and ranged from 1 to 3 K. For that reason, the best use of trees in hot-arid regions is for their shading effect, to reduce the accessibility of the short wave radiation to the ground surfaces and store the energy, and reduce the mean radiant temperature that caused by the emittance of the longwave radiation from the ground, which decreases the pedestrian thermal comfort. The trees could be helpful not only by eliminating the direct solar radiation axes to the horizontal and vertical surfaces but also by the radiative exchange between the surfaces and the trees. Puja Manglani (2003) demonstrate that the difference in surface temperatures between a wall that was shaded by a tree, and another one was exposed reached 11 °C.

Evapotranspiration is the process involving evaporation of water at the stomata of the tree leaves, as well as water trapped in the soil. However, as stated previously, in an urban environment, the tree's shading effect is the primary strategy for improved comfort. (Rosheidat 2014, p 24).

However, the evaporation effect in the hot arid area is ineffective because of continuous wind movement (Rosheidat 2014). Other applications of vegetation have proven to be more effective in the urbanized regions if they were relatively in a large scale like parks with extensive irrigation, the cooling could reach 5.6 °C (McPherson and

Simpson 1995). The efficiency of the urban vegetation is subject to the relative size of the vegetated area and the number of trees and their distances from each other. Also, the Leaf Area Density and Leaf Area Index, Shashua, and Hoffman (2000) measured different vegetated areas like parks and canyons in hot-dry urban sittings and found that 80% of the cooling effect was because of the shading effect of the planted areas.

Moreover, the arrangements and spacing of the trees are critical to increasing the cooling effect of the planted areas. For example, having a group of trees making a more significant shaded area is way more effective than having rows of individual trees along the sidewalks (McPherson 1992, McPherson et al. 1994). A study has pointed out the advantages of trees in urbanized areas and defined the enhancement of the outdoor thermal comfort, reducing induced urban heat and the energy consumption in buildings (Rosenfeld et al, 1996). With that being said, the health, life span and growth, irrigation expenses, and maintenance of trees are the concerns for city officials in hot-dry climates. According to Martin (2006), tree roots should have enough space under the tree, and sufficient air and water, which is necessary to get the most benefits from the tree and for sustainable growth and shading efficiency.

Figure. 2. 9. Visible and infrared (thermal) images for two urban landscapes in Berlin, Germany illustrating the radiation environment (Oke et al., 2017).

2.3. Urban Outdoor Thermal Comfort

Measuring outdoor thermal comfort is even more complex than measuring indoor thermal comfort due to the various parameters that could affect human comfort in urban settings (Cook 2001, Rosheidat 2014, Rowe 1991). The benchmark of human comfort should be referenced by multiple factors, the levels of comfort in the outdoor spaces are higher than the indoor spaces (Cook 2001). Figure. 2. 9. shows visible and infrared (thermal) images for two urban landscapes in Berlin, Germany illustrating the complex radiation environments (Oke et al., 2017). Many outdoor thermal comfort studies have used specific indexes that took multiples factors in to account like Ta , relative humidity RH, and mean radiant temperature Tmrt. Also, psychological factors, person's level of

metabolic activity (MET), person's clothing (CLO) factor (Fanger 1970). The ambient air temperature is not the only indicates the human outdoor thermal comfort, the most effective factor is the Mean Radiant Temperature Tmrt (Emmanuel et al. 2006). The Tmrt is the degree of longwave radiation affecting pedestrians relative to the specific location in the urban setting (Chalfoun 2001). The overall radiation fluxes that the person is exchanging with the surrounding surfaces in the urban environment in every location, which referenced to as the person's sky view factor (SVF) (Chalfoun 2001).

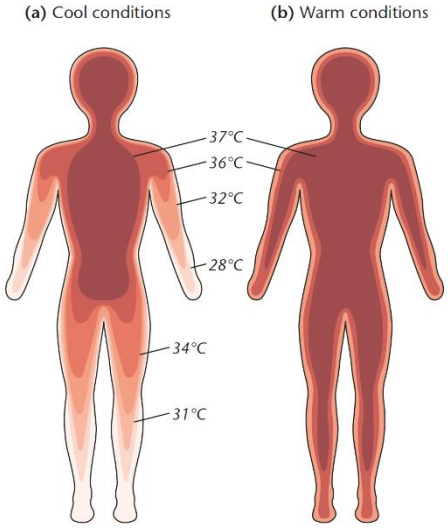

Figure. 2. 11. The temperature distribution in the body during cool and warm conditions. In cool conditions, the warmest temperature (37 C) is confined to the head and trunk only. The temperature of the subcutaneous tissue for the hands and feet is < 28 C. In a warm environment the warm core temperature is found over much of the body (Modified after: Mount, 1979) (Oke et al., 2017).

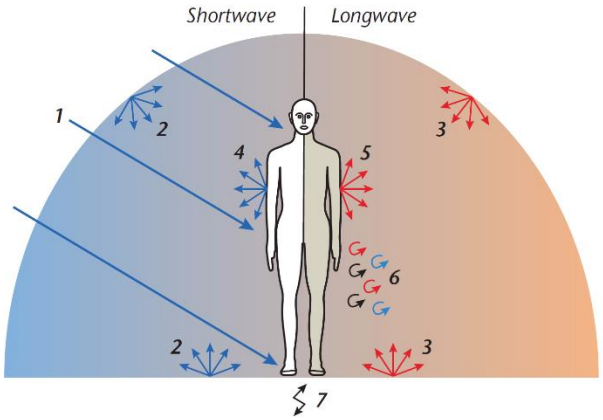

Figure. 2. 10. Energy exchanges at the surface of the human body. These include: (1) direct shortwave radiation that impinges on the sunlit part of the body; (2) diffuse shortwave radiation that originates from the sky as a result of scattering and from the ground as a result of reflection; (3) diffuse longwave radiation that is emitted from the sky vault and from the ground; (4) reflected shortwave radiation that is controlled by the albedo of the clothed body; (5) emitted longwave radiation which is a function of surface temperature; (6) convective heat loss by sensible and latent heat exchange with the ambient air that is partly a function of wind speed and; (7) conductive heat exchange with the ground through physical contact. (Oke et al., 2017).

2.3.1. Human Energy Balance in Urban Spaces

The most effective gain/loss factors in the urban settings on the human energy balance is the total radiation, which could be more than 50% of the whole gain/loss

radiation (Rosheidat 2014). While most of the people take air temperature as the main indicator of comfort, Rowe (1991) have reported that air temperature only represents 7% of the heat exchange between the person and the urban spaces. The various weather parameters interact together to control the way that the human body feels in outdoor spaces. In the summer daytime, Tmrt is the controlling factor of outdoor thermal comfort in the exposed surfaces (Höppe 1999). For that reason, the most effective strategy in hot-dry climates like Phoenix, Arizona, is to reduce the direct sun exposure on the urban pedestrian level (Bryan 2001).

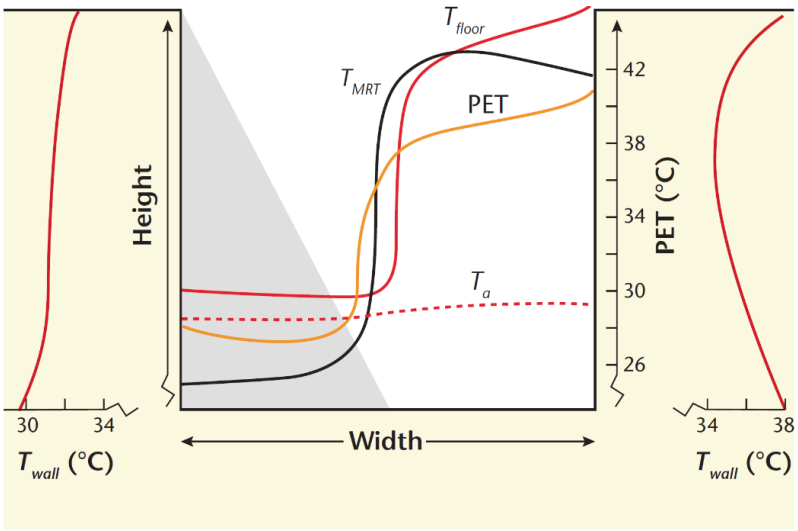

Figure. 2. 12. A cross-section of an urban canyon showing simulated variations in wall (T_{wall}) and floor (T_{floor}) temperatures; air temperature (Ta) and mean radiant temperature (T_{MRT}). Note the impact of sunshine and shade (in grey) on the surface values (Source: G. Jenritzky; with permission) (Oke et al., 2017).

2.3.2. The Thermal Exchange on Microclimate scale

One of the most fundamental studies of the urban climate on heat fluxes in the urban canyon scale is the work of Nunez and Oke (1977) who studied North-South oriented canyons with 1 : 1 aspect ratio in Vancouver, Canada. The walls of the canyon

were painted white with no openings, and little vegetation. They concluded that the orientation was the main factor of the heat exchange efficiency. In the daytime, almost 30% of the heat stored in the canyon surfaces as sensible heat, and about 60% was transferred to the air in the canyon as sensible heat with only 10% of that was latent heat. In the nighttime, the canyon had a low heat loss rate as longwave radiation due to the low wind speed and turbulence. The wind speed and direction have an essential role in the advection effect, parallel or perpendicular to the canyon orientation; either way, the wind could help accelerate the rate of losses in the canyon (Nunez and Oke 1977). Another study by Yoshida et al. (1990/91), confirms many findings of Nunez and Oke's study. They compared East-West canyons with almost 1 : 1 aspect ratio in Kyoto, Japan, to the North-South canyon assumed in Nunez and Oke case study. They found that the East-West canyon surfaces stored 1.5 times more heat than the roofs. Also, about 40% of the heat got lost to the air in the canyon (Yoshida 1991, Toudert 2005).

PMV	PET	Thermal perception	Grade of physiological stress	Universal Thermal Climate Index (UTCI) (°C) range	Physiological responses
		Very cold	Extreme cold stress	< 40	Decrease in core temperature
−3.5	4			−27 to −40	Shivering, average skin temperature will fall below 0°C if exposure is sustained
−2.5	8	Cold	Strong cold stress	−13 to −27	Face temperature < 7°C (numbness), core to skin temperature gradient increases
		Cool	Moderate cold stress	0 to −13	Vasoconstriction, exposed skin temperature < 15°C
−1.5	13	Slightly cool	Slight cold stress	+9 to 0	Localized cooling, need for gloves
−0.5	18				
		Comfortable	No thermal stress	+9 to +26	Comfortable, sweat rate < 100 g h^{-1}
0.5	23				
1.5	29	Slightly warm	Slight heat stress	+26 to +32	Slight heat stress
		Warm	Moderate heat stress	+32 to +38	Positive change in rate of sweating, and of skin temperature
2.5	35	Hot	Strong heat stress	+32 to +38	Sweat rate > 200 g h^{-1}
3.5	41			+38 to +46	Small core to skin temperature gradient (< 1 K). Sweat rate increase (> 650 g h^{-1} at limit)
		Very hot	Extreme heat stress	> 46	Increase in core temperature

Figure. 2. 13. Ranges of the thermal indexes Predicted Mean Vote (PMV) and physiological equivalent temperature (PET) for different grades of thermal perception by human beings and physiological stress on human beings (Modified after: Matzarakis et al., 1999) (Oke et al., 2017).

2.3.3. Human thermal Preference in Urban Spaces

Most of the thermal comfort studies tend to concentrate on indoor spaces, and not many researchers have investigated the outdoor space's thermal comfort (Kaynakli & Kilic 2005). Specifically to the United Sates of America's southwest, Rosheidat (2014) described the lack of studies on the outdoor thermal comfort and how it is "not given enough significance in the urban planning and design processes. Municipal development standards are not adapted to local climatic conditions and are especially poorly suited to the hot arid climate of the Southwest" (Rosheidat 2014, p 1). The American Society of Heating, Refrigeration, and Air-Conditioning Engineers (ASHRAE 1966) defined comfort in as: "a state of satisfaction with the thermal environment". In 2004, ASHRAE 55 had a more precise definition for comfort, "to specify the combinations of indoor

thermal environmental factors and personal factors that will produce thermal environmental conditions acceptable to a majority of the occupants within the space."

Although there are various thermal comfort indexes as illustrated in Figure. 2. 13. the majority of them used the same factors. We could divide them into two main types, rational or empirical. The rational indices include the PPD (percent people dissatisfied), Effective Temperature, the PMV (predicted mean vote), the Standard Effective Temperature (SET), (Toudert 2005). Many scholars have criticized those indexes because of their high humidity saturation level, reaching 100% in most cases, which cannot be representative of the everyday experience for people in the outdoor/indoor spaces. Thom (1957) presented the Effective Temperature with 30% humidity, and after that Gagge, Stolwijk, and Nishi (1971) introduced a new index: the Humid Operative Temperature (Toh), which accounts for sensible and latent heat transfer and their relation to the relative humidity and wetness. However, by (1973) Gagge, Nishi, and Gonzalez proposed a new index and "defined as the temperature of an imaginary environment with a predetermined transfer coefficient in which the total heat exchange from the skin surface (sensible and latent) would match the real environment" (Rosheidat 2014, p 23). They gave it a different name, Standard Effective Temperature (SET) (Gagge 1973).

3. RESEARCH DESIGN & METHOD

The use of microscale atmospheric software by architects, urban designers, landscape architects, town planners, and designers in general in the last two decades has increased the ability to perform detailed studies and simulate the performance of heat mitigation strategies on the urban scale (Crank et al., 2018). For instance, the effects of vegetation, shading devices, and manipulating material thermal properties (i.e., roughness, emissivity, and albedo) can be studied (Bakarman, 2017). The implementation of microscale atmospheric applications by the designer was mainly because the computational models enabled the designers to represent different scenarios of the built environments and measures its performance as a way to mitigate the heat in urban areas. The path involving simulation and evaluation is a cost-effective way to examine different domains of cities where designers and policymakers could draw explicit conclusions and take decisions about specific strategies.

However, Santamouris found inconsistency of similar strategies on different simulated models, and this led to a debate among urban climate scholars about the models and the software. (Santamouris, M., 2014). A recent literature search by Crank et al., (2018) showed that 30% of the published research since 2006 on the atmospheric microclimate modeling in the built environment involved using ENVI-met software in their studies. The extensive use of ENVI-Met is because of its reduced complexity, user-friendly interface, and propositional simulations upfront cost of the software. (Ali-Toudert, 2005; Chow and Brazel, 2012; Roth and Lim, 2017; Singh and Laefer, 2015).

The primary goal of this study is to evaluate suitable possible configurations to the existing urban setting and enforce the spatial thermal perception of the pedestrian

experiences in the outdoor spaces in Downtown Phoenix, Arizona. With a stronger emphasis on design as the essential element of the manifestation of thermal comfort by improving the existing urban settings and finding the suitable urban heat mitigation strategies that could be applied on the hot-arid Phoenix. However, the challenge is to implement these improvements on the existing urban canyons without changing the building's footprint or any radical modification to the existing urban form. One way to do that is by evaluation and analysis of the existing urban conditions then validating a microscale atmospheric software. After that, there is the need to design and test the different urban heat mitigation strategies to find the most effective and resilient strategies that could be implemented to the existing urban setting. To accomplish this, observational field measurements and thermal mapping of North-South canyon were performed in Downtown Phoenix, Arizona, as part of an ongoing study with the SHaDE Lab, ASU. After that, the data was evaluated and analyzed for six different locations. Then, modeling and validating the same area domain was done by using a computational fluid dynamics ENVI-Met 4.4 model. After that, different mitigation strategies were applied to the Urban Canopy Layer (UCL) level of the urban canyons, with the existing structures remaining unaltered. Then the evaluation of three incremental scenarios were done through simulation. Finally, two proposed design solutions were proposed by integrating the best outcomes of the 12 evaluated previously.

3.1. Study location, Phoenix, Arizona

The study location was at Tylor St and 1st St in Phoenix downtown, Arizona State University Campus. The ASU Downtown Phoenix campus is relatively one of the busiest and most walkable streets in the area because of it is location in between the ASU academic and housing buildings, which populate almost 10,000 students in ASU Downtown Phoenix Campus. Also, the campus is located close to Light Rail station and bus station in Downtown Phoenix. As described earlier, the City of Phoenix is projected to grow to more than 2 million by 2040 (The Maricopa Association of Governments, 2013). As a result of the fast and rapid growth of the City of Phoenix, the nighttime temperature has increased by 0.5 °C every decade since 1910 (Brazel et al., 2000). Scholars in many publications have well documented the Urban Heat Island phenomena in the City of Phoenix for different scales and durations (Stabler et al., 2005 ;Brazel et al., 2007, Georgescu et al., 2012, Grossman-Clarkeetal., 2010, Chowand & Brazel., 2012; Middel et al.,2014). Brazel did a time-trend analysis for the summer for Air temperature in the Phoenix Sky Harbor International Airport and found that there was about 6° C difference between the urban and rural areas at nighttime (Brazel et al., 2000). Also, a mobile transect study was conducted in the winter in the City of Phoenix, found intensity of 8° C for the Urban Heat Island (Sun et al., 2009).

Figure. 3. 1. Google Maps views of E Tylor St and N 1st St in ASU Phoenix downtown Campus ASU Downtown campus, City of Phoenix, Arizona.

Figure. 3. 2. Site Plan view of the case study, E Tylor St and N 1st St in ASU Phoenix downtown Campus, Arizona.

Figure. 3. 3. Section view of the case study, E Tylor St and N 1st St in ASU Phoenix downtown Campus, Arizona.

3.2. Field Observation & Validation

The validation process involves focusing on forcing meteorological conditions parameters for a specific period to the simulation software, and then comparing the simulation predictions with measured performance data. The validation process usually does not get the attention it deserves from the simulators and causes inaccurate outcomes (Maggiotto et al., 2014; Middel et al., 2014). To validate a three-dimensional atmospheric model with field observations, we conducted hourly measurements in Downtown Phoenix in summer 2019, as part of an ongoing research at the SHaDE Lab, ASU. After that, we modeled and simulated the ENVI-Met model two times with two different forcing methods to find the most accurate way and the differences between the two ways and how they differ from the actual field measurements.

3.3. Scenarios Evaluation & Proposed Strategies

The goal of this study is to evaluate the performance of different urban heat mitigation strategies on an existing North-South urban canyon in Phoenix, Arizona, by modeling and simulating a variety of scenarios using ENVI-Met 4.4 software. After that, we evaluated each strategy and compared the Mean Radiant Temperatures T_{MRT} at 0.9 m height, and the ground surface temperatures T_{Srf} of the whole canyon area to find the impact of different scenarios on improving pedestrian's thermal comfort. Many scholars have identified the main reasons of the urban heat intensity in hot-arid climates; for example like the effects of the anthropogenic activities, materials thermal properties (Impervious), low tree and shade canopy, and the intensive use of energy and heat generation (Oke, T.R., 1987; Kikegawa et al., 2006; Shahmohamadi et al., 2010). After validating the existing conditions

(Baseline) to the observed measurements of North-South canyon in Downtown Phoenix, Arizona. This study examine four known heat mitigation strategies, each strategy involving three incremental scenarios of different densities and configurations. The evaluation involved studying the effect that each scenario had on the Mean Radiant Temperatures T_{MRT} at 0.9 m height, and on the ground surface temperatures T_{Srf} on the canyon scale.

The first strategy was to increase the permeable material's percentage of the canyon ground surface by adding soil & vegetation through three incremental scenarios 25%, 50%, and 75%. The second strategy, adopted the same ground surfaces materials configurations from the first strategy, and evaluated the tree's cooling effect by adding two types of trees High/Low LAD trees in three incremental configurations and scenarios and a total of six scenarios that had three shading area factors of the canyon; 25%, 50%, and 75%. The third strategy was to replace the three confirmations scenarios in the second strategy with fabric shading to assist the performance of the fabric shading compared to the two types of trees in three incremental scenarios with the same canyon shading area factors. The fourth strategy was by adopting two integrated scenarios of the second and third strategies and evaluating two types of trees and fabric shading with a low shading area factor of 25% and compared them with the high shading area factors. The above steps would allow us to evaluate the performance of each scenario and how much they participated in the mitigation process.

3.3.1. First Strategy, Scenarios 1, 2, and 3 Soil & Vegetation:

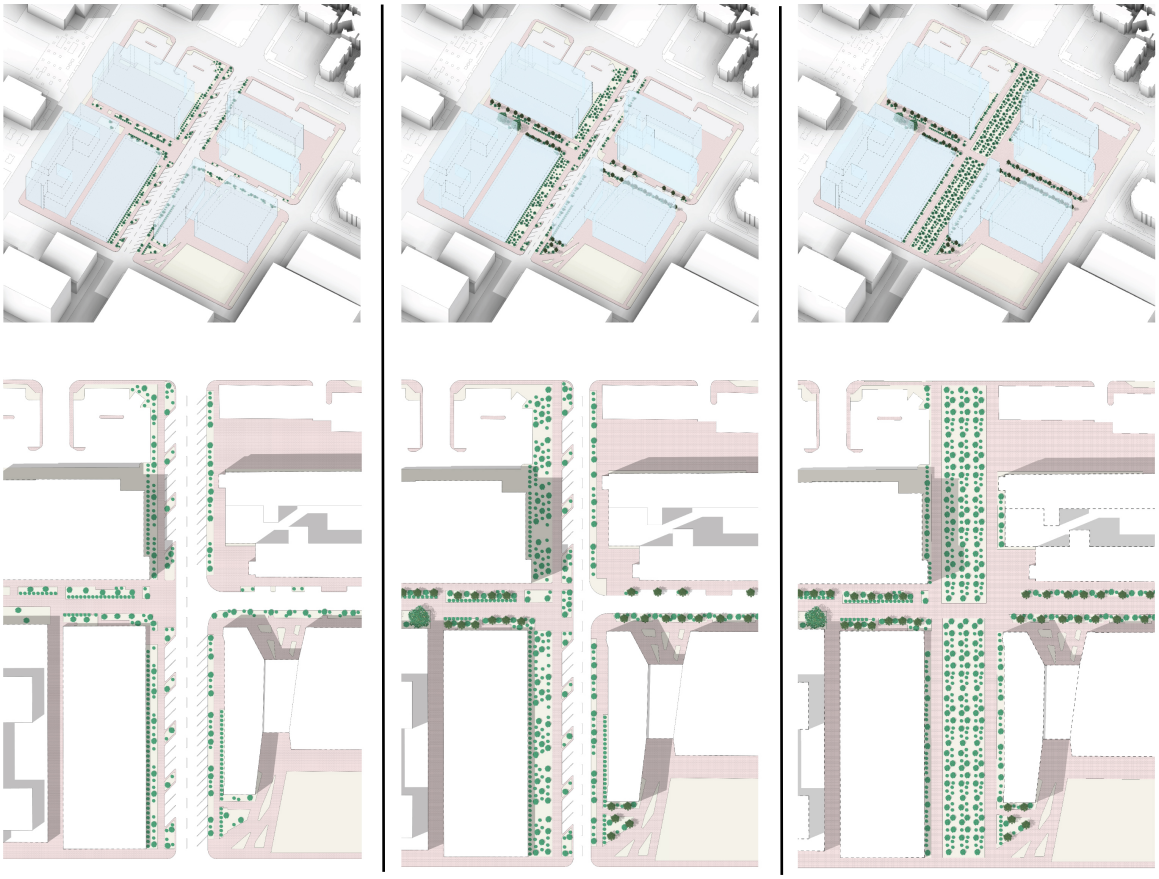

Scenario_1 Soil & Vegetation 25% Scenario_2 Soil & Vegetation 50% Scenario_3 Soil & Vegetation 75%

Figure. 3. 4. Scenarios 1, 2, and 3.

The first strategy focused on the ground surface material thermal property's role to the pedestrian's thermal comfort. To have a better understanding of the ground surface thermal properties, all of the existing trees were removed. After that, the canyon ground surface materials were manipulated with three different incremental scenarios of (Permeable & Impermeable) materials. The first scenario represents the existing ground surface materials configuration, which was 25% of soil and vegetation (Permeable) and 75% of asphalt (Impermeable). The second and third scenarios involved increasing the

percentages of permeable materials, soil, and vegetation in canyon ground surface to 50%, 75%, respectively.

3.3.2. Second Strategy - A & B: High/Low LAD Trees

A- Second Strategy: Scenarios 4, 5, and 6 High LAD Trees:

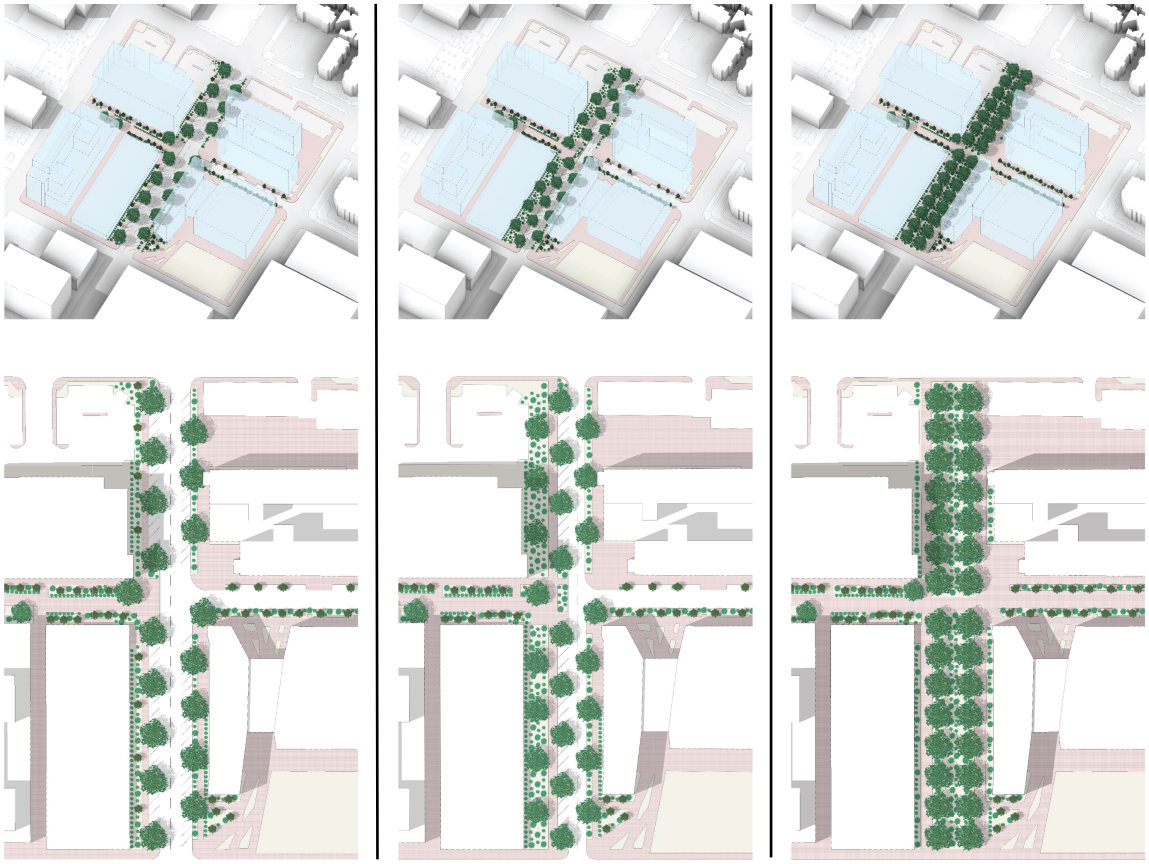

Scenario_4 High (LAD) 25% | Scenario_5 High (LAD) 50% | Scenario_6 High (LAD) 75%

Figure. 3. 5. Scenarios 4, 5, and 6.

B- Second Strategy: Scenarios 7, 8, and 9 Low LAD Trees:

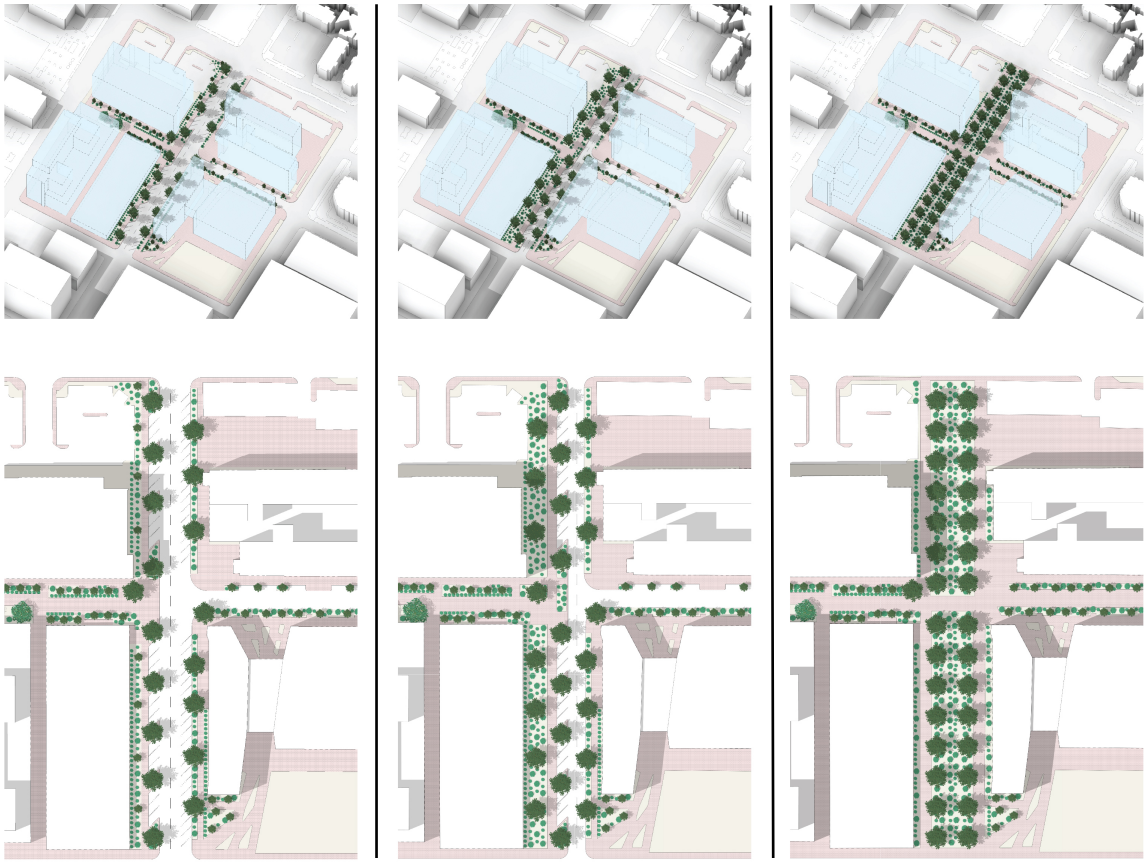

Scenario_7 Low (LAD) 25%

Scenario_8 Low (LAD) 50%

Scenario_9 Low (LAD) 75%

Figure. 3. 6. Scenarios 7, 8, and 9.

Crown diameter, 4 m Height under branch, and 0.18 Leaf albedo. The trees were added to the canyon in three incremental scenarios for each, which provided shade to the canyon ground surfaces by 25%, 50%, and 75% shaded area.

3.3.3. Third Strategy, Scenarios 10, 11, and 12 Fabric Shading:

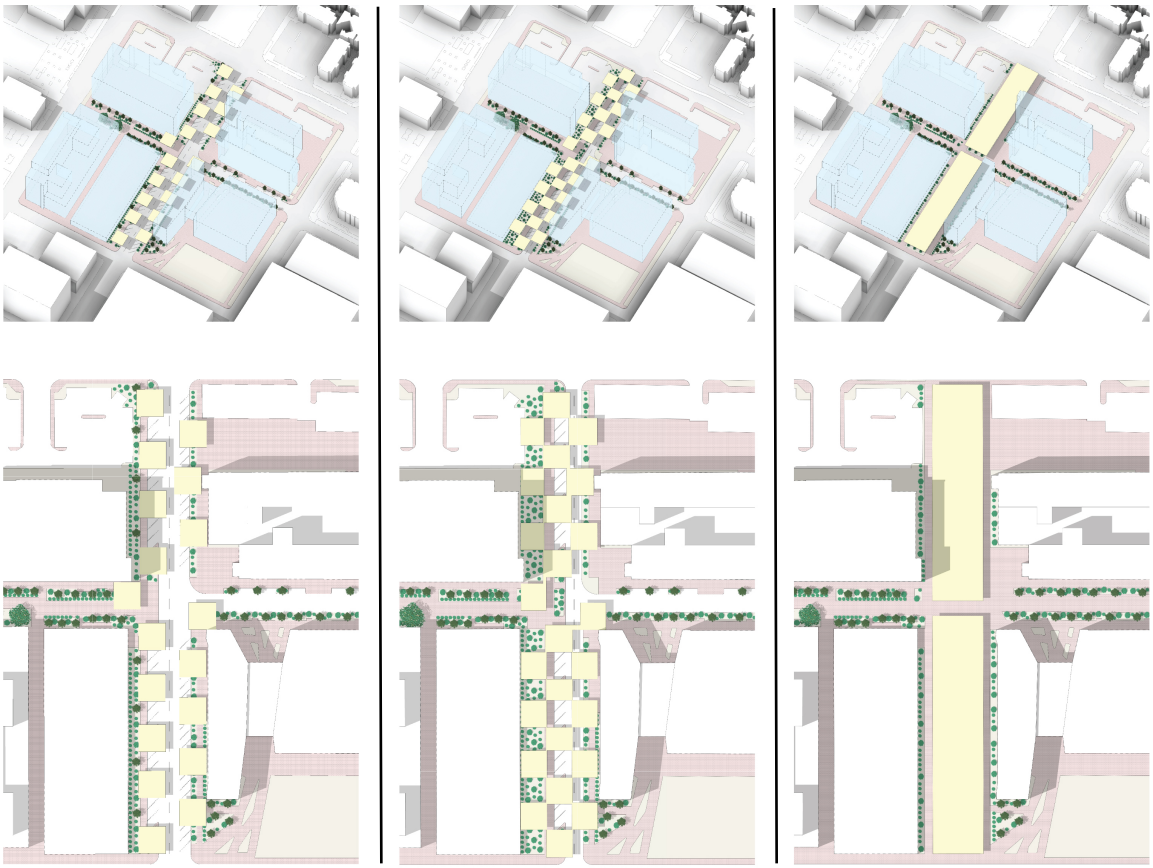

Figure. 3. 7. Scenarios 10, 11, and 12.

The third strategy illustrated in Figure. 3.7. replaced the three configurations of tree in the second strategy with fabric shading devices that has a transmittance of 20%. The shading devices do not need irrigation, with minimal maintenance. This strategy compares the efficiency of the fabric shading to the different types of trees, High/Low

LAD, with a total of three different fabric shading scenarios provides 25%, 50%, and 75% shaded areas. Table.2 is showing the physical parameters of the fabric shading devices, with 10 m height, 9 m Height under branch m, 0.2 Leaf albedo, and 0.2 Fabric Transmittance.

3.3.4. Fourth Strategy, Scenarios 13, 14 High / Low LAD Trees + Fabric Shading:

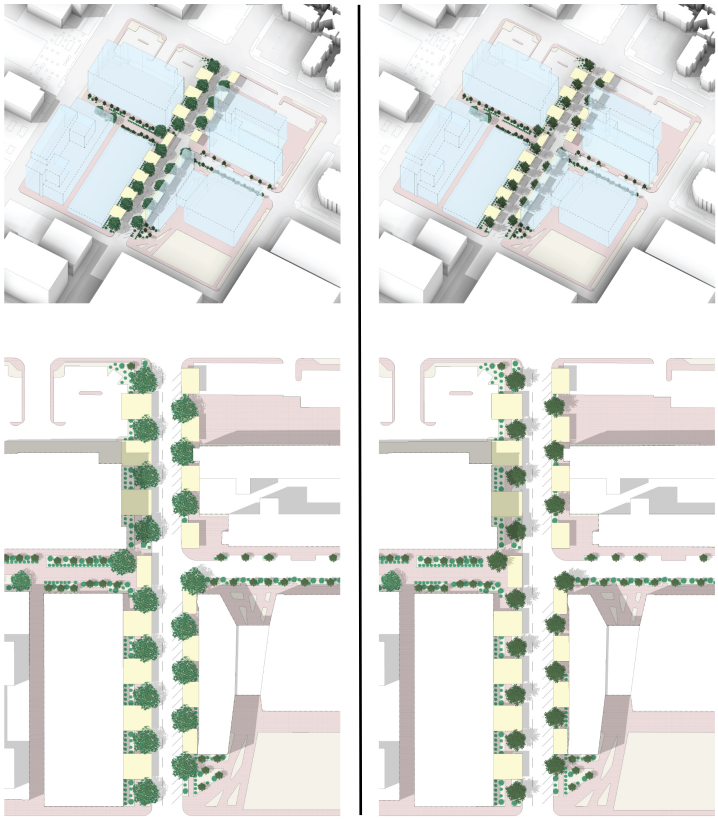

Figure. 3. 8. Scenarios 13 and 14.

After analyzing the results of all the 12 scenarios, an improved fourth strategy proposed with two scenarios. The fourth strategy integrated the most efficient and resilient performance, by having a fixed 25% shaded area of two types of trees, scenarios

4 & 7, Low & High LAD. In addition, a fabric shading scenario were added, where the fabric was providing 25% shaded area of the canyon ground surface, scenario 10. Having a total shaded areas of 50% of the whole of the canyon ground surface, and total of two new proposed scenarios. The main objective of adding fabric shading to the trees scenarios is to determine if the coupling of the two low shading factor strategies (25%) will perform as good as or close to the high shading factor strategies 50% and 75% of the tree shading with two driftnet High/Low LAD. Trees in the desert are using a lot of water and they could be unsustainable if they were used extensively, especially in Phoenix where there is no near natural source of water.

3.3.5. High/Low LAD Trees & Fabric Shading Physical Parameters:

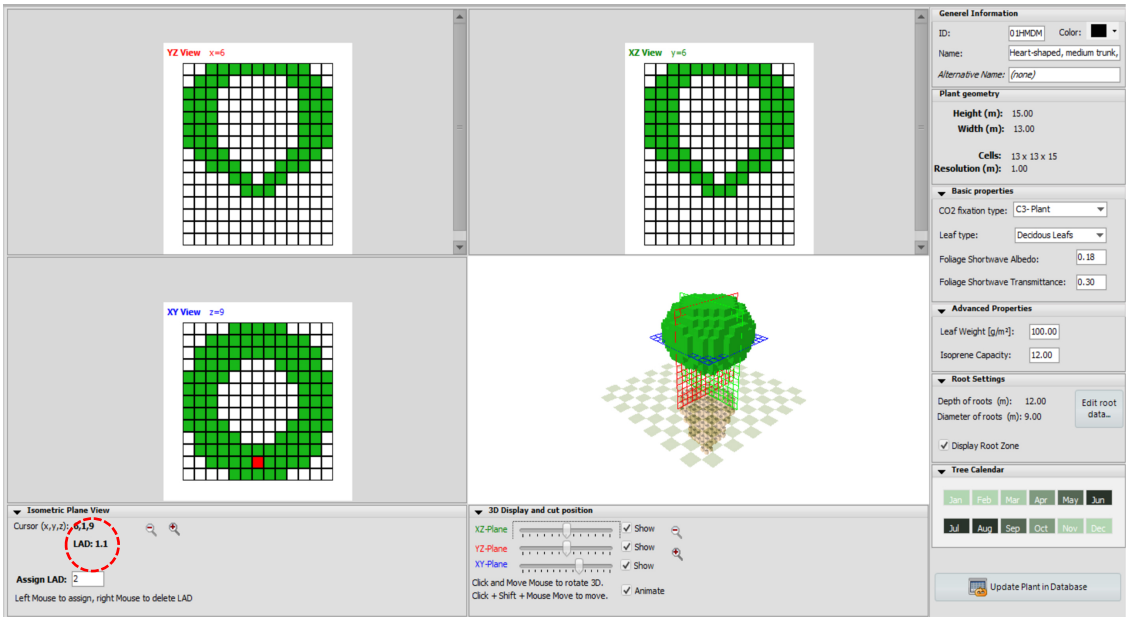

Figure. 3. 9. First tree type, Low LAD trees physical parameters.

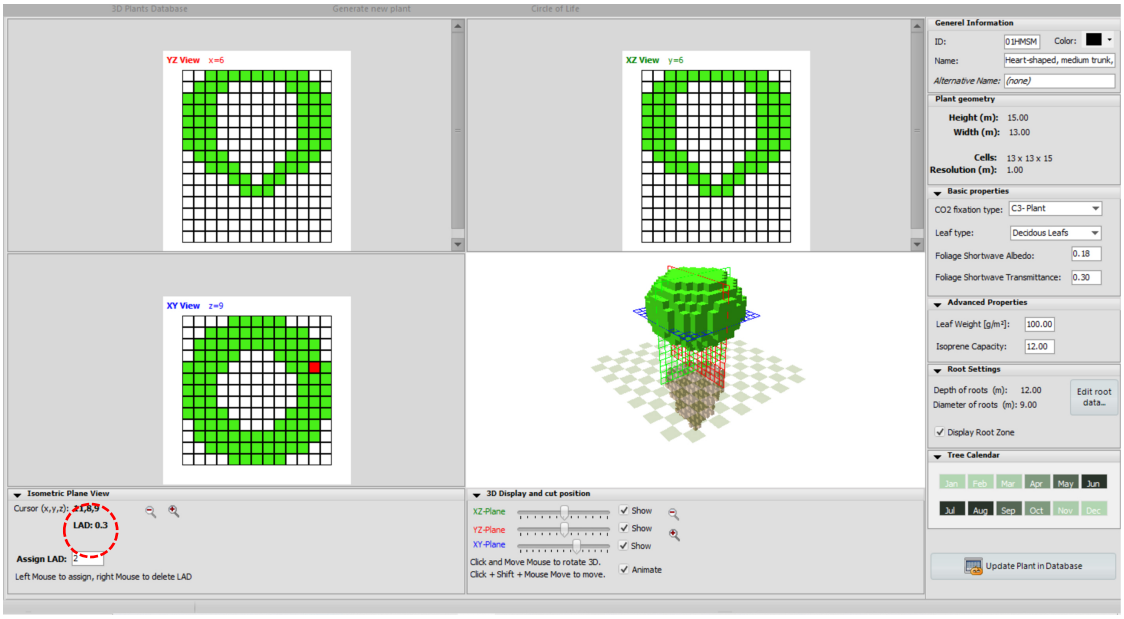

Figure. 3. 10. Second tree type, High LAD trees physical parameters.

Shade type	High LAD Trees	Low LAD Trees	Fabric Shading Devices
Height of tree (m)	15	15	10
Crown diameter (m)	13	13	-
Height under branch (m)	4	4	9
Depth of root (m)	12	12	-
Diameter of root (m)	9	9	-
Leaf albedo	0.18	0.18	0.2
LAI: leaf area index	1	4	-
LAD: leaf area density	0.3	1.1	-
Fabric Transmittance	0.5	0.9	0.2

Table. 3. 1. The physical parameters of the studied trees and fabric shading in ENVI-Met.

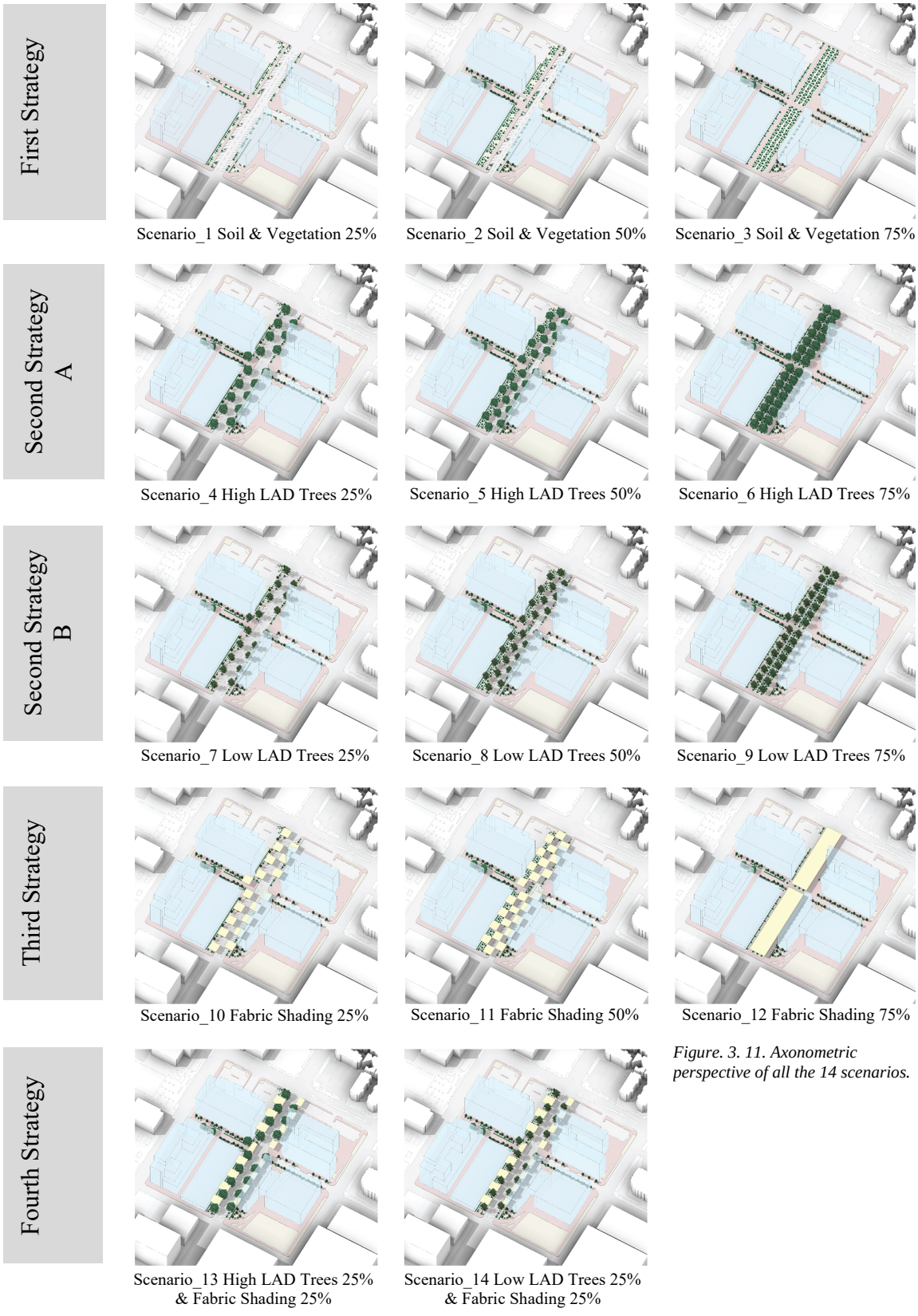

Figure. 3. 11. Axonometric perspective of all the 14 scenarios.

Figure. 3. 13. Top view plan of all the 14 scenarios.

3.4. Data analysis

Four main strategies were simulated, three of which were an evaluation of 12 incremental scenarios, and the fourth strategy proposed two integrated scenarios at the canyon scale in Phoenix, Arizona. The main goal of the simulation was to evaluate the strategy's efficiency of improving the outdoor thermal comfort. To measure the effectiveness of the strategies on pedestrian's comfort level, hourly Mean Radiant Temperatures T_{MRT} at (0.9 m a.g.l) and ground surface temperatures T_{Srf} were extracted from LEONARDO application in ENVI-Met as Excel sheets. Specifically, hourly output of every cell in the studied canyon was obtained. After that, different charts of the data were created to make an analytic evaluation of the results in various data visualizations methodologies. The analysis was based on the cause-effect relationship between different independent variables and a group of dependent variables. The independent variables are the material's thermal properties (permeable & Impermeable), High/Low LAD Trees, and Fabric shading. The dependent variable T_{MRT} at (0.9 m a.g.l) and ground surface temperatures T_{Srf}.

Results are illustrated in three different parts to understand the relationships between the different scenarios for different hours in each scenario, where we could evaluate the performance in higher resolution. The first part involved presenting the results in Line charts of hourly averaged variations for one day and comparing the hourly averaged T_{MRT} at (0.9 m a.g.l) and T_{Srf} for the whole canyon for the scenarios for the same strategies. The second part introduced the four strategies and compared the three scenarios of each strategy by subtracting the scenarios from each other in Area charts for hourly averaged variations for one day. The hourly averaged variations of T_{MRT} at (0.9 m

a.g.l) and T_{Srf} for the whole canyon area were compared. The third part of the analysis looked at the individual strategies in Box & Whisker charts for specific hours and compared the T_{MRT} at (0.9 m a.g.l) and T_{Srf} for the 14 scenarios in one chart for 8:00, 12:00, and 17:00.

Authors Li et al., (2012) presented and explained the Box & Whisker plots, "The box-and-whisker plots were proposed by Tukey in 1977. They are a convenient graphic tool in descriptive analysis to display a group of numerical data through its medians, means, quartiles, and minimum and maximum observations" (Li et al., 2012, p 4). Figure. 3. 15. show the box plot:

> To display the distribution of data, examine symmetry and indicate potential outliers. A box is drawn to represent 50% of the data, where the box's upper boundary represents the upper quartile (Q3) of the data and the lower boundary the lower quartile (Q1). The length of the box represents the interquartile range (IQR). The median (i.e. Q2) is demonstrated by a straight line drawn inside the box, and the mean is marked as a plus (þ) symbol. There are two fences in a box plot. The upper fence is defined as 1:5 × IQR higher than Q3, and the lower fence is defined as 1:5 × IQR lower than Q1. (Li et al., 2012, p 4)

Box & Whisker chart allows us to have a detailed visualization and analysis of a tremendous amount of data sets by dividing the hourly results to 4 Quartiles and a median, where they could be stretched and compressed to show the level of T_{MRT} and T_{Srf} variations in the canyon for every hour.

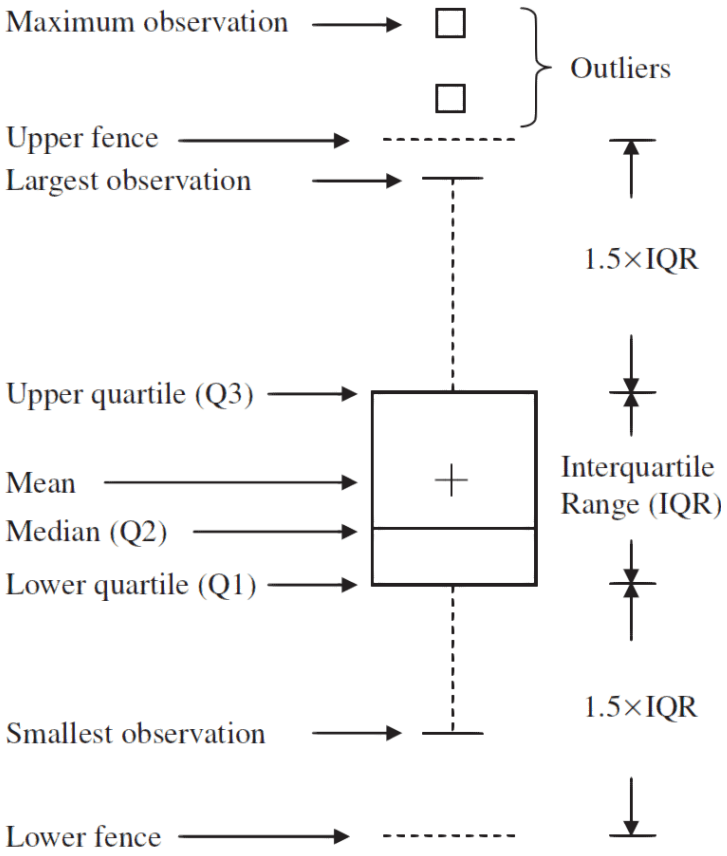

Figure. 3. 15 A distribution is drawn in a box-and-whisker plot (Li et al., 2012).

4. VALIDATION

This study aims to validate a computational fluid dynamics model as it is the first step to evaluate an urban canyon with different mitigation design scenarios and enhance the outdoor thermal comfort on the microclimate scale. The validation process involved applying fully force meteorological conditions and parameters for a specific period of time on the simulation software and then comparing the simulated outcomes with field measurements taken during the same period and getting close results (Maggiotto et al., 2014; Middel et al., 2014). This process usually does not get careful attention from the simulators and causes inaccurate outcomes. Also, as explained by Middel:

> The previous version of the ENVI-met 4.4.3 model does not simulate diurnal cycle for wind or wind direction changes, which would be critical to evaluate for a place with thermal slope valley wind systems such as Phoenix on a diurnal basis. (Middel et al., 2014, p.27)

Moreover, authors like Acero and Arrizabalaga (2016), Buccolieri et al., (2014), and Crank et al., (2018), made systematic review studies comparing the different research results done by using ENVI-met models, and they found that a limited number of researchers validated more than one parameter of the atmosphere. Having a validated computational fluid dynamics model is essential for studying the effects of the modifications and design strategies on the existing urban fabric (Maggiotto et al., 2014; Middel et al., 2014).

In this study, an ENVI-met model used to validate field observations for air temperature (T_{Air}) and the relative humidity (RH) to test the software able to get accurate results. This study evaluated two forcing methods, **full-forcing**, and **simple-forcing** using ENVI-Met software. While the full-forcing method was based on hourly inputs of

variable wind speeds with different directions; on the other hand, the **simple-forcing method** used single averaged wind speed and direction for the whole simulation duration. Note that, up to date, all ENVI-Met forced models validation studies have used a fixed wind speed and wind direction.

ENVI-Met is like any other software, and it has several limitations. Primarily, having a constant wind speed and fixed wind direction for the whole simulation duration, and it is one of the main critics of ENVI-Met, and this is why many scholars have debated on the reliability of ENVI-Met. However, the new version of ENVI-met (V 4.4.4) allows us to account for wind variability, both in terms of speed and direction. The Forcing Manager application within the software could generate files for the full forcing feature based on measured data. Using Phoenix, Arizona as a case study, this part of the study investigates how well a fully forced ENVI-met model that takes wind variability into account, would perform in calculating the T_{Air} and RH values as compared to conventional simple forcing with fixed wind speed and direction.

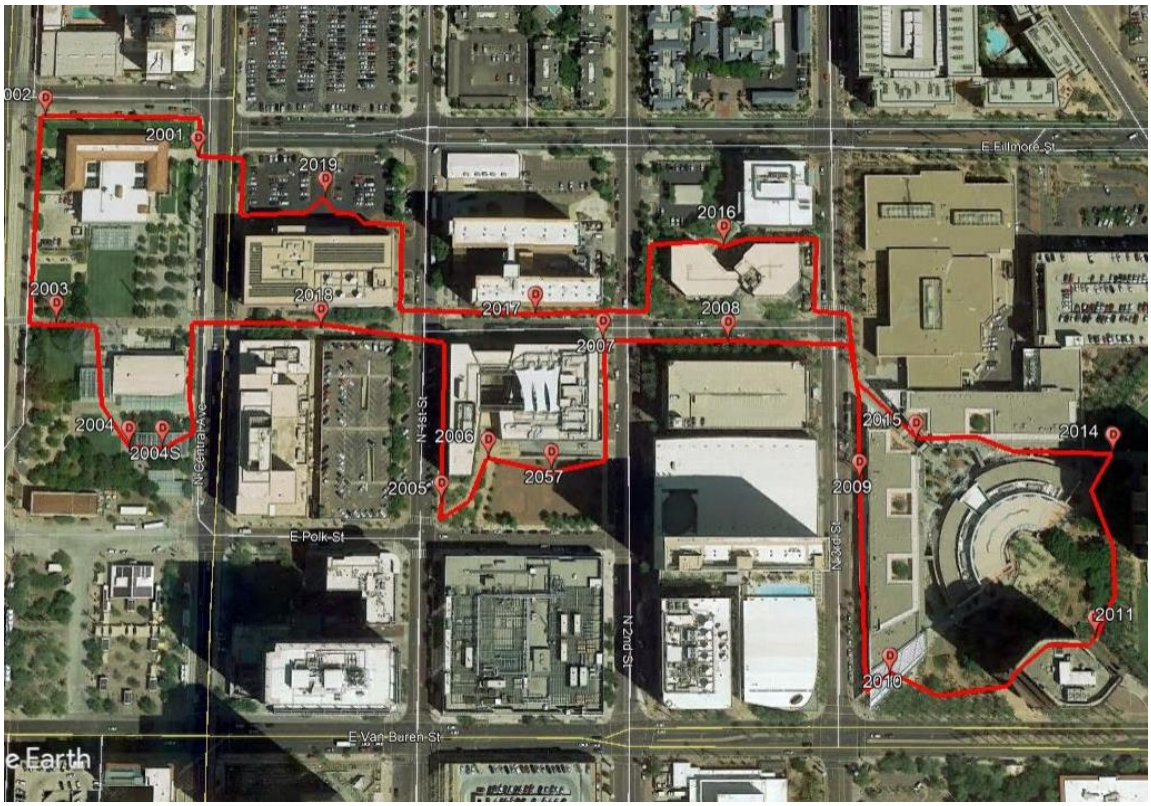

Figure. 4. 1. The field observation locations, Phoenix Downtown, locations: 2018, 2017, 2005, 2006, 2057, and 2019.

4.1. Thermal mapping and data collection

The hourly field measurement campaign was conducted in Downtown Phoenix, Arizona, from 8:00 to 6:00 on July 1, 2019, at Arizona State University's Downtown campus. The field measurements were part of an ongoing research (50 Grades of Shade) and evaluated 19 locations in Downtown Phoenix. Transects of six locations (2018, 2017, 2005, 2006, 2057, and 2019.) across Both North-South and East-West busy pedestrian canyons have been taken as the experimental locations for this study. A mobile human-biometeorological station (MaRTy) used to record the air temperature (1.5-m), relative humidity (1.5-m), 2D wind speed and direction (1.7-m), six-directional radiation flux densities (1.1-m), and GPS location (Middel and Krayenhoff, 2019). Transects were for

six locations in and around the two case study canyon. One location was in the canyon, and five were within the model domain.

4.2. ENVI-Met 4.4 software

Bruse developed ENVI-Met in the 1990s as part of his dissertation in Germany (Bruse and Fleer, 1998). Today it is a widely used Computational Fluid Dynamics (CFD) software, uses RANS equations to calculate the heat energy balance in urban settings and the atmospheric conditions. The software is one of the most straightforward and most used user-friendly in the atmospheric modeling platforms. Since the first release in 1998, the software developed to (V 4.4.4) in 2019 (www. envi-met.com), where it allows several controls for several aspects. For instance, a wide variety of materials and custom materials construction for roofs, walls, payments profiles. Most importantly, a single wall, where it could be used as a horizontal shading device. Also, it allows for unlimited domain range, and different vegetation features, green walls, and roofs. The new feature that we want to test is the effect of forcing weather conditions, such as hourly wind speed and directions.

4.3. Modeling and forcing process in ENVI-Met

An official 2D CAD drawings of the ASU Downtown Phoenix campus and Excel sheets for the building's exact heights were taken from ASU Facilities Management. The drawings were used to generate a 3D Rhino model for the whole campus; after that, the geometry and the properties of the material were exported by using Ladybug Tools to INX file, which used by Spaces in ENVI-Met.

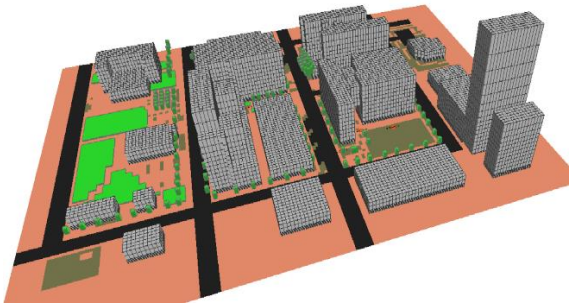

Figure. 4. 2. ENVI-Met model was exported by Dragonfly tool in Grasshopper as INX file to ENVI-Met Spaces.

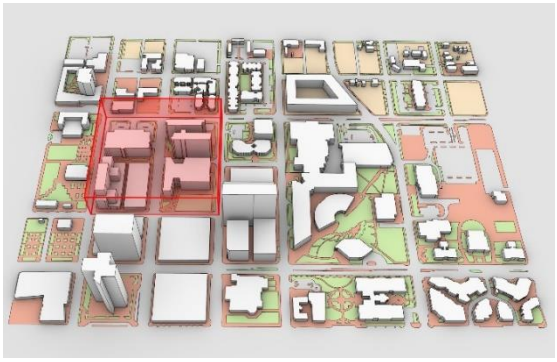

Figure. 4. 3. Rhino 3D model for The City of Phoenix downtown, with exact dimensions and heights from an official CAD drawings ASU facility management.

To make a full forced model, a weather file for the exact observed day was downloaded from mesowest.utah.edu for Phoenix Sky Harbor International Airport, then an average of every half an hour was established for all the 24 hours of the July / 1 / 2019. After that, the Air Temperature, Relative Humidity, wind speed, and direction (the dominant wind speed and direction were taken for every half an hour) and the solar radiation of the City of Phoenix. The second way of forcing was simple-forcing method, where we determine one wind speed and direction and forced the air temperature and relative humidity as we did in the full forcing. The average wind speed in Phoenix Sky Harbor International Airport was found to be 3.5 m/s, and the dominant wind direction was from the south for the whole day.

The model grid size was 3 meters, and the workspace dimensions in ENVI-Met resulted in 157 x 137 x 22 grid cells, a telescoping factor of 19% was used to reduce the Z-axis number of cells and accelerate the simulation run time. Trees, green areas, and materials were observed using Google Street View to determine their locations and magnitude in the modeled domain. The simulation started at 04:00 AM for 26 hours with

constant time steps (2 s) and model output every 60 min; the run time took 65 hours for the full-forcing model and 52 hours for the simple-forcing model.

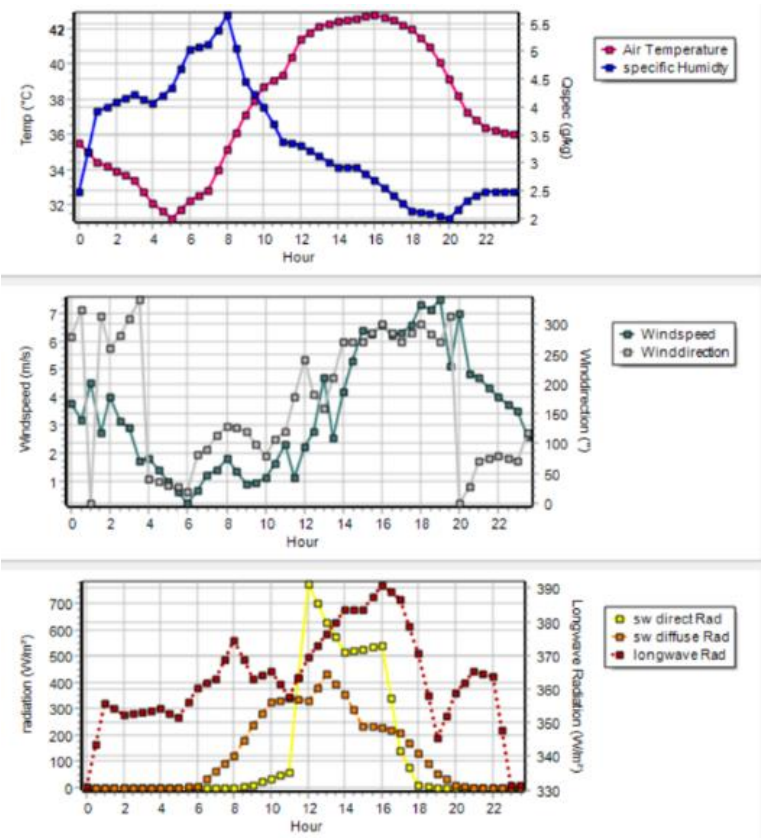

Figure. 4. 4. ENVI-Met Full-forced data, showing the Air temperature, Relative humidity, wind speed and direction, and the direct short-wave and diffused short-wave and long-wave radiations.

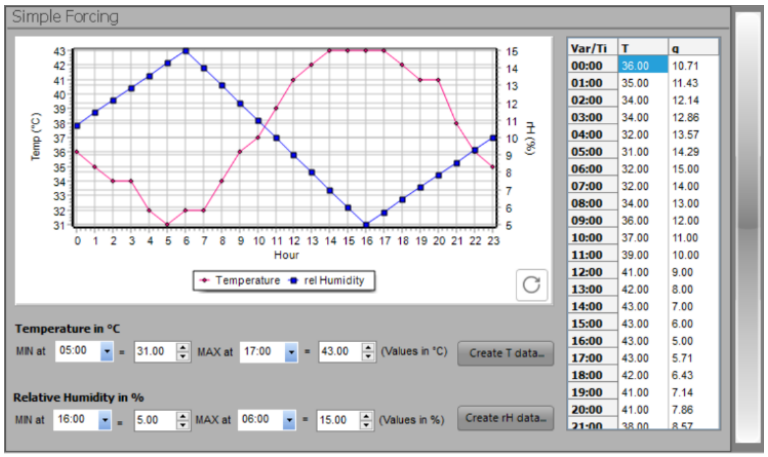

Figure. 4. 5. ENVI-Met Simple-forced data, showing only the air temperature and the Relative humidity.

ENVI-met input parameters for the two forcing scenarios.	Simple Forcing	Full Forcing
Soil data		
Initial temperature, upper layer (0–20 cm) [C]	32	32
Initial temperature, middle layer (20–50 cm) [C]	31	31
Initial temperature, deep layer (>50 cm) [C]	30	30
Relative humidity, upper layer (0–20 cm) [%]	30	30
Relative humidity, middle layer (20–50 cm) [%]	30	30
Relative humidity, deep layer (>50 cm) [%]	30	30
Building data All treatments		
Inside temperature [C]	25	25
Albedo walls [–]	0.3	0.3
Albedo roofs [–]	0.3	0.3
Meteorological data		
Wind speed, 10 m above ground [m s−1]	3.5	varies
Wind direction (0:N, 90:E, 180:S, 270:W) [°]	180	varies
Roughness length at reference point [m]	0.01	0.01
Initial temperature atmosphere [C]	32	32
Relative humidity in 2 m [%]	10	10
Cloud cover [x/8]	0	0

Table. 4. 1. ENVI-Met forced climatic condetions.

Surface type	Material	Albedo
Walls	Default Concrete Wall - Moderate Insulation	0.3
Roofs	Default Concrete Wall - Moderate Insulation	0.3
Paived surfaces	Brik Road (Red Stones)	0.3
Green areas	Grass 25 cm aver. Dense	0.2
Streets	Asphalt Road	0.2
Soils	Defalt Unsealed Soil (Sandy Lome)	0.2
Big Tree	High density 15 m	0.2
Small Tree	Low density 5m	0.2

Table. 4. 2. ENVI-Met materials thermal properties.

4.4. ENVI-Met Validation

The methodology of Willmott (1981, 1982) was used to evaluate the accuracy of the results and calculating the root mean square error (RMSE) and the index of agreement (d) for all of the six study locations. Middel used the same validation evaluation process and described RMSE:

> The RMSE provides insight into the general model performance by measuring the average difference between observed (O) and modeled (P) values, in our case, T2m. The error is further split into a systematic and unsystematic component. The systematic RMSE measures the error introduced by the model design or systematic errors in the initialization values of the model or the observations and should be minimized, while the unsystematic error should approach the overall RMSE. The index of agreement d, ranging from 0.0 to 1.0, is a descriptive measure for model evaluation and measures the degree to which the modeled values are error-free, with d = 1.0 indicating that P equals O. (Middel et al., 2014, p.19)

4.5. Validation results

4.5.1. Air Temperature (T_{Air}) & Relative Humidity (RH) Results

The T_{Air} and the RH values at (0.9 m a.g.l) for both simulated models (simple and full forced) were compared with the observed measurements for 6 locations in the study area. The results for T_{Air} were found acceptable for all locations in the simple forcing model, and for the full-forcing model, were only acceptable for two locations 2006 and 2057 where the d: index of agreement was higher than 0.9. On the other hand, the RH results were acceptable for the simple model in four locations where the d: index of agreement was higher than 0.9, and the full-forcing model did not have an acceptable agreement in all the locations.

The locations of the simple-forcing model where the maximum difference in T_{Air} between the simulated and observed results were at 1.81°C, and the minimum were 0.90°C, and for the RH, the maximum difference between the simulated and observed results were at 1.81%, and the minimum was 0.90%. On the other hand, the Full-forcing model had only two acceptable locations, where the difference between the simulated and the observed values ranged from a maximum of 6.48 % to a minimum of 0.99 %. The methodology of Willmott (1981, 1982) was used to evaluate the accuracy of the results and calculating the root mean square error (RMSE) and the index of agreement (d) for all of the 6 locations for both models as shown in Table. 4.3, and 4.4.

Air T °C Performance	Location 2018		Location 2017		Location 2005		Location 2006		Location 2057		Location 2019	
	Simple Forcing	Full Forcing	Simple Forcing	Full Forcing	Simple Forcing	Full Forcing	Simple Forcing	Full Forcing	Simple Forcing	Full Forcing	Simple Forcing	Full Forcing
MBE	1.51	3.45	1.77	2.94	1.77	2.70	1.05	0.78	0.81	1.39	1.35	3.69
RMSE	1.60	3.69	1.81	3.16	1.81	3.00	1.09	1.19	0.90	1.88	1.42	4.04
MAE	1.51	3.45	1.77	2.94	1.77	2.70	1.05	0.96	0.81	1.41	1.35	3.69
d	0.91	0.72	0.90	0.79	0.90	0.78	0.95	0.95	0.97	0.92	0.92	0.65
MSE_systematic	14.65	14.65	14.71	15.34	14.71	14.71	14.74	14.74	15.00	16.02	14.40	14.40
MSE_unsystematic	6.13	1.77	4.51	1.78	4.51	3.09	7.93	9.76	9.37	8.29	6.46	2.78
RMSE_systematic	3.83	3.83	3.84	3.92	3.84	3.84	3.84	3.84	3.87	4.00	3.79	3.79
RMSE_unsystematic	2.48	1.33	2.12	1.33	2.12	1.76	2.82	3.12	3.06	2.88	2.54	1.67

Table. 4. 3. Air Temperature simulated results: MBE: mean bias error; RMSE: root mean square error; MAE: mean absolute error; d: index of an agreement; MSE: mean square error.

Relative Humidity	Location 2018		Location 2017		Location 2005		Location 2006		Location 2057		Location 2019	
	Simple Forcing	Full Forcing	Simple Forcing	Full Forcing	Simple Forcing	Full Forcing	Simple Forcing	Full Forcing	Simple Forcing	Full Forcing	Simple Forcing	Full Forcing
MBE	-1.96	-8.06	-6.43	7.58	1.88	7.54	1.50	7.54	0.78	6.84	0.91	7.31
RMSE	2.65	8.16	6.48	7.68	2.18	7.62	1.79	7.60	0.99	6.91	1.36	7.39
MAE	2.02	8.06	6.43	7.58	1.88	7.54	1.52	7.54	0.84	6.84	1.12	7.31
d	0.88	0.54	0.70	0.57	0.92	0.58	0.93	0.55	0.98	0.64	0.96	0.61
MSE_systematic	0.49	0.49	0.30	1.98	0.38	1.89	0.31	1.88	0.33	1.87	0.28	1.98
MSE_unsystematic	9.73	67.90	37.86	80.77	5.77	78.64	3.79	78.43	1.63	67.10	1.97	75.67
RMSE_systematic	0.70	0.70	0.54	1.41	0.62	1.38	0.56	1.37	0.57	1.37	0.53	1.41
RMSE_unsystematic	3.12	8.24	6.15	8.99	2.40	8.87	1.95	8.86	1.27	8.19	1.41	8.70

Table. 4. 4. Relieve Humidity simulated results: MBE: mean bias error; RMSE: root mean square error; MAE: mean absolute error; d: index of an agreement; MSE: mean square error.

Overall the simple forcing model predictions were acceptable in T_{Air}, with RMSE (root mean square errors) less than 1.81 °C on all of the six locations. For the RH variable, three locations had RMSE were less than 2.0 % (locations 2006, 2057, and 2019,) also the d index (i.e., index of agreement) of agreement was higher than 0.9 for

four locations (2005, 2006, 2057, and 2019). On the other hand, the full-forced model predicted acceptable T_{Air} values in only for two locations out of six locations (2006 and 2057) with the, same locations also showing a value of d variable higher than 0.9.

The simple-forcing model had the lowest T_{Air} *d* of 0.90 in location 2017, and the highest RMSE (overall: 1.81°C; systematic: 3.84°C; unsystematic: 2.12°C) of all of the locations. We note that the lowest T_{Air} d for the full forcing model was 65 in location 2019 and the highest RMSE (overall: 4.04°C; systematic: 3.79°C; unsystematic: 1.67°C). Eventfully, the location itself will have its unique characteristics, and if it was protected from the wind or not, this is the reason that the full forcing model performed better only in two locations 2006, and 2057 due to the special location characteristics. In the simple forced model, the locations 2006, and 2057 had a slightly higher d value, and that could be for the same reason, i.e., the locale location characteristics helped to have higher validation values. In general, we could conclude that the simple forcing model had higher accuracy in all locations and it is closer to the observed values than the full forcing model.

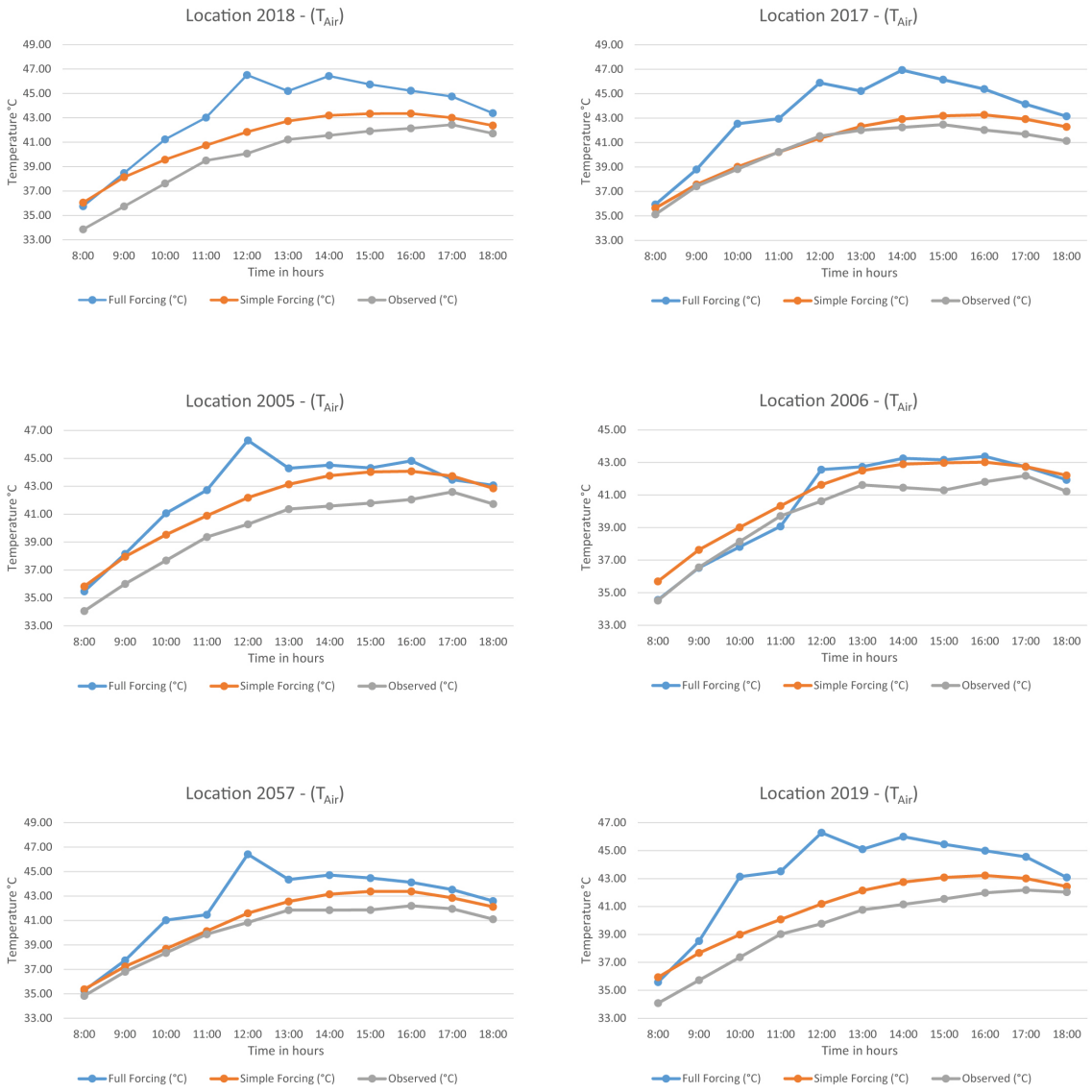

Figure. 4. 6. The results of Air Temperature from the full forcing and simple forcing models compared with the observed measurements on (0.9 m a.g.l) of the same duration time of the observed time.

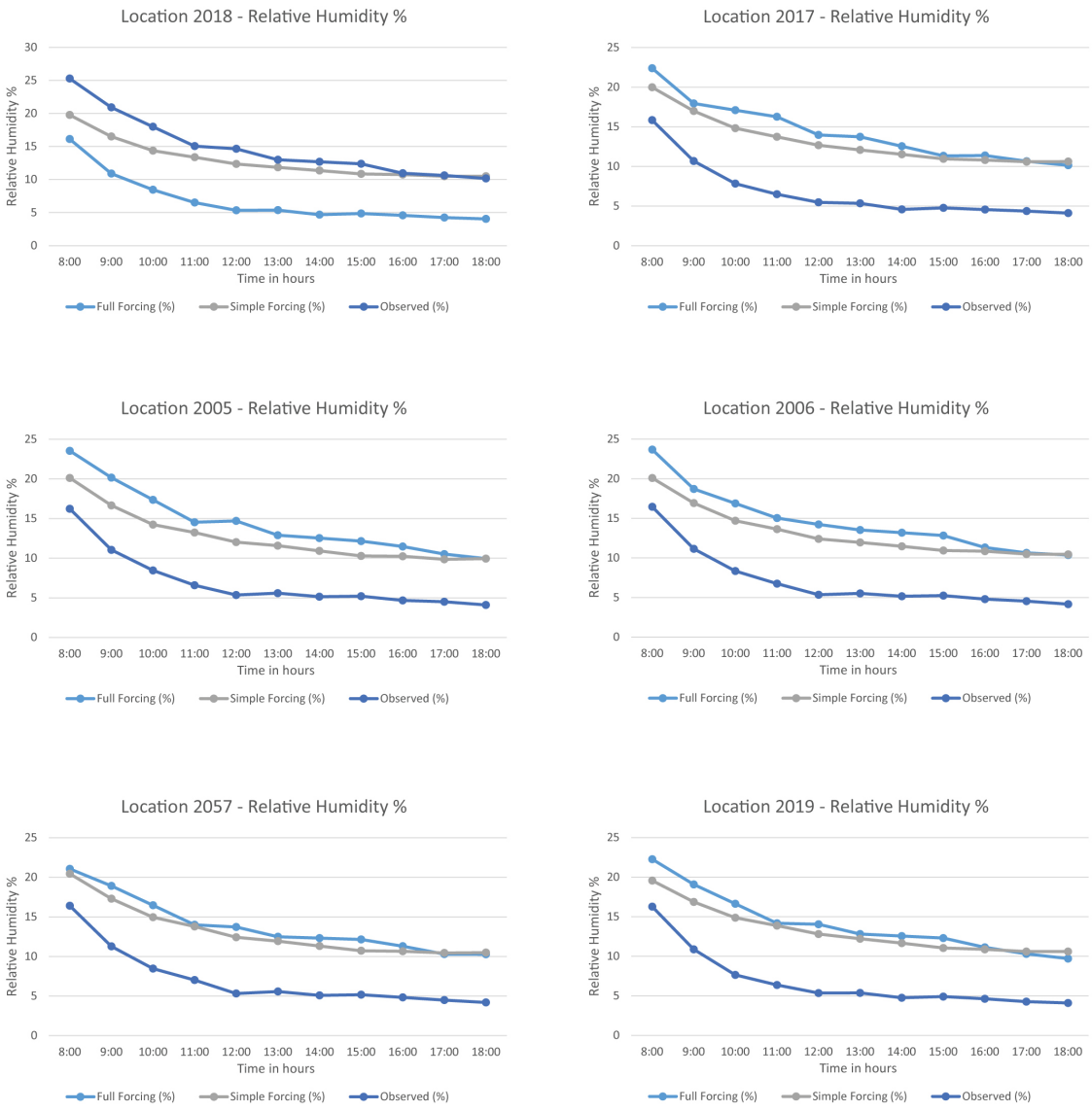

Figure. 4. 7. The results of the Relative Humidity from the full forcing and simple forcing models compared with the observed measurements on (0.9 m a.g.l) of the same duration time of the observed time.

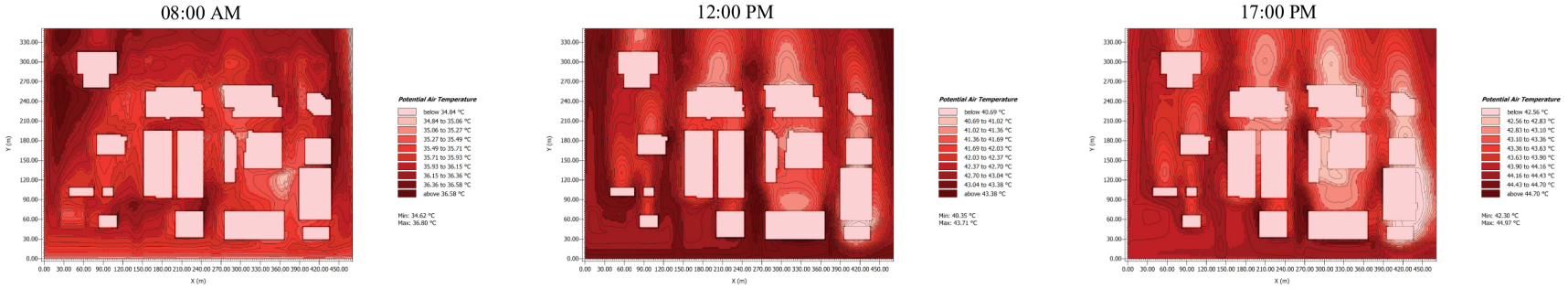

The results of Air Temperature from of the simple forcing on (0.9 m a.g.l).

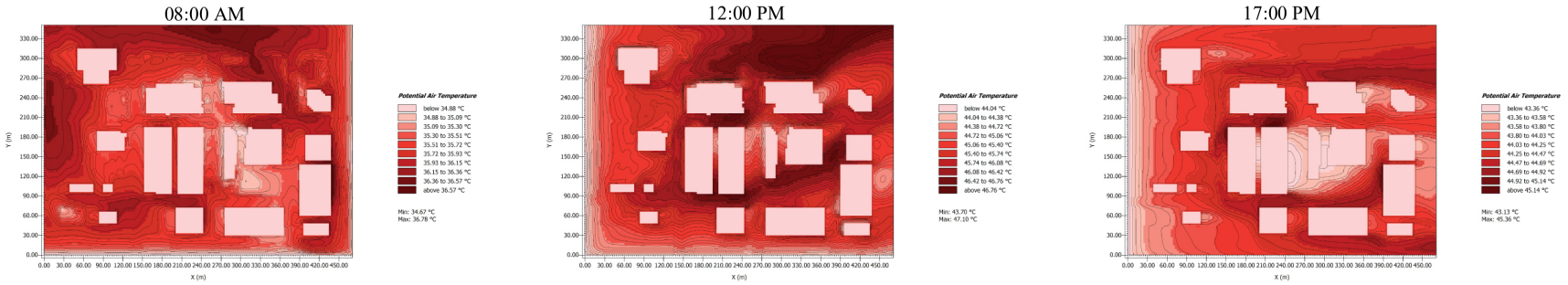

The results of Air Temperature from of the full forcing on (0.9 m a.g.l).

Figure. 4. 8. The results of Air Temperature from of the full & simple forcing models on (0.9 m a.g.l).

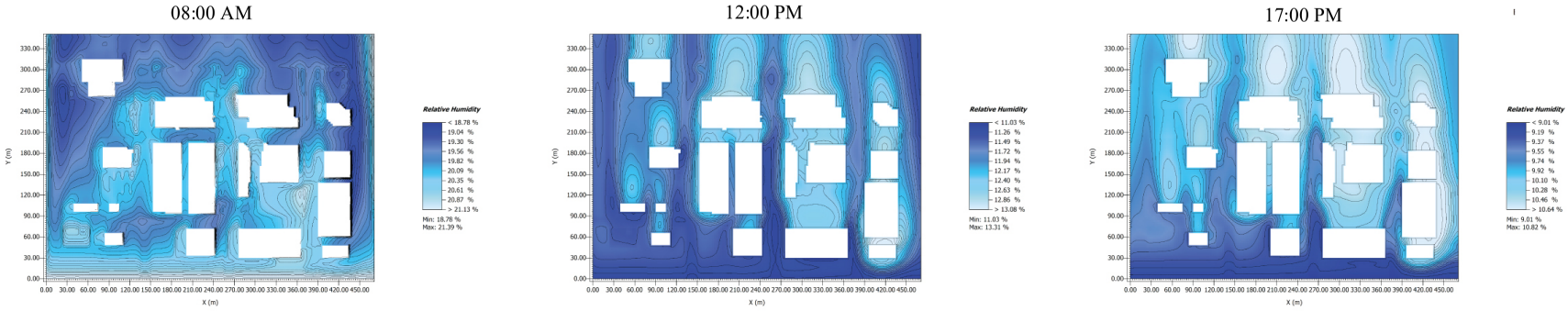

The results of Relative Humidity from of the simple forcing on (0.9 m a.g.l).

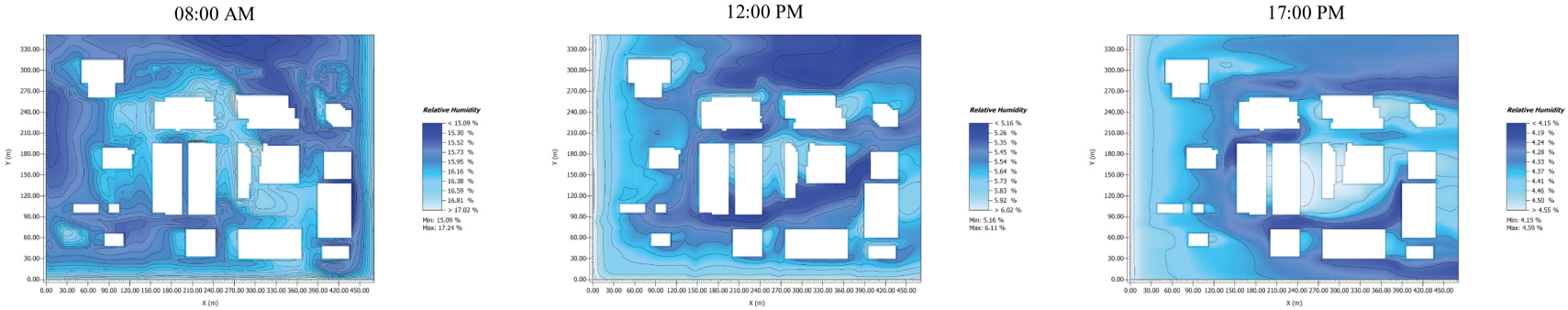

The results of Relative Humidity from of the full forcing on (0.9 m a.g.l).

Figure. 4. 9. The results of Relative Humidity from of the full & simple forcing models on (0.9 m a.g.l).

The modeling approach involving the full forcing model some extra refinements, some parameters may be interacting, and also ENVI-Met may have some embedded calculations to keep things in line and cap some parameters to specific limits. For example, forcing air temperature, then the relative humidity could change some of the air temperature parameters due to the unknown back calculations that the ENVI-Met does to the input parameters. Also, the other way around it does change some of the relative humidity parameters, which makes it hard to force the exact weather conditions on two different models with simple and full forcing. The unstable parameters goes back to the ENVI-Met being a black box, and it is hard to make sure if the parameters that we inputted will not change slightly or affecting other parameters. We can see the full forced model in Figure. 4.8. and 4.9., it has inconsistent air temperature at (0.9 m a.g.l), this is because of the changing wind speeds and directions.

However, because of the unknown exact inputted values and how the model interprets the input weather conditions in ENVI-Met, it is harder for researchers to get closer results to the observed measurements in the full-forced model. Comparing figures. 4.8. and 4.9., we note that the wind effect on air temperature behavior at (0.9 m a.g.l) for both the simple and full-forced models during the whole observation hours. Figure. 4.8. shows the simple-forced model having a consistent fixed south wind for the whole run duration, and explains why we notice cooler areas for the whole simulated duration on the north side of most buildings where they were protected from the advection heat waves. Even though the validation results for the simple-forced model were closer to the observed, the behavior of the lateral boundary conditions is somewhat misleading. The heat sources in the model radiated their heat toward the north by advection effect due to

the fixed wind speed and direction, and the buildings are blocking wind flow which created small cool islands on the north side of most buildings for the whole simulation duration. The wind behavior in the simple forcing model was not realistic, due to the variation of wind flow in actual cases, and this confusion could cause wrong decisions from the designers and policymakers. On the other hand, if we compare the simple and full forced models results in Figure. 8, we can see that the north area of most buildings on the full forced model were not the coolest. Consequently, the heat source locations were changed, and the variation in wind direction caused an advection loses from different sides. Wind transferred the heat from and to different locations in the full-forced model according to the wind direction and speed, where they were shown the coolest in the simple-forced model, namely north sides of the buildings.

The simulation results, as shown in Figure. 4.6. and 4.7. of T_{Air} and RH for both simple and full forced models were in high agreement overall for the simple forcing, and only partly acceptable for the full forcing compared to the observed in the early morning, while they overestimated mid-afternoon and late afternoon. These findings are similar to a validated study using ENVI-Met in the Phoenix metropolitan area done by Middel et al. (2014). On the other hand, other validation study used ENVI-Met in Downtown Phoenix, reported an overestimation during the morning time and underestimation of T_{Air} in mid-afternoon and late afternoon (Emmanuel & Fernando, 2007).

4.5.2. Mean Radiant Temperature (T_{MRT}) results

Figure. 4. 10. The author Abdullah Aldakheelallalh during the field measurements at Arizona State University Downtown campus, with the mobile human-biometeorological station (MaRTy).

In this study, field measurements were taken by a mobile human-biometeorological station (MaRTy), designed and assembled by Ariane Middel (Middel and Krayenhoff, 2019). (MaRTy) measures the six-directional radiation flux densities (S_{str} 1.1-m) of shortwave and longwave radiations. (MaRTy) calculate Mean Radiant Temperature (T_{MRT}), by collecting the directional radiation measurements then multiplied them by a weighting factor F_i (i = 1–6) that represents the shape of the human body, as illustrated in Equation. 4.1 (VDI, 1994). To mimic the standing or walking human body, F_i will have a 0.22 magnitude of the radiation flux from the four main orientations: North, South, East, and West). The weighting of the radiation flux from below and above is 0.06. Knowing F_i (T_{MRT}) can be calculated via Stefan–Boltzmann law in Equation. 4.2 (Thorsson et al., 2007).

$$S_{\mathrm{str}} = \alpha_k \sum_{i=1}^{6} K_i F_i + \varepsilon_p \sum_{i=1}^{6} L_i F_i$$

Equation. 4. 1. Mean Radiant Flux Density, where:
Ki = the short-wave radiation fluxes (i = 1–6).
Li = the long-wave radiation fluxes (i = 1–6).
Fi = weighting factors for a standing person (i = 1–6).
αk = the absorption coefficient for short-wave radiation (standard value 0.7).
εp = the emissivity of the human body. According to Kirchhoff's laws εp is equal to the absorption coefficient for long-wave radiation (standard value 0.97).

$$T_{\mathrm{mrt}} = \sqrt[4]{\left(S_{\mathrm{str}} / \left(\varepsilon_p \sigma\right)\right)} - 273.15$$

Equation. 4. 2. Stefan–Boltzmann law, where:
σ = the Stefan–Boltzmann constant ($5.67 \cdot 10^{-8}$ Wm^{-2} K^{-4})

Moreover, it is important to explain how ENVI-Met calculates T_{MRT}. ENVI-Met uses a cylindrically shaped body to represent the human body in every grid cell (z) and calculates T_{MRT} from longwave as well as direct and diffuse shortwave radiation, as illustrated in Equation.3 (Bruse, 1999).

$$T_{mrt} = \left[\frac{1}{\sigma_B} \left(E_t(z) + \frac{\alpha_k}{\varepsilon_p} \left(D_t(z) + I_t(z) \right) \right) \right]^{0.25}$$

Equation. 4. 3 ENVI-Met Mean Radiant Temperature equation where:
Et (z) = Total longwave radiation fluxes.
Dt (z) = Diffuse and diffusely reflected solar radiation.
It (z) = Direct solar radiation fluxes.

At the canyon level, ENVI-Met calculates longwave radiation emitted from the ground surfaces and the surrounding environment (e.g., buildings, trees) using an upper and lower hemisphere (Ali- Toudert, 2005; Huttner, 2012). Acero & Herranz-Pascual (2015) reported that ENVI-Met overestimates (T_{MRT}). To minimize this bias, this study takes the ENVI-Met (T_{MRT}) for the base case scenario and calculates the difference in T_{MRT} for each shading and heat mitigation strategy. Investigating the data set of a

previous (MaRTy) study (Middel and Krayenhoff, 2019), the daytime difference between observed T_{MRT} under a shade structure and a sun-exposed location ranged between 15 to 22 °C. The results of this study, which will be presented in chapter.5, show a difference ranging from 16 to 18°C between the shaded and exposed surfaces in ENVI-Met the simulated models. Although ENVI-Met tends to overestimated T_{MRT} results, it had shown an acceptable agreement of the T_{MRT} degree reduction with the observed data set. As will be shown in the results section, ENVI-Met is able to produce T_{MRT} reduction ranges despite overestimating absolute magnitudes of T_{MRT}. Therefore, this study will use T_{MRT} differences and not magnitudes as a target goal for the strategies.

Line charts are presented in Figure. 4.13. Comparing the hourly observed and simulated T_{MRT} results for the six validation study locations using simple and full-forcing. We note that ENVI-Met overestimated T_{MRT} by 13.35 °C on average for all hours and locations. However, although the average difference between the simple and full-forcing model was in about 2 °C, the full-forcing model had hourly changed in wind speed and direction, and the wind variability had a direct effect on T_{MRT}. Having variable wind speed and direction is essential to T_{MRT}, due to its sensitivity to the local climatic conditions. Dynamic hourly wind directions will improve advection modeling from surrounding buildings and paved surfaces that function as heat sources. In the following section, after successful validation of the model, this study will adjust the thermal

properties of the paved ground surfaces and add green spaces, trees, or shading devices to investigate heat mitigation impacts.

Figure. 4. 11. The results of the Mean Radiant Temperature from the full forcing and simple forcing models compared with the observed measurements on (0.9 m a.g.l) of the same duration time of the observed time.

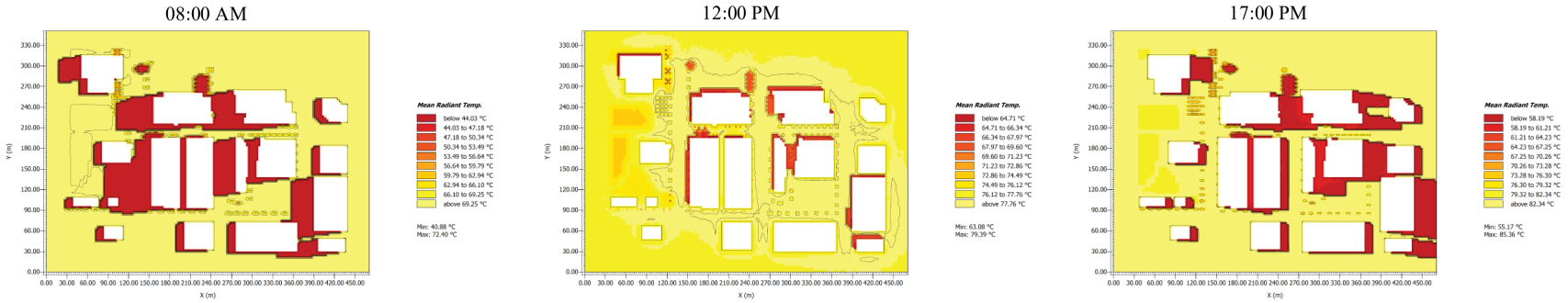

The results of the Mean Radiant Temperature from of the simple forcing model on (0.9 m a.g.l).

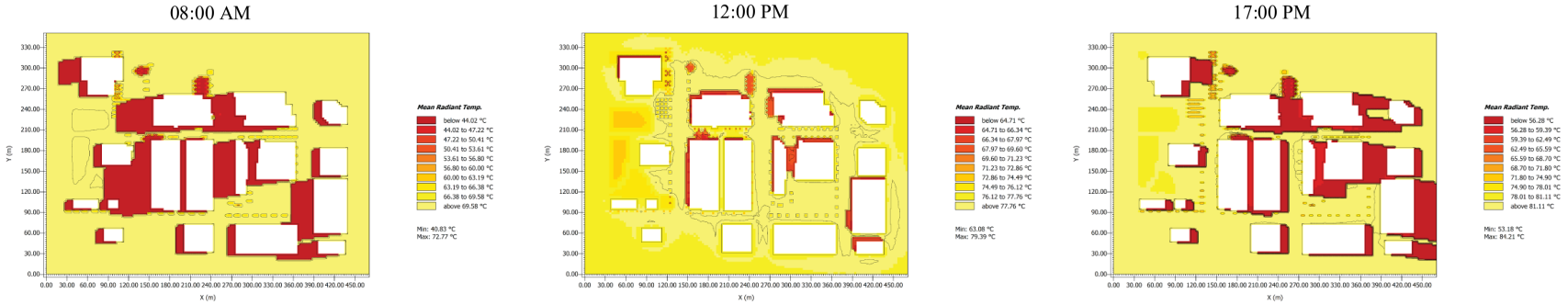

The results of the Mean Radiant Temperature from of the full forcing model on (0.9 m a.g.l).

Figure. 4. 12. The results of the Mean Radiant Temperature from of the full and simple forcing model on (0.9 m a.g.l).

4.6. Validation Conclusion

The results show that both models could be deemed valid with acceptable accuracy. Although, the simple forcing model did slightly better than the full forcing in four locations for the T_{Air}, and that goes to the way that ENVI-Met applies the forced data. However, we could say that previous studies which used the simple forcing in ENVI-Met with one wind speed and direction could be close to the results of the full forcing model. Thus they could be assumed to be credible. There are some unclear results that came from the full-forcing model, and it will be hard to figure them out without knowing how exactly ENVI-Met applies the forcing parameters n its computational algorithm.. It is clear that the air temperature T_{Air} and RH (at 0.9 m a.g.l) have shown more realistic lateral boundary conditions behavior in the full-forcing model, where they were sensitive to the wind speed and direction changes.

The full-forced model is essential to studies where the T_{MRT} results are the focus since local wind conditions are applied in higher resolution, and they help increase or decrease the T_{MRT} drastically on the pedestrian level at (0.9 m a.g.l). On the other hand, air temperature is not as sensitive to wind variation in speed and direction as the T_{MRT}, the air temperature has more resistance than T_{MRT} on the microclimate scale. For that reason, if the goal is to improve the T_{MRT} in the outdoor space on a microscale level, wind speed and direction are critical for getting an accurate, validated model to be the start for different enhanced T_{MRT} scenarios. The realistic wind behavior could be used as an urban heat mitigation design strategy to improve the thermal performance in the outdoor spaces; it will only be effective if the designer had an accurate lateral boundary configuration of the simulated model.

Simple forcing results could be close to the observed measurements if they were taken on calm weather conditions, where the wind variability is not effective. Oke described in his Initial Guidance to Obtain Representative Meteorological Observations at Urban Sites the right techniques to take field observations for urban climate studies (Oke, 2016). One critical step is to choose a day with a clear sky and calm wind to take the field observations. In this way, we validate the observed results by using the simple forced model. Today, we can use the full-forced model to validate a windy day and test the outdoor thermal comfort for different urban arrangements in extreme conditions, but it is important to choose the right locations and have them spread on the study area so that the inaccuracy of the validation a could be determined and evaluated. With that being said, ENVI-Met is still a user-friendly software that helps the designer to make fast decisions on the early design stages. Knowing how to get accurate results by taking decent measurements and validating the model with more than one location will facilitate having an accurate validate model.

5. STRATEGIES EVALUATION & RESULTS ANALYSIS

In this chapter, simulation results were analyzed for all the four strategies and the different scenarios by comparing their performance of improving the outdoor thermal comfort and participation on the pedestrian's level for North-South urban canyon in Downtown Phoenix, Arizona. The pedestrian's thermal comfort is correlated mainly to the Mean Radiant Temperature T_{MRT} as explained earlier in Chapter 2, the ground T_{Srf} is in a close distance to the pedestrians, and the reflected and radiated shortwaves and longwave radiation will be essential to pedestrians comfort (Cook 2001, Rosheidat 2014, Rowe 1991). For that reason, this study will present the findings of the T_{MRT} and T_{Srf} as the main outputs of the different simulated scenarios to evaluate their performance and the potential thermal comfort enhancements. The results were presented in three main parts; the first part looked at the hourly average T_{MRT} at (0.9 m a.g.l) and T_{Srf} variations for the whole canyon area, and grouped all the scenarios of each strategy together in one Line chart so they could be more easily compared. The second part presented area charts of hourly average T_{MRT} at (0.9 m a.g.l) and T_{Srf} results in two different groups. Group A, was by subtracting the incremental shading factor scenarios from each other in each strategy, where we can see how much in degrees did each scenario performed compared to the other scenarios in the same strategies. Group B, was by subtracting scenarios with the same shading factor from each other through all the design strategies, where we could compare the performance of each strategy in different shading factors. The last part presented the use of the Box & Whisker charts also, but for specific hours 8:00 , 12:00, and 17:00 and comparing all the scenarios from different strategies so as to get a better understanding of the strategy's performance relative to the other scenarios.

5.1. First Part

This part of the analysis involving the four strategies and compared the three scenarios of each of strategy by presenting the results in Line charts of hourly averaged variations of the whole canyon area for T_{MRT} at (0.9 m a.g.l) and T_{Srf} in one day duration,

5.1.1. First Strategy, Scenarios_1, 2, and 3 Soil & Vegetation

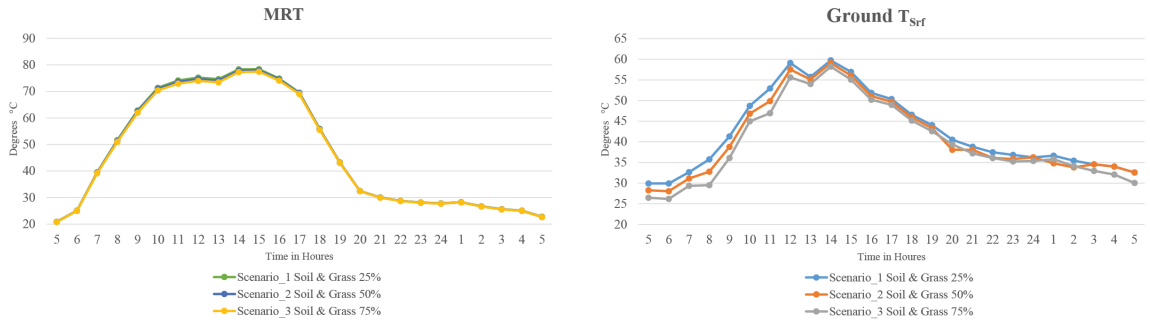

Figure. 5. 1. Hourly average results of (T_{MRT}) at (0.9 m a.g.l) and (T_{Srf}) for all the canyon area.

Hourly averaged variations of the whole canyon area for T_{MRT} at (0.9 m a.g.l) and T_{Srf} are plotted in Figure. 5. 1. for the duration of the day. The results showing the different levels of variation indicate that the T_{MRT} in all three scenarios were almost typical (i.e the effect of removal of all shading devices and trees in scenarios 1, 2, and 3). The ground surface was exposed to the direct solar radiation in the day time and had the maximum sky view factor possible at the night time. The variations between the different scenarios were slightly increased after the 9:00 and decreased after 17:00. Scenario 1 had the maximum T_{MRT} at 14:00 with a magnitude of 74.8 °C, and for scenarios 2 and 3 were 74.5 °C, 74.1 °C, respectively. On the other hand, the results of T_{Srf} varied in the different scenarios; the variations increased in the night time and the first half of the day time until

noon, where scenario 3 had the coolest surface temperatures at a magnitude of 5:00 AM with a magnitude of 26 °C. The variations decreased after 12:00 and the results were close and the variation started to increase again after 20:00, and the hottest surface temperatures was for scenario 1 at 12:00 with a magnitude of 59°C.

5.1.2. Second Strategy-A, Scenarios 4, 5, and 6, High LAD Trees

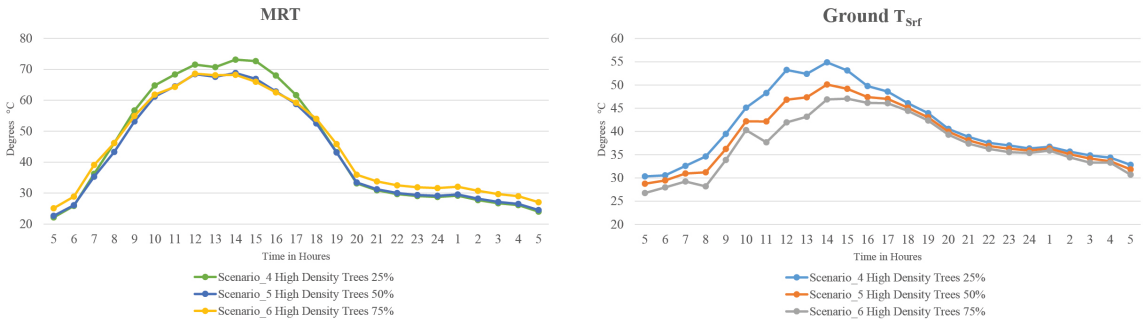

Figure. 5. 2. Hourly average results of (T_{MRT}) at (0.9 m a.g.l) and (T_{srf}) for all the canyon area.

Hourly averaged variations of the whole canyon area for T_{MRT} at (0.9 m a.g.l) and T_{srf} are plotted in Figure. 5. 2. for the whole day duration. The results relate to different levels of variations, and indicate that the variations for scenarios 4 and 5 were at their lowest in early morning hours at 5:00 AM for T_{MRT} at a magnitude of 22.1 °C, 22.6 °C and for the T_{srf} had a magnitude of 30.3 °C, 28.7 °C respectively. After that, results started to vary from 7:00 until 18:00 where they became closer. On the other hand, scenario 6 had a the lowest T_{MRT}, T_{srf} in the early morning at 5:00 with a magnitude of 25.1°C, 26.7°C respectively, due to the high number of trees in the canyon which reduces the sky view factor and the rate of radiation loss and the energy that was stored in the canyon. The highest results between the all scenarios were for Scenario 4, where it had

the maximum T_{MRT}, T_{Srf} at 14:00 with a magnitude of 73.1 °C, 54.8 °C respectively, and the maximum T_{MRT}, T_{Srf} results were for scenario 5 were 68.7 °C, 50.1 °C respectively. Scenario 6 had the coolest T_{MRT}, T_{Srf} results at 14:00 in the afternoon time with 68.2 °C, 46.8 °C, respectively. For scenarios 5 and 6, the variation in the results were close for most of the nighttime, unlike scenario 6, the results show a hotter average of 2 °C degrees for most of the night time compare to other scenario.

5.1.3. Second Strategy-B, Scenarios 7, 8, and 9, Low LAD Trees

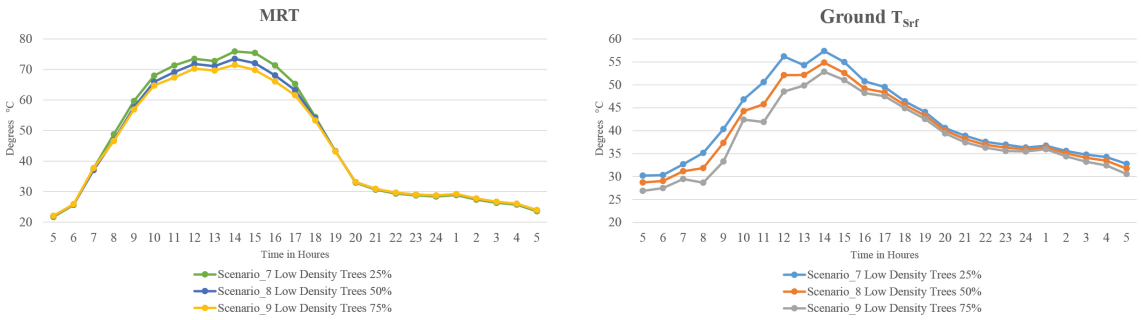

Figure. 5. 3. Hourly average results of (T_{MRT}) at (0.9 m a.g.l) and (T_{Srf}) for all the canyon area.

Hourly variations of the whole canyon area for T_{MRT} at (0.9 m a.g.l) and T_{Srf} were plotted in Figure. 5. 3. For the whole day duration, the results show different levels of variations, where the variations for all the scenarios were low and almost typical T_{MRT} and had virtually 2 °C difference for T_{Srf} from early morning until 8:00, the coolest T_{MRT}, T_{Srf} were at 5:00 with a magnitude of 21.6 °C, 30.2 °C. After that, the variations increased relatively for T_{MRT} and more noticeable for the T_{Srf} from 8:00 for all the scenarios to 18:00 where the variations were at their lowest through the night time. Scenario 7 had the maximum T_{MRT}, T_{Srf} at 14:00 with a magnitude of 75.8 °C, 57.3 °C

due to the low LAD and number of trees in the canyon which allowed relatively more solar radiation to go through to the canyon ground surface than the Second strategy A. For Scenarios 8, and 9 they had lower T_{MRT}, T_{Srf} at 14:00, where they had a maximum T_{MRT} with a magnitude of 73.5 °C, 71.4 °C respectively, and had a maximum T_{Srf} with a magnitude of 54.8 °C, 52.8 °C. This was mainly because of the increased number of trees that reduced the access of the direct solar radiation to the canyon in the day time.

5.1.4. Third Strategy, Scenarios 10, 11, and 12, Fabric shading

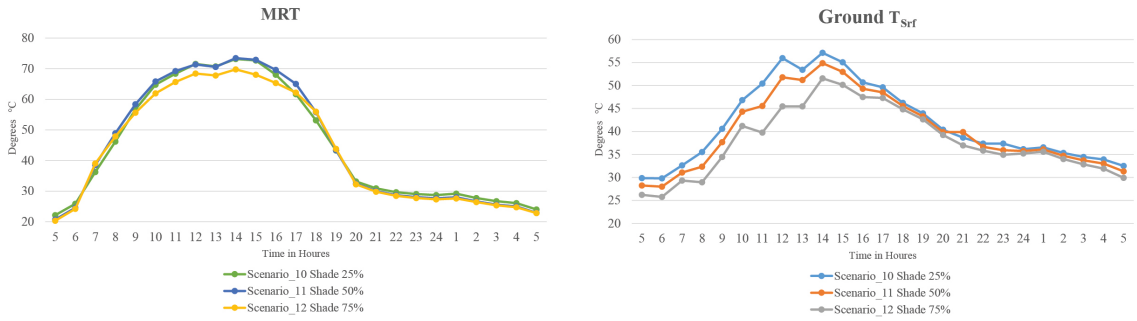

Figure. 5. 4. Hourly average results of (T_{MRT}) at (0.9 m a.g.l) and (T_{Srf}) for all the canyon area.

Hourly variations of the whole canyon area for T_{MRT} at (0.9 m a.g.l) and T_{Srf} are plotted in Figure. 5. 4. For the whole day duration, the results were showing different levels of variations, where the variations for all the scenarios were low in the early morning until 8:00, the coolest T_{MRT}, T_{Srf} at 5:00 were with a magnitude of 20.3 °C, 26.2 °C. After that, the variations increased relatively for T_{MRT} and more considerably for the T_{Srf} from 8:00 for all the scenarios to 18:00 where the variations were at their lowest through the night time. Scenario 10 had the maximum T_{MRT}, T_{Srf} at 14:00 with a magnitude of 75.7 °C, 57.1 °C due to the low fabric configuration shading factor of 25%

and fabric transmittance of 20% in the canyon which allowed the solar radiation to go through to the canyon ground surface more than the Second strategy A and B. Scenario 11, and 12 had lower T_{MRT}, T_{Srf} at 14:00, where they had a maximum T_{MRT} of 73.4 °C and 69.6 °C respectively, and T_{Srf} at 14:00 where they had a maximum magnitude of 54.4 °C and 51.1 °C respectively. This was due mainly because of the increased shading factor of the fabric shading that reduced the direct solar radiation access to the canyon.

5.1.5. Fourth Strategy, Scenarios 13, and 14, High & Low LAD Trees & Fabric shading

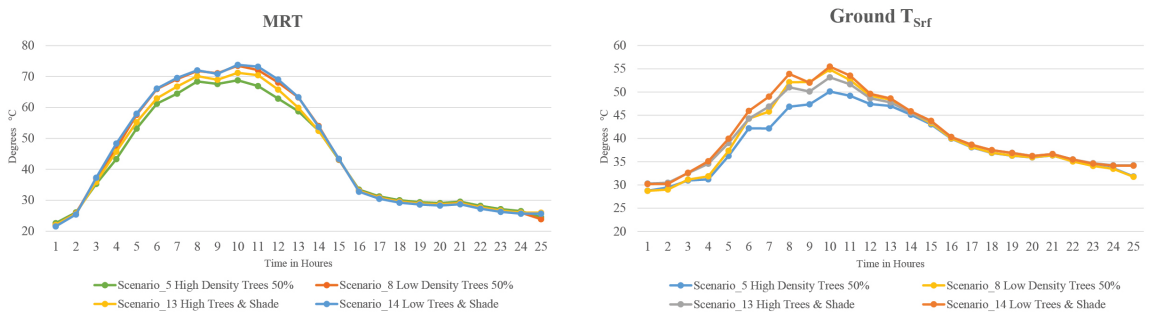

Figure. 5. 5. Hourly average results of (T_{MRT}) at (0.9 m a.g.l) and (T_{Srf}) for all the canyon area.

Hourly averaged variations of the whole canyon area for T_{MRT} at (0.9 m a.g.l) and T_{Srf} illustrated the fourth strategy on a Line chart in Figure. 5.1f. for the whole day duration, the results show different levels of variations, where the variations for all the scenarios were low in the early morning until 7:00 AM. Then the variations increased from 8:00 AM for all the scenarios to 18:00 where the variations were at their lowest through the night time. In this chart, Figure. 4.1f Scenarios 4, 7, 13, and 14 were compared so as to evaluate the performance of the different trees scenarios to the

improved proposed scenario where the fabric shading was integrated with the two different trees LAD scenarios 13 and 14. The two proposed scenarios, 13 and 14, performed better than scenarios 4 and 7. Where scenario 7 had the maximum T_{MRT} at 14:00 with a magnitude of 75.8 °C and T_{Srf} a magnitude of 57.3 °C, due to the low LAD trees shading factor configuration of 25% and fabric transmittance of 20% in the canyon which allowed the solar radiation to go through to the canyon ground surface. Scenario 14, which integrated the low LAD trees and 25% configuration factor with the fabric shading of 25% shaded area, had results close to scenario 4 where it had only high LAD and a shading factor configuration of 25%. The maximum T_{MRT} of scenario 14 had a magnitude of 73.8 °C, and a T_{Srf} had a magnitude of 55.4°C at 14:00. Also, scenario 4 had a T_{MRT} magnitude of 73.1 °C and T_{Srf} of 54.8 °C. Finally, as expected scenario 13 had the best results of the four scenarios, where the maximum values of T_{MRT}, T_{Srf} at 14:00 were with a magnitude of 71.1 °C, 53.1°C, respectively.

5.2. Second Part

This part of the analysis introduces the four strategies and compars scenarios of the different strategies by subtracting the scenarios from each other in Area charts for hourly averaged variations of T_{MRT} at (0.9 m a.g.l) for the whole canyon area for one day duration. Moreover, to have a deep understanding of the performances of all the strategies and scenarios, this part divided the analysis into two groups. The first group identifies the T_{MRT} at (0.9 m a.g.l) differences between scenarios in the same strategies in degree Celsius. The second group finds the T_{MRT} at (0.9 m a.g.l) differences between the scenarios from all strategies that have the same shading area factor to know the exact cooling degrees that each strategy is providing.

5.2.1. First Group

For the whole day duration the results indicate the hourly averaged T_{MRT} differences between the scenarios of the same strategy in Figure. 5.2a. The differences in the first strategy were insignificant in the early morning hours until 7:00, then the variations increased for all the scenarios to the maximum differences of about 0.57°C for (Scenario 2 – Scenario 1), and 0.64°C for (Scenario 3 – Scenario 2) at 12:00. After that, the differences started to reduce until 18:00, where the variations were at their lowest through the night time.

The second strategy-A had higher differences for all the scenarios, from the early morning hours until 7:00, the difference between (Scenario 5 – Scenario 4) was very low and (Scenario 6 – Scenario 5) had up to 3 °C difference. After that, from 8:00 to the end

of the day time at 18:00 the variations increased for all the scenarios to the maximum differences of about 5.7 °C for (Scenario 5 – Scenario 4), and a magnitude of 0.95°C for (Scenario 6 – Scenario 5) at 15:00.

In addition, the second strategy-B had large differences for all the scenarios, where the early morning hours to 7:00 AM, the difference between scenarios were insignificant, and they were around average differences of 0.33 °C. After that, from 8:00 to the end of the day time at 18:00 PM, the variations increased for all the scenarios to the maximum differences of about 3.3 °C for (Scenario 8 – Scenario 4), and 2.2°C for (Scenario 9 – Scenario 8) at 15:00. Moreover, The Third strategy had extreme differences for all the scenarios, wherein early morning hours to 7:00, the differences between scenarios were insignificant, and they were around an average of 0.2 °C. After that, from 8:00 AM to the end of the day time at 18:00 the variations increased for all the scenarios to the maximum differences of about 2.7 °C for (Scenario 11 – Scenario 10), and 4.8 °C for (Scenario 12– Scenario 11) at 15:00.

Finally, the fourth strategy had only two scenarios and was compared with scenario 1 as the baseline, which had no trees and 75% of paved surfaces; for that reason, it had the hottest T_{MRT} results of all scenarios. The early morning hours until 7:00, the difference between the (Scenarios 1 – Scenarios 14) exceeded 5 °C, and had insignificant variations for (scenarios 13 – scenarios 14) where they were less than 0.2 °C. After that, from 8:00 AM to the end of the day time at 18:00, the variations increased for all the scenarios to the maximum difference of about 14.2 °C for (Scenario 14 – Scenario 1), and 3.1 °C for (Scenario 13 – Scenario 14) at 10:00.

First Strategy

Subtracting three incremental scenarios of the materials thermal properties, Soil & Vegetation covering 25%, 50%, and 75% of the canyon's ground surface.

Second Strategy-A

Three incremental scenarios of the High leaf density trees covering 25%, 50%, 75% of the canyon.

Second Strategy-B

Three incremental scenarios of the Low leaf density trees covering 25%, 50%, 75% of the canyon.

Third Strategy

Three incremental scenarios of the Low leaf density trees covering 25%, 50%, 75% of the canyon.

Fourth Strategy

Three incremental scenarios of the fabric shading covering 25%, 50%, 75% of the canyon.

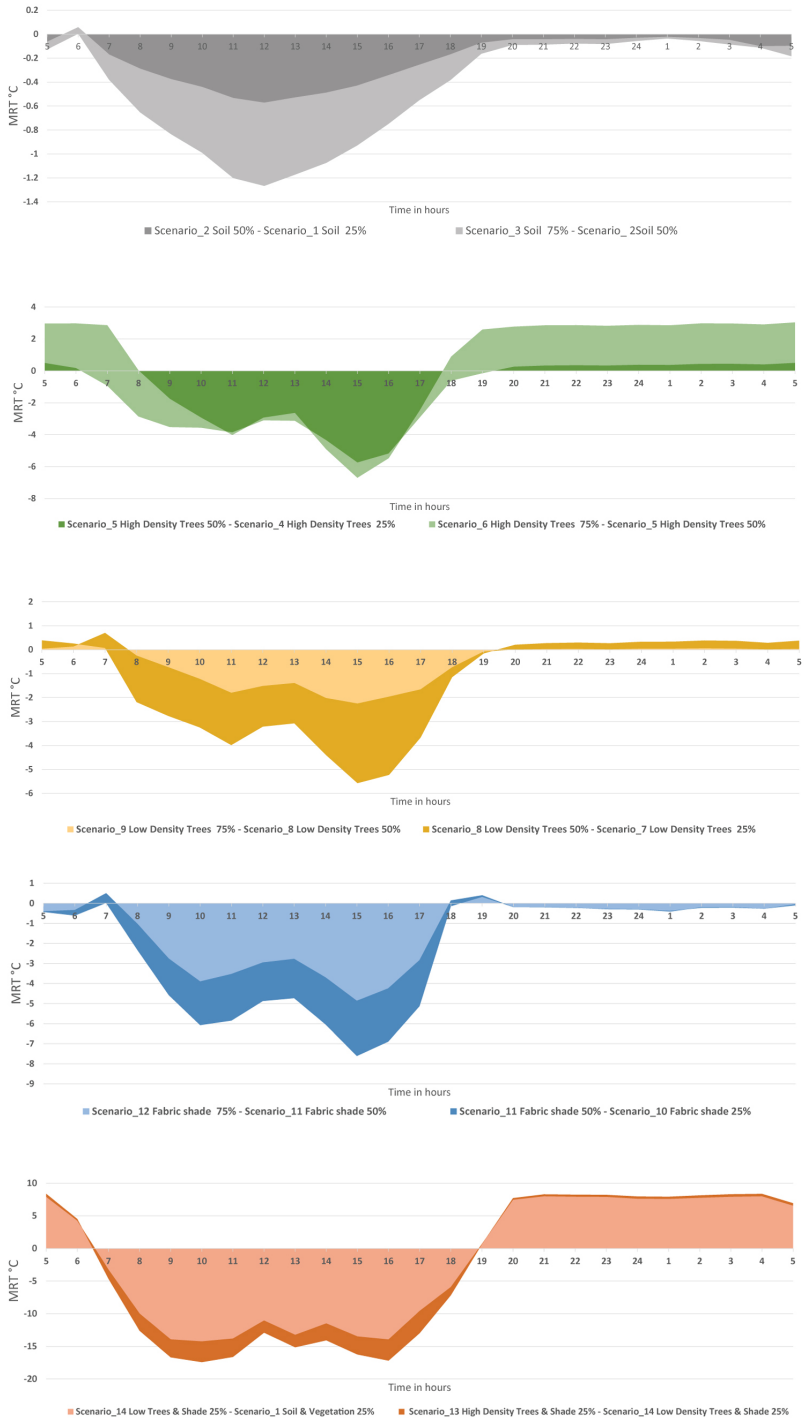

Figure. 5. 6. Area charts for all the 14 scenarios comparing hourly variation for all the scenarios results of T_{MRT} on (0.9 m a.g.l) for all the canyon area.

5.2.2. Second Group

For the whole day duration the results show the hourly averaged variations of whole canyon area for T_{MRT} differences in degree Celsius between the scenarios from all the different strategies in Figure. 5.2b. While the difference in the first comparison was significant for all the scenarios, the differences were very low in the early morning hours until 7:00 of less than 1 °C for all the scenarios. After that, the variations increased for all the scenarios to the maximum differences of about 6.6 °C for (Scenario 4 – Scenario 1), and a magnitude of 3.2 °C for (Scenario 7 – Scenario 4) at 10:00, and 3.2 °C for (Scenario 10 – Scenario 7) at 17:00. After that, the differences started to decline until 18:00, where the variations were at their lowest through the night time with an average of 1 °C.

The second comparison had significant differences in temperature for all scenarios, since the early morning hours until 7:00 the difference between (Scenario 5 – Scenario 2) was relatively high with a magnitude of 1.8 °C and had the lower differences between (Scenario 11 – Scenario 8) with a magnitude of 1.3 °C. The lowest difference in this comparison was between (Scenario 8 – Scenario 5) with a magnitude of 0.6 °C. After that, since 8:00 to the end of the day time at 18:00 the variations increased for all the scenarios to the maximum difference of 11.6 °C for (Scenario 5 – Scenario 2), and a difference of 1.52 °C for (Scenario 8 – Scenario 5) at 17:00. In addition, the third comparison revealed considerable differences in the late afternoon for all the scenarios, since the early morning hours to 7:00 AM the difference between the scenarios were relatively significant, the differences were around an average of 0.33 °C. After that, from 8:00 AM to the end of the day time at 18:00 the variations increased for all the scenarios

to the maximum differences of about 3.3 °C for (Scenario 8 – Scenario 4), and 2.2°C for (Scenario 9 – Scenario 8) at 15:00.

Finally, the fourth comparison involving only two scenarios 13 and 14, were compared to Scenario 7 – Scenario 4, which shows the performance of the new proposed strategy that integrated two different trees LAD and 25% of shaded factor configurations with the fabric shading that has 25% shade factor. The results have shown that the difference between the scenarios in early morning hours until 7:00 was insignificant, and had an average magnitude of 1 °C. From 8:00 AM to the end of the day time at 18:00 the variations increased for all the scenarios to the maximum difference of magnitude of 3.57 °C for (Scenario 7 – Scenario 4) at 17:00, and magnitude of 2.01 °C for (Scenario 13 – Scenario 7) at 16:00, and a magnitude of 3.3°C for (Scenario 13 – Scenario 15) at 17:00. Finally, a magnitude of 3.5°C for (Scenario 5 – Scenario 13) at 15:00 was noted.

1-Comparing Strategies
Three different scenarios with the same shading area factor of 25% from First, second, and third strategies.

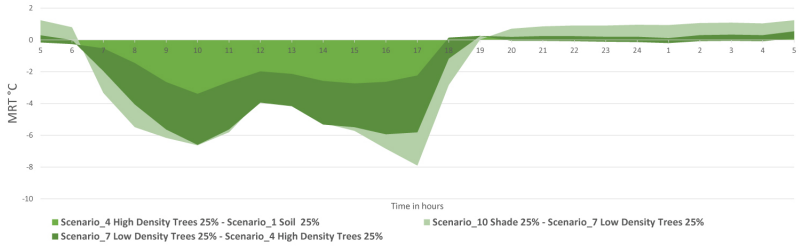

2-Comparing Strategies
Three different scenarios with the same shading area factor of 50% from First, second, and third strategies.

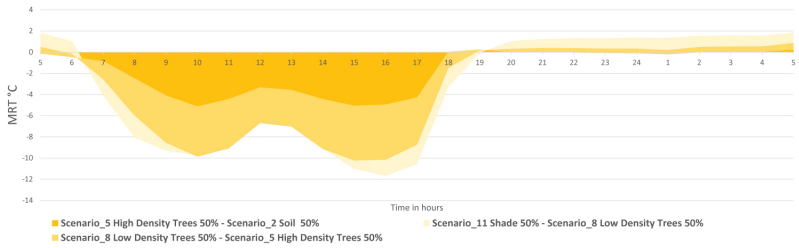

3-Comparing Strategies
Three different scenarios with the same shading area factor of 75% from First, second, and third strategies.

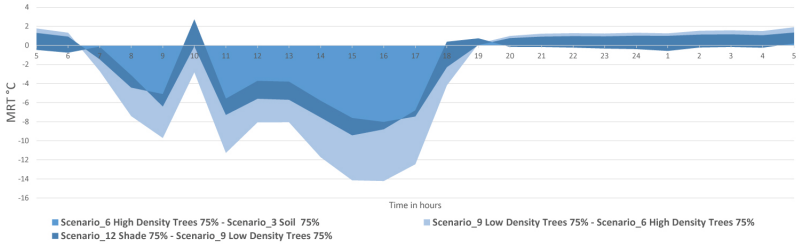

4-Comparing Strategies
Three different scenarios with the same shading area factor of 25%, 50% from the second and third strategies.

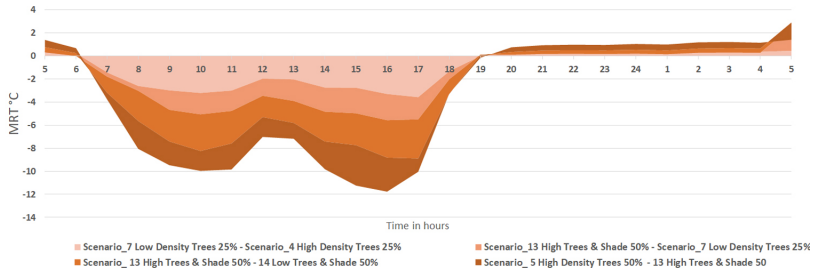

Figure. 5. 7. Area charts for all the 14 scenarios comparing hourly variation for all the scenarios results of T_{MRT} on (0.9 m a.g.l) for all the canyon.

5.3. Third Part

This group of the analysis included all the scenarios of the whole strategies in Box & Whisker charts for specific hours and compared the T_{MRT} at (0.9 m a.g.l) and T_{Srf} for the 14 scenarios. The results were plotted for different critical hours of the day for pedestrian behavior in ASU Downtown Phoenix campus, where hours 8:00, 12:00, and 17:00 were presented as the most active pedestrian's active hours of the daytime. The Box & Whisker plot is a way to study the data points of the canyon hourly and show the range of T_{MRT} and T_{Srf} points along the canyon area. Also, one can identify the median of the results.

5.3.1. The scenarios evaluation at 8:00

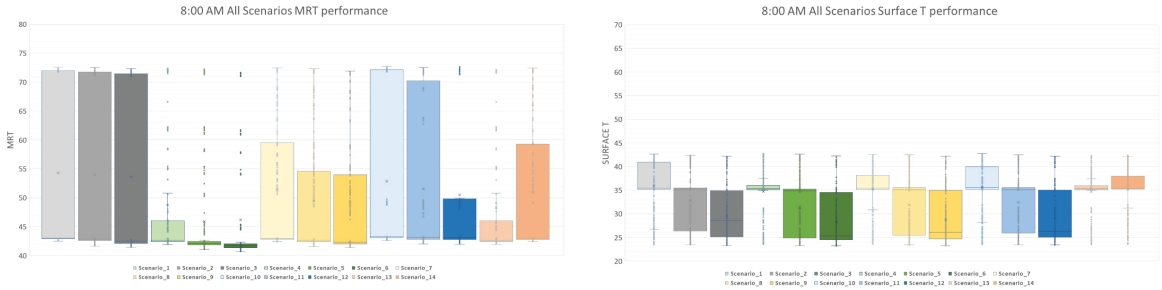

Figure. 5. 8. Box & Whisker charts for all the 14 scenarios comparing 8:00 average results of all the canyon area for the (T_{MRT}) on (0.9 m a.g.l) and (T_{Srf}) for all the canyon cells.

The results of all the scenarios were plotted for 8:00 to compare the performance of the different strategies applied on the canyon of T_{MRT} at (0.9 m a.g.l) and T_{Srf} in Figure. 5. 14. The boxes for scenarios 1, 2, and 3 had the longest ranges of the T_{MRT} results, where they started on average at 42.5 °C and ended on average at 71.5 °C with an average median at 43 °C. The second strategy-A had the shortest box ranges T_{MRT} results

of all strategies, where scenarios 4, 5, and 6 had a minimum magnitude of 42.5, 42, 41.5 °C respectively, and had a maximum magnitude of 46, 42.5, 42 °C respectively, and an averaged median magnitude of 42 °C. Moreover, scenario 4 had a relatively longer Whisker range that scenarios 5 and 6, and this is because of the increased high leaf density trees amount in scenarios 5 and 6 with 50% and 75%, respectively. The second strategy-B had the second shortest box ranges of the other scenarios, where the minimum T_{MRT} results for scenarios 7, 8, and 9 had a magnitude of 43, 42.5, 42°C respectively, and a maximum magnitude of 59.5, 54.5, 54 °C respectively, with an average median magnitude of 43 °C. The second strategy-B had a longer Whiskers ranges for all the strategies compared to the second strategy-A due to the use of low LAD trees which allowed the direct solar radiation to reach the ground surface of the canyon, where the Whiskers average maximum T_{MRT} for scenarios 7, 8, and 9 was at 72.5°C. The third strategy replaced the three trees scenarios and configurations in the second strategy with fabric shading. The result was showing relatively high Boxes & Whiskers ranges compared to the second strategy especially for scenarios 10 and 11, where the Boxes had a minimum T_{MRT} for scenarios 10, 11, and 12 with a magnitude of 43, 42.8, 42.2 °C respectively. Furthermore, the maximum Boxes ranges for T_{MRT} results at a magnitude of 72, 70, 50 °C, respectively. The fourth strategy, we integrated the second and the third strategies to test the performance of reducing the use of trees and fulfilling fabric shading devices to reach a higher shaded area. The Boxes minimum ranges for T_{MRT} were at magnitude 42.5, 42.8 °C for scenarios 13, 14 respectively, and the Boxes maximum ranges were at a magnitude of 46, 59.7 °C for scenarios 13, 14 respectively. Moreover,

the average median magnitude was relatively low compared to the maximum Boxes levels, where it had a magnitude of 42.8, 43 °C for scenarios 13, 14, respectively.

On the other hand, the T_{Srf} results of all the scenarios were plotted for 8:00 to compare the performance of the different strategies that been applied to the canyon of T_{Srf} shown in Figure. 5. 14. the results had a relatively close maximum Whiskers ranges with an average magnitude of 43 °C. However, the minimum Boxes & Whiskers ranges had higher variability, where scenarios 2, 3, 5, 6, 8, 9, 11, and 12 had an average T_{Srf} Whiskers ranges with a magnitude of 23 °C, due to the extensive shaded area throughout the canyon that reached 50% & 75%. Scenarios 1, 7, 10 had a higher average minimum Boxes & Whiskers ranges with a magnitude of 27°C, and Scenarios 4 and 13 had the highest minimum T_{Srf} Boxes & Whiskers ranges with a magnitude of 35 °C, due to the low shading area with 25% and less.

5.3.2. The scenarios evaluation at 12:00

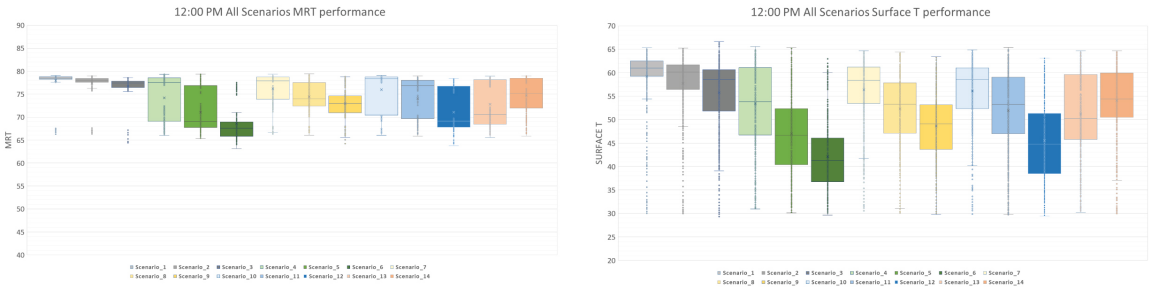

Figure. 5. 9. Box & Whisker charts for all the 14 scenarios comparing 12:00 average results of all the canyon area for the (T_{MRT}) on (0.9 m a.g.l) and (T_{Srf}) for all the canyon cells.

The results of all the scenarios were plotted for 12:00 to compare the performance of the different strategies that had been applied to the canyon for T_{MRT} at (0.9 m a.g.l) and T_{Srf} results in Figure. 5. 15. The boxes for scenarios 1, 2, and 3 had the shortest ranges of

the results of the different scenarios, where the Whiskers started at 72.5, 71.3, 70.5 °C respectively, and they ended at an average of 78.57 °C, and with an average median magnitude of 78 °C. The second strategy-A had the longest T_{MRT} stretched Boxes & Whiskers ranges of all the other strategies at 12:00, where scenarios 4, 5, and 6 had a minimum magnitude of 66, 65, 63°C respectively, and had a maximum magnitude of 79.4, 79.2, 71 °C respectively, and a median magnitude of 77.5, 69, 67.5 °C. Moreover, scenario 6 had a relatively shorter Whisker range than scenarios 4 and 5 at 12:00, due to the increased number of high LAD trees in the scenarios 6 with 75% of the shaded area throughout the canyon. The second strategy-B had the relatively shorter Boxes & Whiskers ranges of the second strategy-A, where the minimum T_{MRT} results for scenarios 7, 8, and 9 had a magnitude of 66.8, 66, 65.5 °C respectively, and a maximum magnitude of 79.4, 79.2, 78.8 °C respectively, with a median magnitude of 77, 74, 73 °C. The second strategy-B had a higher median range for all the scenarios compared to the second strategy-A due to the use of low leaf density trees, which allowed the direct solar radiation to reach the ground surface of the canyon. The third strategy replaced the three trees scenarios and configurations in the second strategy with fabric shading. The result was showing relatively longer Boxes & Whiskers ranges compared to the second strategy A and B, The Whiskers had a minimum T_{MRT} for scenarios 10, 11, and 12 with a magnitude of 66, 65.8, 64°C respectively. Furthermore, the maximum Whiskers ranges results were at a magnitude of 79, 79, 78.5 °C, respectively. Also, the median magnitudes for T_{MRT} were at 78.5, 77, 69 °C. The fourth strategy, the second and the third strategies were integrated to test the performance of reducing the use of trees and fulfilling fabric shading devices to reach a higher shaded area. The Whiskers minimum ranges for T_{MRT}

were at magnitudes of 65.5, 66 °C for scenarios 13, 14, respectively, and the maximum Whiskers ranges were at a magnitude of 79 °C for both scenarios. Moreover, the median magnitude was relatively higher, compared to the maximum Boxes & Whiskers ranges, where it had a magnitude of 70.5, 75.5 °C for scenarios 13, 14, respectively.

On the other hand, the T_{Srf} results of all the scenarios were plotted for 12:00 to compare the performance of the different strategies that been applied on the canyon for T_{Srf} shown in Figure. 5. 15. the results had a considerable variability for each strategy, where scenarios with the same shaded area percentage had close T_{Srf} boxes ranges. For instance, scenario 1, 2, and 3 had a minimum Boxes ranges with magnitudes of 62.5, 61.5, 60.5 °C, respectively. However, the Boxes ranges had higher variability on the second strategy-A, where the minimum ranges for scenarios 4, 5, and 6 had a T_{Srf} ranges with a magnitude of 61, 52.5, 46 °C respectively, due to the extensive shaded area throughout the canyon that reached 50% & 75%. Moreover, Scenarios 7, 8, and 9 had a relatively lower minimum Boxes ranges with a magnitude of 53.5, 46, 43.6 °C, due to the low LAD trees that were used. Finally, the fourth strategy had low variation in the maximum T_{Srf} Box ranges and relatedly higher variation in the boxes median and the minimum ranges. Whereas, scenario 13, 14 had an average maximum Boxes ranges with a magnitude of 64.8 °C for both scenarios. Also, it had a minimum boxes range with a magnitude of 45.5, 50.1 °C, respectively, and a median of magnitudes of 50.2, 54.4 °C.

5.3.3. The scenarios evaluation at 17:00

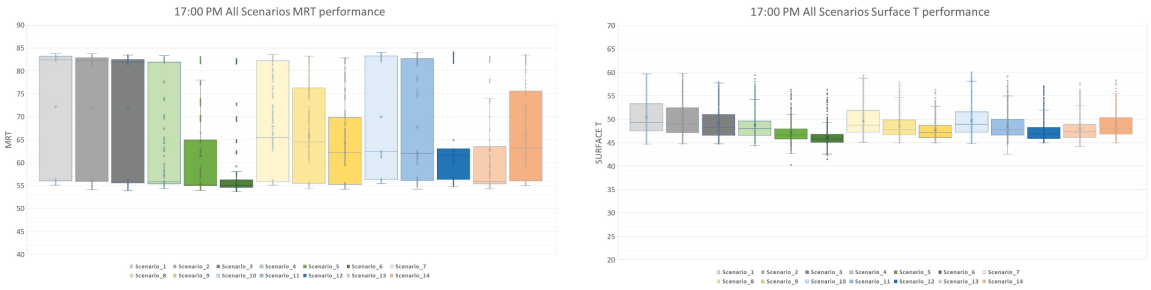

Figure. 5. 10. Box & Whisker charts for all the 14 scenarios comparing 17:00 average results of all the canyon area for the (T_{MRT}) on (0.9 m a.g.l) and (T_{Srf}) for all the canyon cells.

The results of all the scenarios were plotted for 17:00 to compare the performance of the different strategies that had been applied to a North-South canyon and evaluate the T_{MRT} at (0.9 m a.g.l) and T_{Srf} results in Figure. 5. 16. in the first strategy, the boxes for scenarios 1, 2, and 3 had the longest ranges of the T_{MRT} compared to the different scenarios. Where the Whiskers had a T_{MRT} magnitudes at 55, 54.2, 54 °C, respectively, and they ended at an average of 83.8 °C, and with an average median magnitude of 82.2 °C, due to the removal of all the trees and shading devices in the first strategy and manipulates the ground surface material's thermal properties. The second strategy-A had the crucial difference of T_{MRT} results between it's scenarios, where the maximum Boxes & Whiskers ranges for scenario 4 at 17:00 had a T_{MRT} with a magnitude of 83.3 °C, where scenarios 5 and 6 had a minimum magnitude of 65 and 55.2 °C respectively. Also, a median T_{MRT} magnitude of 55 °C for all the scenarios. Since scenario 6 had high LAD trees with a 75% shaded area for all the canyons, the canyon ground surface was protected from the direct solar radiation for most of the daytime and worked as a practical cooling effect. The second strategy-B had the relatively longer Boxes & Whiskers ranges

for scenarios 8 and 9 from the scenarios of the second strategy-A. Where the minimum T_{MRT} Whiskers results for scenarios 7, 8, and 9 had an average magnitude of 54.5 °C, and a maximum Boxes magnitudes of 82.2, 76.2, 69.8 °C respectively, with a median magnitude of 65.4, 64.5, 62.2 °C. The second strategy-B had a higher median range for all the scenarios compared to the second strategy-A due to the use of low LAD trees, which allowed the direct solar radiation to reach the ground surface of the canyon.

The third strategy replaced the three trees scenarios and configurations in the second strategy with fabric shading. The result was showing relatively longer Boxes & Whiskers ranges compared to the second strategy A and B, especially scenarios 10 and 11. For instance, scenarios 10, 11, and 12 had an average minimum T_{MRT} Whiskers with a magnitude of 56 °C. Also, the maximum Whiskers ranges results were at a magnitude of 83.2, 82.8, 63 °C, respectively. Furthermore, the T_{MRT} average median magnitudes were at 62 °C. By comparing scenarios 11, 8, and 5, we can see that even though the fabric shading devices had the same area, but the trees in strategies A and B had cooler results due to the additional moisture that the trees are providing to the canyon and relatively improving the T_{MRT}. The fourth strategy, the second and the third strategies were integrated to test the performance of reducing the use of trees and fulfilling fabric shading devices to reach a higher shaded area. The minimum ranges for T_{MRT} Whiskers were at a magnitude of 54.5, 55 °C for scenarios 13, 14, respectively, and the maximum Whiskers ranges were at a magnitudes of 74, 83.5 °C for scenarios 13, 14 respectively. Moreover, the median magnitude had high differences, where it had a magnitude of 56, 63 °C for scenarios 13, 14, respectively.

On the other hand, the T_{Srf} results of all the scenarios were plotted for 17:00 to compare the performance of the different strategies that been applied on the canyon for T_{Srf} shown in Figure. 5. 16. The results had an almost similar behavior for all the strategies, where scenarios with the same shaded area percentage had close T_{Srf} boxes ranges, and the hierarchy of the T_{Srf} level was clear in each strategy. The scenarios with higher soil and vegetation, trees, and fabric shading have shown a similar hierarchy. For instance, scenarios 4, 7, and 9 were higher than the other scenarios in the same strategy. The Boxes & Whiskers range for most of the scenarios between 43 and 60 °C, which, except scenarios 6, 9, and 12 where they had an average median of 46.2 °C.

Figure. 5. 11. Box & Whisker charts for all the 14 scenarios comparing 8:00 AM, 9:00 AM, and 12:00 average results of all the canyon area for the (T_{MRT}) on (0.9 m a.g.l) and (T_{Srf}) for all the canyon cells.

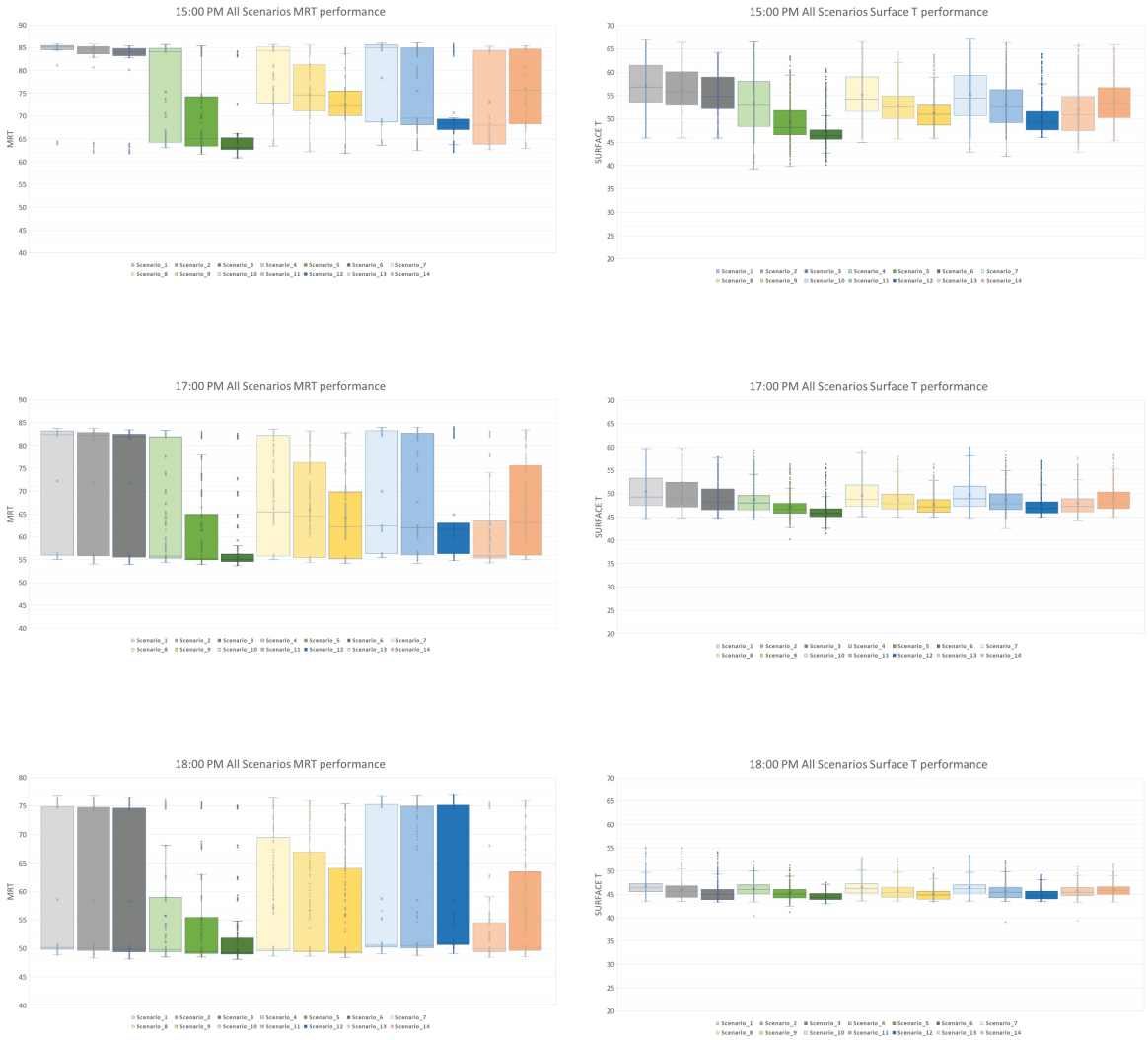

Figure. 5. 12. Box & Whisker charts for all the 14 scenarios comparing 13:00 PM, 17:00 PM, and 18:00 average results of all the canyon area for the (T_{MRT}) on (0.9 m a.g.l) and (T_{srf}) for all the canyon cells.

6. CONCLUSIONS & DISCUSSIONS

The primary objective of this study was to evaluate different pragmatic design solutions to an existing urban form. This was achieved by finding best possible configuration to enhance spatial thermal perception with a stronger emphasis on design as the essential element of manifestation of social patterns. Specific urban heat mitigation strategies were evaluated that could be applied to the existing urban settings in the hot-arid Phoenix, Arizona, without changing the building's footprint or any radical modification in the existing urban structures. An existing North-South canyon in Arizona State University Downtown campus was selected for study involving thermal mapping in six locations within and around the urban canyon. Subsequently, the data from the former exercise was analyzed and later evaluated to determine the different microclimates within the study area, and a computational fluid dynamics ENVI-Met model was validated against measurements by forcing actual climatic conditions.

Three main urban heat mitigation strategies targeting the UCL level were evaluated under three incremental scenarios. The three strategies included (a) increasing the permeable materials in the ground surface; (b) adding different configurations of high/low Leaf Area Density (LAD) trees, and; replacing existing tree configurations with fabric shading, all of which had three incremental scenarios. While the existing structures remained unaltered, the results of each strategy were evaluated and analyzed, and then compared to identify those with most efficient performance. Subsequently, the most successful and resilient scenarios were integrated into two proposed scenarios and evaluated against the three strategies. This study presented a scientific framework meant to improve the outdoor thermal comfort in the existing urban fabric by observation,

validation, simulation evaluation, and design decision and integration. Also, it has demonstrated that the local hot-arid climate improvements and mitigation strategies could be influential factors in improving the thermal perception and walkability likelihood in the outdoor spaces of Downtown Phoenix on an urban scale.

6.1. The study findings

This part of the conclusion & discussions chapter aims to answer the study questions:

6.1.1. The first question

What is the most efficient/durable urban heat mitigation strategy that could be applied to the existing urban canyon, with respect to the pedestrian's thermal comfort?

After evaluating the three strategies with three incremental scenarios, the best performance was recorded by scenario 6, which was under the second strategy-A, with 75% shaded area and trees of high LAD. Although this scenario was the most effective, it requires a large number of trees, and it is unrealistic to apply this scenario to the majority of the city's environments. For that reason, scenario 6 was used as the maximum degree of mitigation possible that could be reached through the main three strategies, and we seek to identify a scenario that could be realistic and effective in terms of the number of trees, and, consequently requiring lower use of water. Shading 50% of the canyon with scenarios 5, 8, and 11 are considered realistic and applicable to streets with busy daytime pedestrian activities. However, scenario 5 involved shaded 50% of the canyon with high LAD trees, thus requiring relatively large amounts of irrigation water when compared to

the low LAD trees proposed in scenario 8, or no water irrigation for scenario 11. Accordingly, this study proposed two scenarios, namely 13 and 14, which involved shading 50% of the canyon using a combination of integrating the high/low LAD trees and fabric shading. The strategies performed similarly (and better sometimes in the afternoon and late evening) than all the scenarios 5, 8, and 11. Scenarios 13 and 14, which requires half of the number of trees as scenarios 5 and 8, and had similar cooling effect with 50% reduction in irrigation water use and thus could be considered useful strategies to improve outdoor spaces in hot-arid cities like Phoenix.

6.1.2. The second question

To which level do the permeable surfaces on the ground level participate in outdoor thermal comfort for pedestrians?

The first strategy evaluated the role of material thermal properties on the ground surface level to the T_{MRT} at (0.9 m a.g.l) and T_{Srf} with three incremental scenarios. The first scenario represented the existing pavement layout, with 75% of asphalt, and only 25% of soil and vegetation. The second and third scenarios increased the soil and vegetation to 50% and 75%, respectively. Results of average hourly T_{mrt} and T_{Srf} across the canyon showed a limited cooling effect on T_{MRT} at (0.9 m a.g.l) and a relatively considerable cooling effect on T_{Srf}. Both scenarios included more permeable surfaces, which allows for more latent heat fluxes, and were found to be helpful for T_{Srf}.

6.1.3. The third question

Between the fabric shading devices and High/Low LAD trees, which one has the highest cooling effect in hot-arid Phoenix, Arizona?

The second strategy had two parts, A and B, and included three incremental scenarios for each part. Scenarios 4, 5, and 6 had different trees configurations shading 25%, 50%, and 75% of the canyon area. Leaf Area Density was at 1.1, and considered to be high therefore providing a greater shading factor to the canyon area. Scenarios 7, 8, and 9 had different tree configurations that shade 25%, 50%, and 75% of the canyon, respectively. The low LAD of 0.3 used in scenarios 7, 8 and 9 results with a low and provided low shading factor on the canyon area. The high LAD scenarios had considerably more cooling effect on the T_{MRT} at (0.9 m a.g.l) and T_{Srf}. Fabric shading devices found in the third strategy replaced the tree scenarios in the second strategy. The transmittance of those shading devices was set at 20%, and had the same configurations of 25%, 50%, and 75% of the canyon area. Although the fabric shading scenarios performed better than the low LAD tree scenarios, they were outperformed by high LAD tree scenarios. The fourth strategy integrated scenarios 4 and 10 to define to propose scenario 13, and scenarios 7 and 10 to define scenario 14 as two additional proposed scenarios. The total shading factor for both scenarios 13 and 14 was 50% of the canyon area, but with 50% less need for irrigation and maintenance. Scenario 14, which had a low LAD tree with 25% shaded area and fabric shading with 25% shaded area with a total of 50% shaded area, was very close and almost the same as the performance of the cooling effect of scenario 4, which had only High LAD trees. Such a result tells us the benefit of how powerful are the high LAD trees to improve the thermal performance of

the outdoor thermal comfort. Although high LAD trees require more irrigation and maintenance than the fabric shading, the high LAD trees could be an effective strategy to improve the outdoor thermal comfort if designed to be in the proper crowded and human-centered spaces. Moreover, we could reach even more comfortable levels if we integrated a few high LAD trees with fabric shading devices, which will improve the outdoor spaces drastically, as shown in scenario 13 results in chapter.5.

6.2. Design implementations & Recommendations

This study has presented an evaluation and analysis of the most common strategies that could be applied to an existing urban canyon in hot-arid climates. Many municipalities believe in increasing the number of trees on all streets as a way to reduce urban heat and improve the life quality in cities. However, when we want to improve the thermal performance in urban canyons, it is necessary to know the right location and type of trees we should be using. The methodology we have used in this research had different incremental scenarios of High/Low LAD trees and fabric shading strategies to examine their performance and found a threshold for each strategy. The limits of each strategy's cooling effect on a specific number of trees or ratio of the shade of the canyon ground area were determined. Knowing the threshold of each strategy could help us determine a range of the necessary amount of each strategy. This will help to avoid high initial capital costs, the need for irrigation, and maintenance in water scarcity regions.

However, each canyon will have its unique sun path and climatic conditions due to the different urban arrangements long the canyon. Also, the type of outdoor activity of some parts on the canyons, due to the low pedestrian's activities, may not necessarily

need the same cooling effect increase. As an example, this would apply to the long and consistent sidewalks between two buildings, where pedestrians will pass through without any attraction points along the sidewalk. Consequently, Low cooling effect could be applied with a limited number of trees additional to shading devices. On the other hand, other outdoor spaces where we expect high human activity, gatherings, and sitting for longer times the increase of cooling effect will be necessary, which could be achieved by adding high LAD trees with shading devices. Understanding the pedestrian's behavior in the outdoor spaces is essential to design strategies for specific behaviors, which could help to save the expenses of the initial costs, the need for irrigation, and maintenance for green and gray infrastructures.

This study evaluated the performance of different scenarios on North-South canyon, where the buildings block the direct solar radiation during the early morning hours and the late afternoon. The person's location in the canyon for a point of time in the daytime will determine the intensity of the direct solar radiation. Moreover, knowing that T_{Air} will be at it is maximum after noontime until the late afternoon, pedestrians will be uncomfortable walking at that time due to the high T_{Air}. Furthermore, due to the limited resources for most of the municipalities, it is not necessary to have symmetric mitigation implementations on both sidewalks of the canyons. Instead of improving the cooling effect of both canyon's sidewalks, we could choose one sidewalk to be improved. In the case of this study, North-South orientation, the west sidewalk of the canyon will be protected from the direct solar radiation when the T_{Air} at its maximum. Improving cooling effect performance of the west sidewalk could be beneficial to the pedestrian's thermal comfort because of the limited exposure to the direct solar radiation at the midafternoon

to sunset period. On the other hand the east sidewalk, where pedestrians could be exposed to direct solar radiation on the hottest times of the day would be an area where any strategy will prove futile.

Finally, the first strategy evaluation results have shown a perceptible cooling effect by increasing the permeable surfaces area on the ground $T_{Srf.}$ However, it did not have a considerable cooling effect on the T_{MRT} at (0.9 m a.g.l) for the whole canyon area, which could be due to the limitation of the ENVI-Met algorithm in terms of accuracy in the T_{MRT} calculation. However, increasing the permeable surface in the canyon ground surfaces will undoubtedly participate positively to the cooling effect, especially if the areas of permeable materials (e.g. soil, gravel, aggregate, etc.) exceeded 50% of the canyon area. This will reduce the heat absorption and decrease the chances of having high longwave radiation emittance around the pedestrian's sidewalls. Moreover, having light colors (high albedo) permeable surfaces could increase their reflectivity, and eventually their thermal storage. Typical paved applications (e.g. asphalt, concrete, etc.) should be rethought and redesigned in a way to allows more permeable materials in the canyon's ground surfaces.

6.3. Future Research Approaches & Limitations

This study has several limitations, one obvious limitation was the evaluation of only North-South canyon's orientation. A broader study scope would require the evaluation of the strategies on different canyon's orientations and find determine their performance on East-West, North East-South West, and North West - South East orientations. Moreover, the T_{MRT} simulated calculation in ENVI-Met are overestimated, and it is important to find a way to fix that bias in the software or using different programs which allow better agreements with the T_{MRT} measurements. Furthermore, the field observation of choosing the different study locations could have a drastic effect on the collected data, due to the unique characteristics of each location. One way to improve that is by having a grid with equal distances between the data collection locations on the domain study area, which will reduce the bias probability in the observed data. In addition, it is essential for improving the pedestrian's outdoor thermal comfort to associate their behavior to the locations that needs heat mitigation treatments the most in the city. By observing and detecting pedestrian's activities and social norms, the strategies evaluation and the design process for the specific locations can be performed. Finally, the outdoor thermal comfort and the microclimate are directly influencing the energy consumptions in the surrounding buildings. For that reason, it is crucial to study and evaluate the reduction magnitude that the urban heat mitigation strategies could achieve in terms of the energy consumption in buildings.

REFERENCES

Acero, J. A., & Arrizabalaga, J. (2018). Evaluating the performance of ENVI-met model in diurnal cycles for different meteorological conditions. Theoretical and applied climatology, 131(1-2), 455-469.

Akbari H., Rosenfeld A.H., Taha H. 1995: Cool construction materials offer energy saving and help reduce smog. ASTM standardization news 23, 11: 32 -37.

Akbari, H. (2008). Reducing Urban Heat Islands: Compendium of Strategies–Urban Heat Island Basics. US Environmental Protection Agency. Chapter 1: 1–22.

American Meteorological Society, 63(11), 1309–1313.

Arnfield, A. J. (2003). Two decades of urban climate research: a review of turbulence, exchanges of energy and water, and the urban heat island. International Journal of Climatology, 23(1), 1-26.

Asaeda T., Ca V.T., Wake A. 1993. Exchange Processes at the Land Surface for a Range of Space and Time Scales (Proceedings of (he Yokohama Symposium, July 1993). IAHS Publ. no. 212.

Asaeda T., Ca V.T., Wake A. 1996: Heat storage of pavement and its effect on the lower Atmosphere. Atmospheric Environment Vol.30, No.3: pp. 413-427.

Bakarman, M. A. (2017) Evaluating the Influence of Urban Canyon Geometry on Air and Surface Temperatures inside Modern Residential Neighborhoods in Hot-arid Climates: A Case Study of Riyadh, Saudi Arabia. University of Kansas.

Bin Ayyaf, A. (2015). dimension in municipal work, Riyadh as a case]. Riyadh, Saudi Arabia: Tarah International.

Bosselmann, P. (2012). Urban transformation: Understanding city form and design. Island Press.

Brazel, A., Gober, P., Lee, S. J., Grossman-Clarke, S., Zehnder, J., Hedquist, B., & Comparri, E. (2007). Determinants of changes in the regional urban heat island in metropolitan Phoenix (Arizona, USA) between 1990 and 2004. Climate Research, 33(2), 171-182.

Brazel, A., Selover, N., Vose, R., & Heisler, G. (2000). The tale of two climates Baltimore and Phoenix urban LTER sites. Climate Research, 15(2), 123-135.

Bryan, Harvey Ph.D., FAIA. “Outdoor Design Criteria for the Central Phoenix/East Valley Light Rail Transit System” Cooling Frontiers: The advanced edge of Cooling Research and Applications in The Built Environment, Herberger Center for Design Excellence, 2001, pp 5.1-5.7.

Burton, E., & Mitchell, L. (2006). Inclusive Urban Design: Streets for Life. Oxford: Elsevier.

Burton, E., Mitchell, L., & Lynne Mitchell, M. E. S. (2006). Inclusive urban design: Streets for life. Elsevier.

Carmona, M. (2014b). Investigating urban design. In M. Carmona (Ed.), Explorations in Urban.

Carmona, M. (Ed.). (2014). Explorations in urban design: An urban design research primer. Ashgate Publishing, Ltd.

Carmona, M., Heath, T., Tiesdell, S., & Oc, T. (2010). Public places, urban spaces: the dimensions of urban design. Routledge.

Chalfoun, N. V. (2001, November). Thermal comfort assessment of outdoor spaces using MRT© and fish-eye lens photography of architectural scale models: a case study of the “arts oasis” plaza at the university of Arizona, USA. In Proc. 18th Int. Conf. on PLEA, Florianopolis, Brazil (pp. 1021-1025).

Chow, W. T., & Brazel, A. J. (2012). Assessing xeriscaping as a sustainable heat island mitigation approach for a desert city. Building and Environment, 47, 170-181.

Cilliers, E. J., & Timmermans, W. (2016). Transforming spaces into lively public open places: case studies of practical interventions. Journal of Urban design, 21(6), 836-849.

Cook, J., and H. Bryan. 2001. Climate, Comfort and Health. Central Phoenix/East Valley Light Rail Transit, Phoenix, AZ.

Crank, P. J., Sailor, D. J., Ban-Weiss, G., & Taleghani, M. (2018). Evaluating the ENVI-met microscale model for suitability in analysis of targeted urban heat mitigation strategies. Urban climate, 26, 188-197.

Doll D., Ching J.K.S., Kaneshiro J. 1985, Parameterization of Subsurface Heating for Soil and Concrete Using Net Radiation Data. Boundary−Layer Meteorol. 32: 351-372.

Fishman, R. (1982). Urban Utopias in the Twentieth Century: Ebenezer Howard, Frank Lloyd Wright, and Le Corbusier. MIT Press.

Fung, W. Y., Lam, K. S., Hung, W. T., Pang, S. W., & Lee, Y. L. (2006). Impact of urban temperature on energy consumption of Hong Kong. Energy, 31(14), 2623-2637.

Fürst, D. (2009). Planning Cultures en Route to a Better Comprehension of 'Planning Processes'? In J. Knieling, & F. Othengrafen (Eds.), Planning cultures in Europe, decoding cultural phenomena in urban and regional planning.

Garba, S. B. (2004). Managing urban growth and development in the Riyadh metropolitan area, Saudi Arabia. Habitat International, 28(4), 593-608.

Gehl Institute. (2016, January). The Public Life Toolkit. Gehl Institute. Retrieved from https://gehlinstitute.org/work/public-life-diversity-toolkit/

Gehl, J. (2010). Cities for people. Washington, DC: Island Press.

Gehl, J., & Gemzøe, L. (2008). New City Spaces (3 edition). Copenhagen: Danish Architectural Press.

Georgescu, M., Mahalov, A., & Moustaoui, M. (2012). Seasonal hydroclimatic impacts of Sun Corridor expansion. Environmental Research Letters, 7(3), 034026.

Golden, J.S. and Kaloush, K. 2006. Meso-Scale and Micro-Scale Evaluations of Surface Pavement Impacts to the Urban Heat Island Effects. The International Journal of Pavement Engineering. 7(1): 37-52. March 2006.

Grossman-Clarke, S., Zehnder, J. A., Loridan, T., & Grimmond, C. S. B. (2010). Contribution of land use changes to near-surface air temperatures during recent summer extreme heat events in the Phoenix metropolitan area. Journal of Applied Meteorology and Climatology, 49(8), 1649-1664.

Hassid, S., Santamouris, M., Papanikolaou, N., Linardi, A., Klitsikas, N., Georgakis, C., & Assimakopoulos, D. N. (2000). The effect of the Athens heat island on air conditioning load. Energy and Buildings, 32(2), 131-141.

Höppe P. 1999: The Physiological Equivalent Temperature - A Universal Index for the Biometeorological Assessment of the Thermal Environment. Int. J. Biometeorol. 43: 71- 75.

Jacobs, J. (1961). The Death and Life of Great American Cities (Reissue edition). New York: Vintage.

Jacobs, J. (2016). The death and life of great American cities. Vintage.

Jauregui, E. (1997). Heat island development in Mexico City. Atmospheric Environment, 31(22), 3821-3831.

Kaynakli, O., & Kilic, M. (2005). Investigation of indoor thermal comfort under transient conditions. Building and Environment, 40(2), 165-174.

Kikegawa, Y., Genchi, Y., Kondo, H., & Hanaki, K. (2006). Impacts of city-block-scale countermeasures against urban heat-island phenomena upon a building's energy-consumption for air-conditioning. Applied Energy, 83(6), 649-668.

Knieling, J., & Othengrafen, F. (Eds.). (2009). Planning cultures in Europe: Decoding cultural phenomena in urban and regional planning. Ashgate Publishing, Ltd..

Kolokotroni, M., Zhang, Y., & Watkins, R. (2007). The London Heat Island and building cooling design. Solar Energy, 81(1), 102-110.

Krieger, A., & Saunders, W. S. (Eds.). (2009). Urban design. U of Minnesota Press.
Landscapes: integrating multidisciplinary perspectives. University of Washington Press. Seattle: 150-160.

Lang, J. T. (2005). Urban design: a typology of procedures and products (1st éd.). Oxford: Elsevier/Architectural Press. UdeM Amenag. NA, 9031, L36.

Lenzholzer, S., Klemm, W., Vasilikou, C., 2016. Qualitative methods to explore thermo-spatial perception in outdoor urban spaces. Urban Climate.

Li, D. C., Chen, C. C., Chang, C. J., & Chen, W. C. (2012). Employing box-and-whisker plots for learning more knowledge in TFT-LCD pilot runs. International Journal of Production Research, 50(6), 1539-1553.

Lynch, K. (1984). Good City Form (Reprint edition). Cambridge, Massachusetts: The MIT Press.

Lynch, K. (1984). Good city form. MIT press.

Madanipour, A. (1998). Social Exclusion and Space. In A. Madanipour, G. Cars, & J. Allen (Eds.), Social exclusion in European cities, processes, experiences and responses (pp.75–89). Jessica Kingsley.

Madanipour, A. (Ed.). (2010c). Whose Public Space?: International Case Studies in Urban Design and Development.

Madanipour, A. (Ed.). (2013). Whose public space?: International case studies in urban design and development. Routledge.

Maggiotto, G., Buccolieri, R., Santo, M. A., Leo, L. S., & Di Sabatino, S. (2014). Validation of temperature-perturbation and CFD-based modelling for the prediction of the thermal urban environment: The Lecce (IT) case study. Environmental Modelling & Software, 60, 69-83.

Maggiotto, G., Buccolieri, R., Santo, M. A., Leo, L. S., & Di Sabatino, S. (2014). Study of the urban heat island in Lecce (Italy) by means of ADMS and ENVI-MET. International Journal of Environment and Pollution. Accepted for publication.

Maloutas, T. (2018). Travelling concepts and universal particularisms: A reappraisal of gentrification's global reach. European Urban and Regional Studies, 25(3), 250-265.

Manglani, Puja, Radiative Exchange Analysis between a Tree and a West Wall, PLEA 2003 Conference proceedings, page 487.

McPherson E.G., Rowntree R.A, Wagar J.A. 1994: Energy efficient landscapes. Urban Forest.

Mehta, V. (2013). The street, a quintessential social public space. New York: Routledge.

Michelson, W. M. (1975). Behavioral research methods in environmental design. Dowden, Hutchinson & Ross.

Michelson, W. M. (1977). Environmental choice, human behavior, and residential satisfaction. Oxford University Press.

Middel, A., & Krayenhoff, E. S. (2019). Micrometeorological determinants of pedestrian thermal exposure during record-breaking heat in Tempe, Arizona: Introducing the MaRTy observational platform. Science of the Total Environment, 687, 137–151. https://doi.org/10.1016/j.scitotenv.2019.06.085

Middel, A., Häb, K., Brazel, A. J., Martin, C. A., & Guhathakurta, S. (2014). Impact of urban form and design on mid-afternoon microclimate in Phoenix Local Climate Zones. Landscape and Urban Planning, 122, 16-28.

Middel, A., Häb, K., Brazel, A. J., Martin, C. A., & Guhathakurta, S. (2014). Impact of urban form and design on mid-afternoon microclimate in Phoenix Local Climate Zones. Landscape and Urban Planning, 122, 16-28.

Mirzaei, P. A., & Haghighat, F. (2010). Approaches to study Urban Heat Island – Abilities and limitations. Building and Environment, 45(10), 2192-2201.

Moulay, A., Ujang, N., & Said, I. (2017). Legibility of neighborhood parks as a predicator for enhanced social interaction towards social sustainability. Cities, 61, 58-64.

Mumford, L. (1981). The Highway and the City. Westport, Conn: Praeger.

NACTO. (2013). Urban street design guide. Island Press.

Nunez M., Oke, T. R. 1977: The energy balance of an urban canyon. J. Appl. Meteorol.16: 11-19.

Oke T. 1988: Street design and urban canopy layer climate. Energy and Buildings 11:103-113.

Oke, T. R. (1981). Canyon geometry and the nocturnal urban heat island: comparison of scale model and field observations. Journal of Climatology, 1(3), 237-254.

Oke, T. R. (1987). Boundary Layer Climates. London: Routledge.

Oke, T. R. (1997). Urban Climates and Global Environmental Change. Applied Climatology: Principles & Practices, 273-287.

Olgyay, V. (1963). Design with Climate: Bioclimatic Approach to Architectural Regionalism.

Panofsky, E. (1951). Gothic Architecture and Scholasticism. Archabbey Press.

Rapoport, A. (1987). Pedestrian street use: Culture and perception. Public streets for public use, 80-94.

Reijndorp, A., & Hajer, M. A. (2001). In Search of the New Public Domain. Rotterdam: NAI Publishers.

Rosheidat A. (2014). Optimizing the Effect of Vegetation for Pedestrian Thermal Comfort and Urban Heat Island Mitigation in a Hot Arid Urban Environment. Arizona State University.

Rowe, Dave (English version), “Climatic Control of Outdoor Spaces in EXPO’ 92,”, Sociedad Estatal para la Exposicion Universal Sevilla 92, S.A. 1991.

Santamouris, M. (2001). Energy and climate in the urban built environment. London: James & James.

Santamouris, M. (2014). On the energy impact of urban heat island and global warming on buildings. Energy and Buildings, 82, 100-113.

Santamouris, M., Papanikolaou N., Koronakis I., Livada I., Asimakopoulos D. 1999: Thermal and Schivelbusch, W. (2014). The Railway Journey: The Industrialization of Time and Space in the Nineteenth Century. Univ of California Press.

Santamouris, M., Papanikolaou, N., Koronakis, I., Livada, I., & Asimakopoulos, D. (1999). Thermal and air flow characteristics in a deep pedestrian canyon under hot weather conditions. Atmospheric Environment, 33(27), 4503-4521.

Sayer, A. (2010). Method in social science: revised 2nd edition. Routledge.

Sayer, R. A. (1992). Method in social science: A realist approach. Psychology Press.

SEC. (2013). SEC Annual Report Retrieved from http://www.se.com.sa/SEC/English/Panel/Reports/

Shahmohamadi, P., Che-Ani, A., Ramly, A., Maulud, K., & Mohd-Nor, M. (2010). Reducing urban heat island effects: A systematic review to achieve energy consumption balance. International Journal of Physical Sciences, 5(6), 626-636.

Shashua-Bar L., Hoffman M.E. 2000: Vegetation as a climatic component in the design of an urban street. Energy and Buildings 31: 221-235.

Souza, L. C. L., Postigo, C. P., Oliveira, A. P., & Nakata, C. M. (2009). Urban heat islands and electrical energy consumption. International Journal of Sustainable Energy, 28(1-3), 113-121.

Stabler, L. B., Martin, C. A., & Brazel, A. J. (2005). Microclimates in a desert city were related to land use and vegetation index. Urban forestry & urban greening, 3(3-4), 137-147.

Sun, C. Y., Brazel, A. J., Chow, W. T., Hedquist, B. C., & Prashad, L. (2009). Desert heat island study in winter by mobile transect and remote sensing techniques. Theoretical and applied climatology, 98(3-4), 323-335.

Sun, Y., & Augenbroe, G. (2014). Urban heat island effect on energy application studies of office buildings. Energy and Buildings, 77(0), 171-179.

Taha, H. (1997). Modeling the Impacts of Increased Urban Vegetation on the Ozone Air Quality in the South Coast Air Basin. Atmospheric Environment, 30, 3423–3430.

Thorsson, S., Lindberg, F., Eliasson, I., & Holmer, B. (2007). Different methods for estimating the mean radiant temperature in an outdoor urban setting. International Journal of Climatology: A Journal of the Royal Meteorological Society, 27(14), 1983-1993.

Toudert, F.A. (2005), Dependence of Outdoor Thermal Comfort on Street Design. PhD Thesis, University of Freiburg, Freiburg.

UNESCO. (2016). Culture: urban future: global report on culture for sustainable urban development. Paris, France: UNESCO Publishing.

VDI, 1994: VDI 3789, Part 2: Environmental Meteorology, Interactions between Atmosphere and Surfaces; Calculation of the short- and long wave radiation. Beuth, Berlin. pp. 52.

Watkins, R., Palmer, J., Kolokotroni, M., & Littlefair, P. (2002). The balance of the annual heating and cooling demand within the London urban heat island. Building Services Engineering Research and Technology, 23(4), 207-213.

Whyte, W. H. (1980). The Social Life of Small Urban Spaces. New York: Project for Public Spaces Inc.

Willmott, C. J. (1981). On the validation of models. Physical Geography, 2, 184–194.

Willmott, C. J. (1982). Some comments on the evaluation of model performance. Bulletin of the American Meteorological Society, 63(11), 1309-1313.

World Population Prospects, the 2012 Revision. (2014). Retrieved November 2014, from United Nation's Population Division http://www.un.org/en/development/desa/population/publications/index.shtml

Yang, X., Zhao, L., Bruse, M., & Meng, Q. (2012). An integrated simulation method for building energy performance assessment in urban environments. Energy and Buildings, 54(0), 243-251.

Yoshida A., Tominaga, K., Watani S. 1990/91: Field measurements on energy balance of an urban canyon in the summer season. Energy and Buildings 15-16: 417-423.

APPENDIX. I

HOURLY BOX & WHISKER PLOTS, COMPARING HOURLY AVERAGE RESULTS FROM 8:00 TO 20:00 FOR (T_{MRT}) ON (0.9 M A.G.L) AND (T_{SRF}) FOR ALL THE CANYON AREA.

I.1. Hourly Box & Whisker Plots

This part of the appendix intruded the four strategies and compared the three scenarios of each strategy by presenting the results in a Box & Whisker charts for hourly variations of the whole canyon area for 12 hours of the day, from 8:00 to 20:00, and comparing the results of the T_{MRT} at (0.9 m a.g.l) and T_{Srf} of the canyon area for the three scenarios of each strategy. Box & Whisker is a way to plot the data points set and showing the ranges of T_{MRT} and T_{Srf} for every hour.

I.1.1. First Strategy, Scenarios 1, 2, and 3 Soil & Vegetation

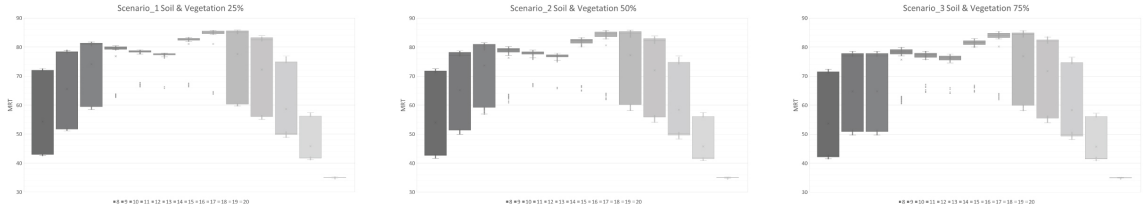

(T_{MRT}) on (0.9 m a.g.l)

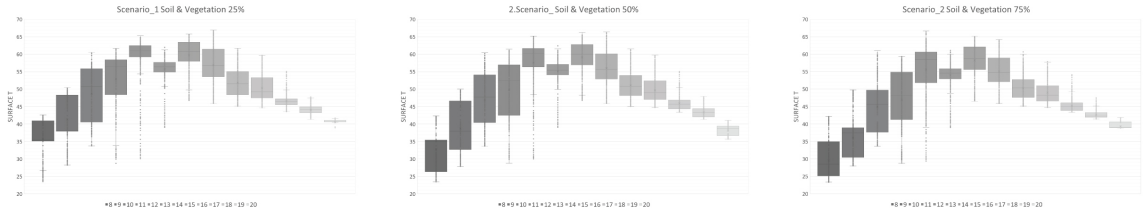

(T_{Srf}) results

APPENDIX I. 1. Hourly Box & Whisker charts for the first strategy, comparing the scenarios 1, 2, and 3. Showing: Hourly average results of (TMRT) on (0.9 m a.g.l) and (TSrf) for all the canyon area.

Mean Radiant Temperature. Hourly Box & Whisker charts are comparing the T_{MRT} at (0.9 m a.g.l) for three scenarios of the first strategy illustrated in Figure. 5. 8. For 12 hours duration, the results were showing low levels of variations due to the removal of all the shading and trees in scenarios 1, 2, and 3. The ground surface was exposed to the direct solar radiation in the day time and had the maximum sky view factor possible at the night time. The highest differences in the results between the different scenarios started increasing after 9:00 AM and begun to decrease after 17:00. The Boxes of hours 8:00 and 9:00 in scenarios 2 and 3 were stretched to cooler degrees compared to scenario 1, due to the different materials thermal properties for the ground surface materials, where the area of soil and vegetation increased relatively they affected the T_{MRT} in a large area of the canyon at those hours. Comparatively, the same thing happened in Scenario 2

and 3 at 11:00 to 15:00, the Boxes of those hours were stretched to slightly cooler degrees. Scenario 1 had the maximum T_{MRT} at 14:00 with 74.8 °C, the maximum T_{MRT} for scenario 2 and 3 were 74.5 °C, 74.1 °C respectively.

Ground Surface Temperature. Hourly Box & Whisker charts are comparing the T_{Srf} for three scenarios of the first strategy illustrated in Figure. 5. 8. The results presented simulated outcomes for 12 hours of duration, starting from 8:00 to 20:00. The results of the different scenarios varied, the Boxes of all the hours in scenarios 2 and 3 were stretched to cooler degrees, which means there were cooler areas in the canyon. For instance; at 11:00 AM in scenario 1 the minimum T_{Srf} was 34 °C and the median was at 56.5 °C, compared to scenarios 2 where the lowest T_{Srf} was at 28 °C and median was at 52.5 °C, and scenario 3 had the lowest T_{Srf} at 27 °C and the median at 48.2 °C, due to the amount of additional soil and vegetation that were increased in scenarios 2 and 3 for 50% and 75%, respectively. Most of the hour's ranges were stretched to cooler degrees, and more areas had cooler T_{Srf} by only changing the materials of asphalt to soil and vegetation. At the night time and the first half of the day time, scenario 3 had the coolest surface temperatures at 5:00 with a magnitude of 26 °C. The variations decreased after 12:00 and the results were close, and the variation started to increase again after 20:00, where the hottest surface temperatures were for scenario 1 at 12:00 with a magnitude of 59 °C.

I.1.2. Second Strategy-A, Scenarios 4, 5, and 6, High LAD Trees

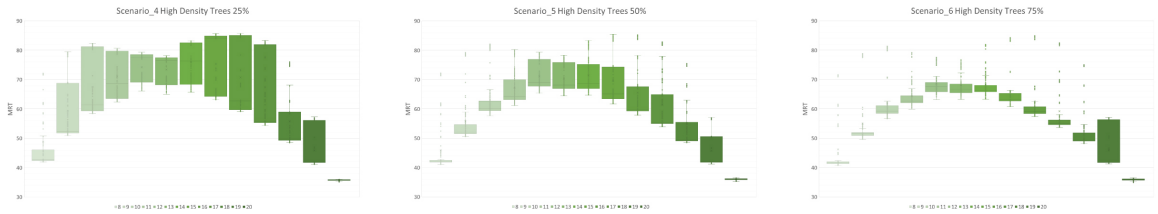

(T_{MRT}) on (0.9 m a.g.l)

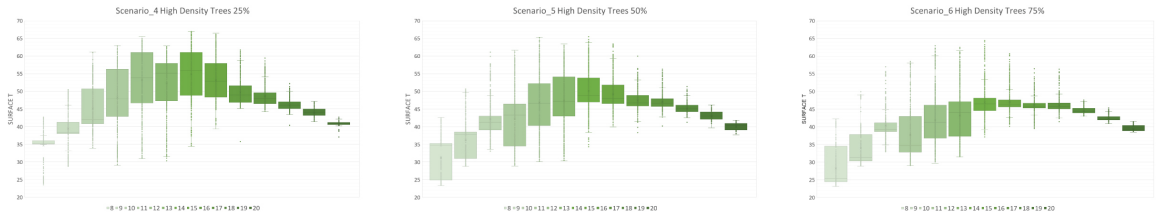

(T_{Srf}) results

APPENDIX I. 2. Hourly Box & Whisker charts for the first strategy, comparing the scenarios 4, 5, and 6. Showing: Hourly average results of (TMRT) on (0.9 m a.g.l) and (TSrf) for all the canyon area.

Mean Radiant Temperature. Hourly Box & Whisker charts are comparing the T_{MRT} at (0.9 m a.g.l) for three scenarios of the second strategy-A illustrated in Figure. 5. 9. For 12 hours duration, the results were showing high variability levels between the results due to the high LAD trees in the second strategy. The ground surface, which is a main contributor to the T_{MRT} on the pedestrian's level, was mostly covered with high LAD trees from the direct solar radiation during the day time. The Box & Whisker charts in Figure. 5. 9. shows that there was a cooling effect mostly in early morning hours until 14:00 due to the cool air temperatures and the protection from the direct solar radiation. However, from mid-afternoon to the late evening hours, there was a relatively limited cooling effect due to the increased air temperatures, which helped to keep the T_{MRT} higher. The cooling effect of the high LAD trees in different scenarios, as illustrated in Box & Whisker charts at 14:00, scenario 1 had the T_{MRT} the median magnitude of 75.5°C

and the lowest T_{MRT} magnitude at 66 °C. Where the scenario 2 had a T_{MRT} the median magnitude of 68 °C and the lowest T_{MRT} magnitude at 63 °C. Finally, scenario 3 had the lowest T_{MRT} median of 66 and the lowest T_{MRT} magnitude at 62 °C.

Ground Surface Temperature. Hourly Box & Whisker charts are comparing the T_{Srf} for three scenarios of the second strategy-A illustrated in Figure. 5. 9. The results presented hourly simulated data points for 12 hours from 8:00 to 20:00 duration. The results of the different scenarios had a drastic drop due to the cooling effect by the high leaf density trees; the Boxes of all the hours in scenarios 2 and 3 were stretched to cooler degrees, which means there were cooler areas in the canyon. However, the results were showing that the cooling effect had a higher effect on the early morning hours through the afternoon due to the low air temperatures in the morning time which helped with the shading strategies to reduce the T_{Srf} in some areas of the canyon. For example; at 11:00 in scenario 1 had a minimum T_{Srf} at 29 °C, and the median was at 48 °C, compared to scenarios 2 where the lowest T_{Srf} was at 28.5 °C and median was at 43.5 °C, and scenario 3 had the lowest T_{Srf} at 28 °C and the median at 43.3 °C, due to the different high LAD trees configurations in different scenarios. Almost all of the hour's ranges were stretched to cooler degrees, and more areas had cooler T_{Srf} whenever we have more dense trees. At the night time and the first half of the day time, scenario 3 had the coolest surface temperatures at 5:00 with 26 °C. The variations between scenarios decreased after 12:00 and the results were closes, then the variation started to increase again after 20:00, where the hottest surface temperatures were for scenario 1 at 12:00 with a magnitude of 59 °C.

I.1.3. Second Strategy-B, Scenarios 7, 8, and 9, Low LAD Trees

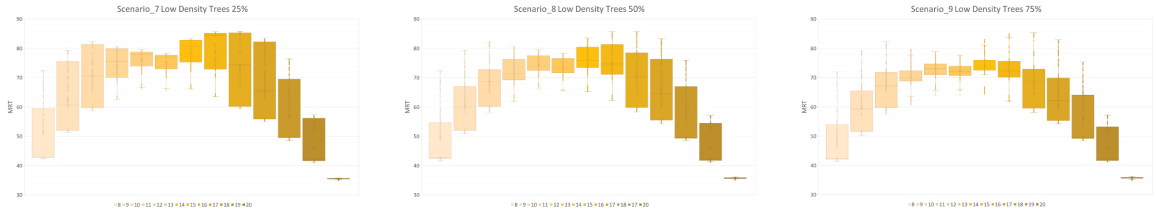

(T_{MRT}) on (0.9 m a.g.l)

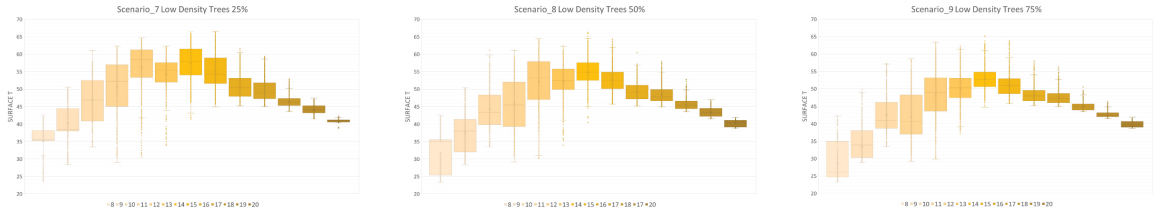

(T_{Srf}) results

APPENDIX I. 3. Hourly Box & Whisker charts for the first strategy, comparing the scenarios 7, 8, and 9 Showing: Hourly average results of (T_{MRT}) on (0.9 m a.g.l) and (T_{Srf}) for all the canyon area.

Mean Radiant Temperature. Hourly Box & Whisker charts are comparing the T_{MRT} at (0.9 m a.g.l) for three scenarios of the second strategy-B illustrated in Figure. 5. 10. For 12 hours duration from 8:00 AM to 20:00. The results were showing high variability levels between the different scenarios, especially scenario 9, due to the incremental number of low LAD trees in the third strategy. The ground surface, which is a primary contributor to the T_{MRT} on the pedestrian's level, was mostly covered with low leaf density trees, in scenarios 8 and 9, from the direct solar radiation during the day time. The Box & Whisker charts in Figure. 5. 10. Showed that there was a noticeable cooling effect mostly in early morning hours until 14:00 due to the cooler air temperatures and the protection from the direct solar radiation. However, from mid-afternoon to the late evening hours, there was a relatively limited cooling effect due to the increased air temperatures, which helped to keep the T_{MRT} higher. The cooling effect of the low LAD

trees in different scenarios, as illustrated in Box & Whisker charts at 14:00; for instance, scenario 7 had the T_{MRT} the median magnitude of 81 °C and the lowest T_{MRT} magnitude at 66 °C. Where scenario 8 had a T_{MRT} the median magnitude of 76 °C and the lowest T_{MRT} magnitude at 65 °C. Finally, scenario 3 had the lowest T_{MRT} median of 72.2 and the lowest T_{MRT} magnitude at 62°C.

Ground Surface Temperature. Hourly Box & Whisker charts are comparing the T_{Srf} for three scenarios of the second strategy-B illustrated in Figure. 5. 10. The results presented hourly simulated data points for 12 hours, from 8:00 to 20:00 duration. The results of the different scenarios had a relatively significant drop due to the cooling effect by the low LAD trees; most of the Boxes of scenarios 8 and 9 were stretched to cooler degrees, which means there were cooler areas in the canyon. However, the results were showing that the cooling effect had a higher effect on the early morning hours through the afternoon due to the low air temperatures in the morning time which helped with the shading strategies to reduce the T_{Srf} in some areas of the canyon. For instance; at 11:00 AM in scenario 7, the minimum T_{Srf} was at 45 °C and the median was at 54.5 °C, compared to scenarios 8 where the lowest T_{Srf} was at 39.5 °C and median was at 45.5 °C, and scenario 9 had the lowest T_{Srf} at 37 °C and the median at 40.5 °C, due to the different number of low LAD trees configurations in the different scenarios. Almost all of the hour's Boxes ranges were stretched to cooler degrees, and more areas had cooler T_{Srf} whenever we have more trees. At the night time and the first half of the day time, scenario 9 had the coolest surface temperatures at 5:00 AM with 26 °C. The variations between the scenarios decreased after 12:00 and the results were close, then the variation

started to increase again after 20:00, where the hottest surface temperatures were for scenario 7 at 14:00 for 57.3 °C.

I.1.4. Third Strategy, Scenarios 7, 8, and 9, Low LAD Trees

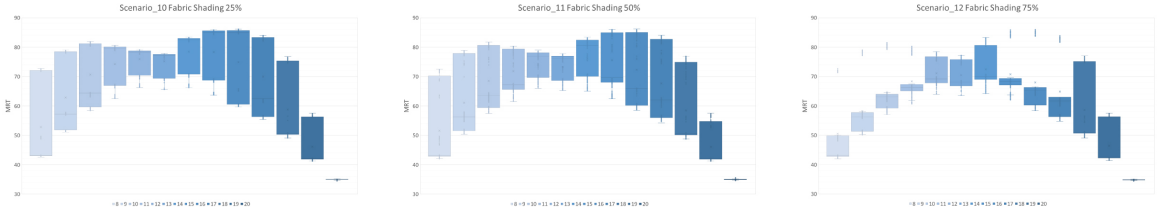

(T_{MRT}) on (0.9 m a.g.l)

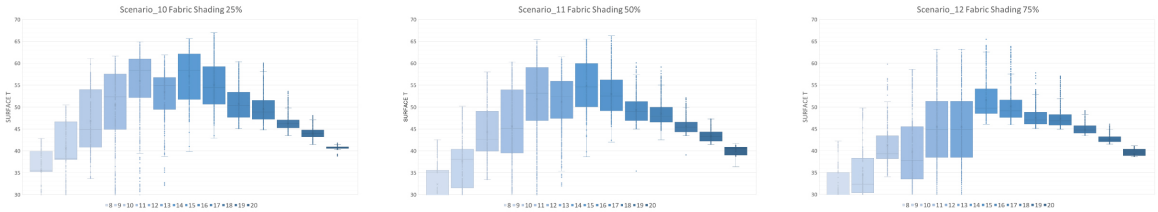

(T_{Srf}) results

APPENDIX I. 4. Hourly Box & Whisker charts for the first strategy, comparing the scenarios 10, 11, and 12 Showing: Hourly average results of (T_{MRT}) on (0.9 m a.g.l) and (T_{Srf}) for all the canyon area.

Mean Radiant Temperature. Hourly Box & Whisker charts are comparing the T_{MRT} at (0.9 m a.g.l) for three scenarios of the third strategy illustrated in Figure. 5. 11. For 12 hours, from 8:00 AM to 20:00 duration, the results were showing high variability levels between the results, due to the fabric shading in the fourth strategy. The ground surface, which is a main contributor to the T_{MRT} on the pedestrian's level, was mostly covered with fabric shading from the direct solar radiation during the day time. The Box & Whisker charts in Figure. 5. 11 showed that there was a cooling effect mostly in early morning hours until 14:00 due to the cool air temperatures and the protection from the

direct solar radiation. However, from mid-afternoon to the late evening hours, there was a relatively limited cooling effect due to the increased air temperatures, which helped to keep the T_{MRT} higher. The cooling effect of the high LAD trees in different scenarios as illustrated in Box & Whisker charts at 14:00; scenario 10 had the T_{MRT} the median magnitude of 82.2 °C and the lowest T_{MRT} magnitude at 71 °C. Where the scenario 11 had a T_{MRT} the median magnitude of 81 °C and the lowest T_{MRT} magnitude at 70 °C. Finally, scenario 12 had the lowest T_{MRT} median of 70 and the lowest T_{MRT} magnitude at 69 °C.

Ground Surface Temperature. Hourly Box & Whisker charts are comparing the T_{Srf} for three scenarios of the third strategy illustrated in Figure. 5. 11. The results were presenting hourly simulated data points for 12 hours, from 8:00 to 20:00 duration. The results of the different scenarios had a drastic drop due to the cooling effect by the fabric shading, the Boxes ranges of all the hours in scenarios 11 and 12 were stretched to cooler degrees which means there were cooler areas in the canyon. However, the results were showing that the cooling effect had higher performance on the early morning hours through the afternoon due to the low air temperatures in the morning time which helped with the shading strategies to reduce the T_{Srf} in some areas of the canyon. For example; at 11:00 in scenario 10 had a minimum T_{Srf} at 45 °C, and the median was at 52.2 °C, compared to scenarios 11 where the lowest T_{Srf} was at 39.5 °C and median was at 45.2 °C, and scenario 12 had the lowest T_{Srf} at 33.5 °C and the median at 37.5 °C, due to the different fabric shading configurations in different scenarios. Almost all of the hour's ranges were stretched to cooler degrees, and more areas had cooler T_{Srf} whenever we have more fabric shading. At the night time and the first half of the day time, scenario 12

had the coolest surface temperatures at 5:00 with 26.2 °C. The variations between scenarios decreased after 12:00 PM, and the results were closes, then the variation started to increase again after 20 PM, where the hottest surface temperatures were for scenario 10 at 14:00 with 57.1 °C.

I.1.5. Fourth Strategy, Scenarios 13, and 14, High & Low LAD Trees + Fabric shading

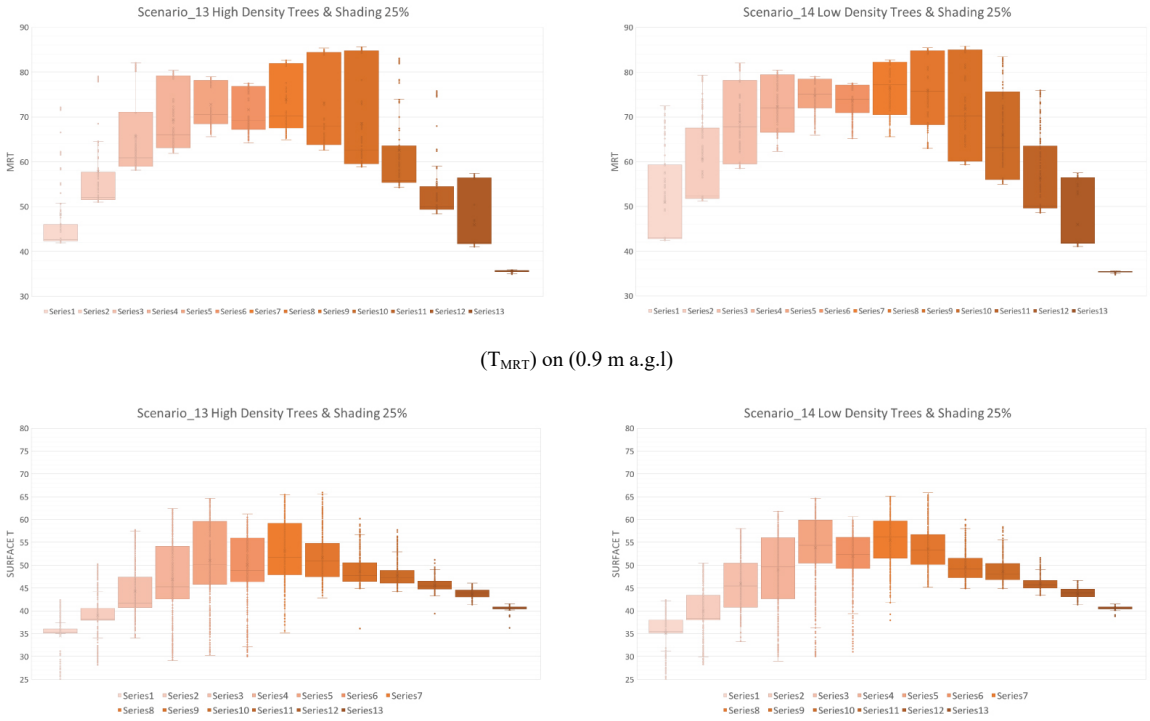

(T_{MRT}) on (0.9 m a.g.l)

APPENDIX I. 5. Hourly Box & Whisker charts for the first strategy, comparing the scenarios 13 and 14 Showing: Hourly average results of (T_{MRT}) on (0.9 m a.g.l) and (T_{Srf}) for all the canyon area.

Mean Radiant Temperature. Hourly Box & Whisker charts are comparing the T_{MRT} at (0.9 m a.g.l) for two scenarios of the fourth strategy illustrated in Figure. 5.12. For 12 hours, from 8:00 to 20:00 duration, the results were showing noticeable variability

levels between the results, due to the mixing of high and low LAD trees plus the fabric shading devices in the fourth strategy. The ground surface, which is a main contributor to the T_{MRT} on the pedestrian's level, was 50% covered with high and low leaf density trees plus the fabric shading devices the direct solar radiation during the day time. The Box & Whisker charts in Figure. 5.12. shows that there was a cooling effect mostly in early morning hours until 14:00 due to the cool air temperatures and the protection from the direct solar radiation. However, from mid-afternoon to the late evening hours, there was a relatively limited cooling effect due to the increased air temperatures, which helped to keep the T_{MRT} higher. The cooling effect of the high and low LAD trees plus the fabric shading devices in the two scenarios were illustrated in Box & Whisker charts at 14:00, scenario 13 had the (T_{MRT}) the median magnitude of 70.2 °C and the lowest T_{MRT} magnitude at 77.5 °C. Where the scenario 14 had a T_{MRT} the median magnitude of 75 °C and the lowest T_{MRT} magnitude at 71 °C.

Ground Surface Temperature. Hourly Box & Whisker charts are comparing the T_{srf} for the two scenarios of the fourth strategy illustrated in Figure. 5. 12. the results were presenting hourly simulated data points for 12 hours, from 8:00 to 20:00 duration. The results of the different scenarios had a drastic drop compared to the same stagey two and three, due to the cooling effect by high and low LAD trees plus the fabric shading devices. The Boxes ranges of all the hours in scenarios 11 and 12 were stretched to cooler degrees, which means there were cooler areas in the canyon. However, the results were showing that the cooling effect had higher performance on the early morning hours through the afternoon due to the low air temperatures in the morning time which helped with the shading strategies to reduce the T_{srf} in some areas of the canyon. For illustration;

at 11:00 in scenario 13 had a minimum T_{Srf} at 68 °C, and the median was at 72 °C, compared to scenarios 14 where the lowest T_{Srf} was at 63 °C and median were at 66 °C, due to the different fabric shading configurations in different scenarios. Almost all of the hour's ranges were stretched to cooler degrees, and more areas had cooler T_{Srf} whenever we have more fabric shading. At the night time and the first half of the day time, scenario 14 had the coolest surface temperatures at 5:00 with a magnitude of 30.1 °C. The variations between the two scenarios decreased after 12:00, and the results were close, then the variation started to increase again after 20:00, where the hottest surface temperatures were for scenario 13 at 14:00 with 53.1 °C.

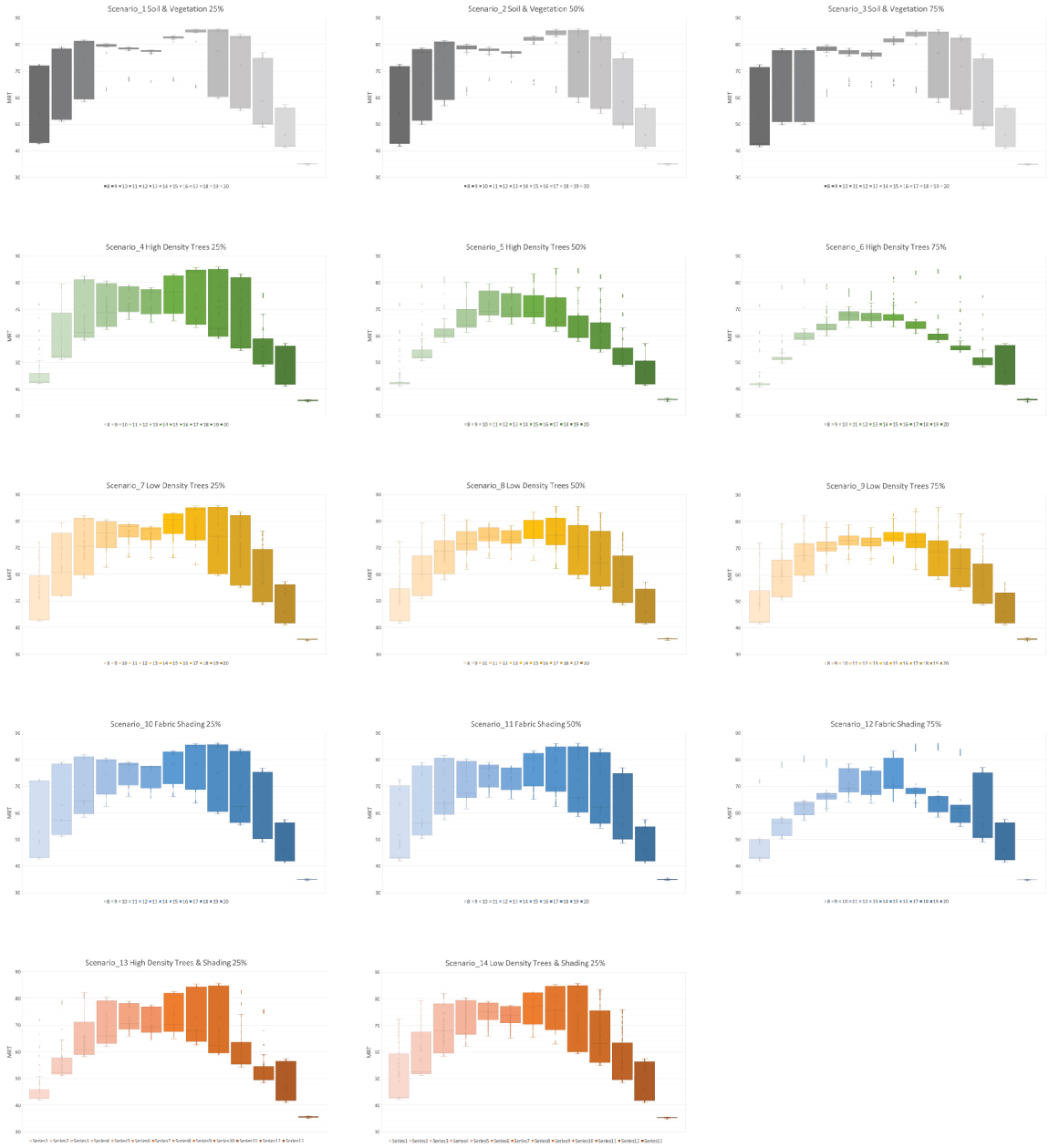

APPENDIX I. 6. Hourly Box & Whisker charts for the first strategy, comparing all the scenarios, and showin hourly average results of (T_{MRT}) on (0.9 m a.g.l) for all the canyon area.